PHILOSOPHICAL TRANSACTIONS OF THE ROYAL SOCIETY A MATHEMATICAL, PHYSICAL & ENGINEERING SCIENCES

The Breakdown of Superfluidity in Liquid ^{4}He. IV. Influence of ^{3}He Isotopic Impurities on the Nucleation of Quantized Vortex rings

G. G. Nancolas, R. M. Bowley and P. V. E. Mcclintock

Phil. Trans. R. Soc. Lond. A 1985 **313**, 537-606
doi: 10.1098/rsta.1985.0003

Phil. Trans. R. Soc. Lond. A **313**, 537–606 (1985) [537]
Printed in Great Britain

THE BREAKDOWN OF SUPERFLUIDITY IN LIQUID ^{4}He. IV†. INFLUENCE OF ^{3}He ISOTOPIC IMPURITIES ON THE NUCLEATION OF QUANTIZED VORTEX RINGS

By G. G. NANCOLAS‡, R. M. BOWLEY§ and P. V. E. McCLINTOCK‡

‡ *Department of Physics, University of Lancaster, Lancaster LA1 4YB, U.K.*
§ *Department of Physics, University of Nottingham, Nottingham NG7 2RD, U.K.*

(*Communicated by W. F. Vinen, F.R.S. – Received 25 April 1984*)

CONTENTS

	PAGE
1. Introduction	538
(*a*) The vortex nucleation problem	540
(*b*) The negative ion in dilute ^{3}He–^{4}He solutions	543
(*c*) Surface states of ^{3}He on the negative ion	544
2. Experimental details	547
(*a*) Measurement and control of the isotopic ratio	547
(*b*) Thermometry	549
(*c*) Measurement of the nucleation rate in low electric fields	550
3. Experimental results	551
4. Theory of the linear régime	559
(*a*) Outline of the model	560
(*b*) Process 1: 'thermal equilibrium'	561
(*c*) The absorption cross-section	566
(*d*) Process 2: roton-assisted ^{3}He emission	568
(*e*) Generalization of the model for many bound states	569
5. Data analysis for the linear régime	571
(*a*) Values of ν' and ν''	572
(*b*) Determination of the binding energy E_b	575
(*c*) Fitting the model to the data	576
(*d*) Extension to higher temperatures	579
(*e*) Critical velocity for the creation of the vortex rings	581

† Parts I–III appeared, respectively, in *Phil. Trans. R. Soc. Lond.* A **284**, 179–224 (1977), *Phil. Trans. R. Soc. Lond.* A **296**, 581–595 (1980) and *Phil. Trans. R. Soc. Lond.* A **307**, 201–260 (1982).

 [Published 30 May 1985

PAGE

6. Further discussion 584
(*a*) Nonlinear behaviour 584
(*b*) Theory of the nonlinear terms 585
(*c*) Fit to the data 589
(*d*) Rate of emission of ^{3}He with a pair of rotons 591
(*e*) Implications for the microscopic mechanism of vortex nucleation 592

7. Conclusions 594
Appendix A. Glossary of symbols 595
Appendix B. Tabular vortex nucleation data 598
Appendix C. ^{3}He concentration adjustment 599
Appendix D. The vortex-borne current 600
Appendix E. Equations for the nonlinear terms 603

References 605

We have investigated the rate ν at which negative ions nucleate charged vortex rings in a series of extremely dilute superfluid ^{3}He/^{4}He solutions. Measurements of ν were made at a pressure $P = 23$ bar (23×10^5 Pa) for temperatures, T, electric fields, E, and ^{3}He/^{4}He isotopic ratios, x_3, within the ranges: $0.33 < T < 0.61$ K, $1.0 \times 10^4 < E < 1.5 \times 10^6$ V m^{-1}, $2.1 \times 10^{-8} < x_3 < 1.7 \times 10^{-7}$. A few data were also recorded at other pressures within the range $19 < P < 25$ bar. For each concentration, and also for nominally pure ^{4}He ($x_3 = 1.9 \times 10^{-10}$), ν was measured for the same set of E and T. For all the chosen values of x_3 and P, the form of $\nu(E, T)$ was qualitatively much the same, and considerably more complicated than for pure ^{4}He. It was found that ν became equal to the nucleation rate ν_0 in pure ^{4}He for large E, but that $\nu \gg \nu_0$ for smaller values of E at low T. The ^{3}He-influenced contribution to the overall nucleation rate, $\Delta\nu = \nu - \nu_0$, passed through a pronounced maximum at a value of E that increased with increasing T; but the magnitude of $\Delta\nu$ itself decreased rapidly with increasing T. Plots of ν against x_3 for fixed P, E and T show a marked upward curvature for the lower values of E and T, but become linear within experimental error above *ca.* 0.5 K. A model is proposed (in two variants) in which the complicated behaviour of $\nu(E, T)$ is accounted for in terms of changes in the average occupancy by ^{3}He atoms of trapping states on the surface of the ion, it being proposed that the nucleation rate ν_1, due to ions each having one trapped ^{3}He atom, is very much greater than ν_0 for bare ions. The nonlinearities in $\nu(x_3)$ are interpreted in terms of the simultaneous trapping of two (or more) ^{3}He atoms on a significant fraction of the ions. It is shown that the model can be fitted closely to the experimental data, thereby yielding numerical values of ν_1, of the ^{3}He binding energy on the ion, and of a number of other relevant quantities. From the form of $\nu_1(E)$, it is deduced that the addition of a ^{3}He atom to a bare ion affects its propensity to create vortex rings in two ways: the critical velocity for the process is reduced by *ca.* 4 m s^{-1}, and the rate constant is increased by a factor of *ca.* 10^3. The implications of these results for microscopic theories of the vortex nucleation mechanism are discussed.

1. Introduction

An unexpected observation made earlier in our research programme on the breakdown of superfluidity in liquid ^{4}He was that the presence of minute proportions of ^{3}He isotopic impurity could exert a quite astonishingly potent influence on the propensity of negative ions to create quantized vortex rings. Under some conditions, even the small proportion of ^{3}He present in commercial helium (for which the ^{3}He/^{4}He ratio x_3 is typically 2×10^{-7}) was sufficient to alter

by an order of magnitude, or more, the rate ν at which rings were nucleated. For this reason, our initial experimental studies (Bowley *et al.* 1982) of vortex nucleation in liquid helium were completed on the basis of ^{4}He which had been isotopically purified to a very high standard. In the present paper we report and discuss the results of a new series of experiments in which we have investigated systematically the effect on ν of the deliberate addition of tiny traces of ^{3}He to pure ^{4}He. In view of the extraordinary sensitivity of ν to x_3, the phenomenon may be regarded as one that is of very considerable interest in its own right. An additional and, in some ways, more important motivation for the measurements described below, however, has been our hope that such studies might yield information about the nature of the microscopic vortex nucleation mechanism itself. A brief preliminary report (Bowley *et al.* 1984) summarizing some of the more important results and conclusions from the work has already been published.

The earlier papers in this series on the breakdown of superfluidity in liquid ^{4}He have been: Allum *et al.* (1977), hereinafter referred to as I, describing an experimental test of Landau's explanation of superfluidity; Ellis *et al.* (1980), hereinafter referred to as II, on excitation emission from negative ions travelling at extreme supercritical velocities; and Bowley *et al.* (1982), hereinafter referred to as III, on vortex nucleation by negative ions in isotopically pure liquid ^{4}He. Paper III is, of course, the most directly relevant to the present work, and we shall make frequent reference to it throughout the rest of this paper.

The plan of the paper is as follows. In §1 (*a*) we review briefly some important developments in the theory of vortex nucleation that have occurred since the publication of III. Relevant earlier work on the negative ion in dilute ^{3}He–^{4}He solution is discussed in §1 (*b*), and the ^{3}He surface states that are believed to exist on the negative ion are described in §1 (*c*). Experimental details are presented in §2. The methods developed for the control and adjustment of x_3 are described in §2 (*a*); and the precision and accuracy of the thermometry near 0.3 K (which were unimportant for the pure ^{4}He measurements of III because ν was then temperature independent) are discussed in §2 (*b*). Although a full exposition of the technique used for the measurement of ν was presented in III, the work described here has required an extension of the measurements to considerably lower values of electric field than were used in III. Accordingly, a justification for the use of the same technique under these conditions is given in §2 (*c*). An extensive set of experimental data is given in the form of graphs in §3 and, of these, a further small selection is also presented in tabular form in Appendix B.

As we shall see, it turns out that, in the limiting case of low concentration, as $x_3 \to 0$, the ^{3}He contribution to ν varies linearly with x_3. A theoretical model describing this linear régime is developed in §4. The model is first presented, in §4 (*a*)–(*d*), in the simplest possible form, on the assumption that only one state for bound ^{3}He exists on each ion. In §4 (*e*) we generalize the model to allow for the fact that, in reality, there will be many such bound states, with a range of energies, on each ion as discussed in §1 (*c*). We do so in two different ways. In the first of these, we propose a model in which all the parameters involved (the instantaneous nucleation rate, the ^{3}He absorption cross-section and the ^{3}He + rotons emission rate) are independent of l, the angular momentum quantum number. We call this model A. In the second model, we take the ^{3}He + rotons emission rate to vary with the energy ϵ_l of the bound ^{3}He atom in a specific way: since the energy is already known, this assumption introduces no additional unknown parameters into the model. We call this model B. By comparing the values obtained for the parameters of these models, we can infer the uncertainty in them arising from our approximations.

In §5 (*a*)–(*d*) we fit these two variants of the model to the experimental data, thereby

PHILOSOPHICAL TRANSACTIONS OF THE ROYAL SOCIETY A MATHEMATICAL, PHYSICAL & ENGINEERING SCIENCES

obtaining numerical values of a number of important parameters, including the ^{3}He binding energy on the negative ion and a characteristic rate ν_1 (dependent on electric field) for the nucleation of vortex rings by an ion with a single trapped ^{3}He atom. Information about the (weakly temperature-dependent) ionic absorption cross-section for ^{3}He, and the emission rate of ^{3}He atoms from the ion with rotons, is also obtained; but only in the form of a ratio of the respective constants. We shall see that both forms of the model give gratifyingly good agreement with the data, but that model B appears on balance to be superior. In §5(*e*) we discuss the form of the deduced values of $\nu_1(E)$ and show how it can be accounted for in terms of a reduced critical velocity and an increased instantaneous vortex nucleation rate, as compared with those of a bare ion.

The nonlinear régime is discussed in §6(*a*)–(*c*). It is suggested in §6(*a*) that the nonlinearities correspond to the onset of conditions such that an increasing number of ions have *two* trapped ^{3}He atoms at any one time. The necessary extensions to the model of §4(*a*)–(*e*) are developed in §6(*b*) and fitted to the experimental data in §6(*c*). As we shall see, fitting the data of the nonlinear régime in this way is especially advantageous in that it then becomes possible to derive absolute values of the ^{3}He absorption cross-section. By comparison of these with the ratio of constants obtained from fits in the linear régime in §5(*c*), it then also becomes possible (in §6(*d*)) to determine absolute values of the (electric-field-dependent) ^{3}He emission rate. In §6(*e*) we discuss in a fairly speculative way some possible mechanisms underlying the ^{3}He effect, and the extent to which the data presented in this paper may help to illuminate the vortex nucleation process itself.

Finally, in §7, we try to sum up the current experimental and theoretical situation, by taking stock of what has now been established with reasonable certainty and what still remains obscure; and we suggest some further avenues which might with advantage be explored in the future.

A glossary of the main symbols used in the paper is given as Appendix A.

(*a*) *The vortex nucleation problem*

The experimental and theoretical background to the present work has already been discussed in some detail, in III. After the publication of that paper, however, some important developments have occurred in the theory (Muirhead *et al.* 1984; Bowley 1984). These are believed to be potentially of great significance for the interpretation of the ^{3}He effect studied in the experiments reported here, and we therefore present a very brief summary of what has been achieved. This should be considered in conjunction with the discussion in III, particularly including §1(*a*)–(*c*) and §4(*c*) and (*d*).

Although they differ in a number of important details, both Muirhead *et al.* (1984) and Bowley (1984) adopt the same basic approach in tackling the fundamental problem of how a vortex ring is created *ab initio* in the superfluid by a moving ion. They start from a suggestion put forward by Vinen (1963) more than twenty years ago, namely that the creation of a vortex in the liquid is impeded by an energy barrier; and they develop this idea within the context of the generalized Landau argument (Rayfield & Reif 1964; Schwarz & Jang 1973) that has already been discussed in III.

Muirhead *et al.* treat each of the two possible configurations that have been proposed for the initial vortex relative to the ion: the loop suggested by Donnelly & Roberts (1971) and the encircling ring of Schwarz & Jang (1973). Bowley considers only the latter configuration but does so starting from a more fundamental standpoint. Both papers make explicit allowance

for the quantum zero point energy of the initial vortex and both recognize that the principal difficulty in making accurate quantitative predictions lies in our present ignorance of the detailed structure and energy of the vortex core, this being of considerable importance on account of the small scale of the nucleating configuration.

At the risk of over-simplification, but in the interests of conveying the main physical ideas, we will now try to summarize the basis and the principal conclusions of these calculations. It is assumed in both cases that, in the transition from bare ion to ion plus vortex, impulse must be conserved. Hydrodynamics is then used as a basis for calculating the energy difference ΔE between the initial and final states as a function of the radius of the vortex (assumed to be an arc of a circle, for loops), for different initial velocities v_i of the ion. The results of these calculations take the forms sketched in figure 1 (*a*) and (*b*) for rings and loops respectively

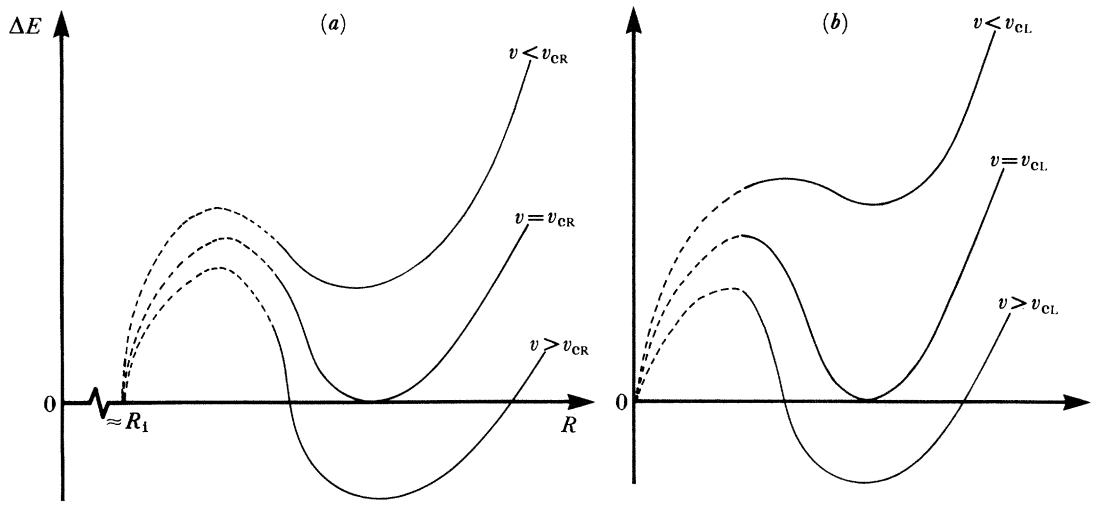

FIGURE 1. Sketch of the energy barrier that is believed to impede the creation of a vortex in the superfluid by a moving ion (after Muirhead *et al.* 1984) for two possible nucleating configurations: (*a*) vortex rings; and (*b*) vortex loops. In each case, the difference in energy ΔE between a bare ion and an ion + vortex is plotted as a function of the radius R of the vortex for three initial velocities v. The critical values v_{cR} and v_{cL} refer to the creation of rings or loops respectively. The full curves indicate regions where ΔE can be calculated explicitly and the dashed ones represent reasonable guesses of the form which must be taken by $\Delta E(R)$ in the core-dominated region, where quantitative calculations are currently not feasible.

(Muirhead *et al.* 1984). The dashed regions of the curves, lying in the core-dominated region where ΔE cannot at present be calculated, are based on plausibility arguments. It is thus being suggested that ΔE must be zero for a ring of a radius such that it effectively coalesces with its hydrodynamic image in the ion; and that a vortex loop of zero radius must also have $\Delta E = 0$. In each case, it is argued, the energy difference ΔE will be likely to rise smoothly from zero, eventually joining up with the relevant full curve in the region where the energy resides mainly in the flow field around the core and the calculation of ΔE can be carried through explicitly. For the transition to occur at all, ΔE must of course be zero, which can only be so if v exceeds a critical value v_{cR} or v_{cL} for rings or loops respectively. Calculated values of these critical velocities are uncertain to the extent that the vortex core parameters are unknown, but they appear to be consistent with the experimental values reported for the first critical velocity v_{v1} in III.

Considered in this way, vortex creation can be viewed as an example of quantum tunnelling:

no matter whether the initial vortex is a ring or a loop, it is clear from figure 1 that the initial and final states are separated by an energy barrier in the sense that there are no energetically allowed intermediate states through which the system can pass during the nucleation process. However, this viewpoint does present some conceptual difficulties. One can quite reasonably enquire as to the nature of the entity that is doing the tunnelling. There appear to be two possible approaches to this question. The first of these is to say that one is observing a transition between two different stable flow patterns of the superfluid as a whole, starting without a vortex and ending with a vortex present; that these states are separated by an energy barrier; and that it is the whole system that tunnels from the initial to the final state. Alternatively, perhaps, one might envisage the vortex itself as existing transiently in some kind of virtual state, at vortex ring radius $r = R_i$, the ionic radius, or $r = 0$ respectively for rings or loops, before tunnelling through the barrier in the usual quantum mechanical way.

The latter picture does not really seem to stand up to close scrutiny, however. To calculate the tunnelling rate in the W.K.B. approximation, an attempt rate is required; and this then determines the scale of the nucleation rate. One immediately encounters a philosophical difficulty for, if an entity does not exist, how can it attempt to tunnel? If the entity does exist before tunnelling, but only in a virtual state, what then will govern the attempt rate? Muirhead *et al.* argue that the only frequency scale in the problem is the cyclotron frequency of the vortex

$$\omega = \rho_4 \kappa / M,$$

where κ is the circulation of the vortex, M is its effective mass per unit length and ρ_4 is the ^{4}He density. This interesting suggestion still does not fully resolve the conceptual problems referred to above, however, because the cyclotron motion in question must surely refer to the vortex *after* creation, and not before. We may also note that it would appear to be inconsistent, in a formal sense, to couple the idea of a virtual state with calculations based upon a tunnelling model: the concept of a virtual state is derived from perturbation theory and automatically carries with it the implication that nucleation rates should be calculated not on the assumption of tunnelling, but by use of the formulae of traditional perturbation theory. In any case, the process under discussion clearly differs in important respects from, for example, the tunnelling of an individual electron from a metal during field emission, where the electron exists as a discrete entity both before and after the tunnelling event occurs. Furthermore, the latter process involves only one electron, whereas vortex nucleation involves a discontinuous change in the collective motion of a very large number of helium atoms. If, therefore, vortex nucleation is indeed to be regarded as occurring through tunnelling, then it must be an example of *macroscopic* (or semi-microscopic) quantum tunnelling.

Muirhead *et al.* have shown that the critical velocity for the formation of a vortex loop is apparently less than that for the formation of a ring. The two calculations in question each incorporated exactly the same assumptions about the vortex core so that, although these are quite likely to turn out not to be exactly correct, there seems no good reason to suppose that a more refined version of their theory would invert the relative magnitudes of the two critical velocities (although their absolute values could well be in error). Muirhead *et al.* have also been able to demonstrate that the rate of tunnelling through the calculated barrier for loops would probably be of the right order of magnitude to account for the experimental data of III.

Bowley's calculations refer exclusively to the encircling ring of Schwarz & Jang (1973).

PHILOSOPHICAL TRANSACTIONS OF THE ROYAL SOCIETY A MATHEMATICAL, PHYSICAL & ENGINEERING SCIENCES

Taking advantage of certain simplifications that arise because of the cylindrical symmetry of this configuration, he has been able to treat the initial vortex explicitly as a quantum object, which consequently has zero point motion and quantized energy levels within the well which exists beyond the energy barrier of figure 1(*a*). He makes appropriate allowance for the existence of the zero point energy in calculating the critical velocity and he also considers other possible transitions to excited states of the vortex–ion system. The nucleation rate is calculated on the basis of Fermi's golden rule. The step-like increase in the nucleation rate observed in the experiments (see III) is ascribed to the onset of a new set of allowed transitions, corresponding to occupation of the first excited cyclotron level (transitions to excited states involving vortex waves being considered relatively improbable in view of the cylindrical symmetry assumed by the model). The magnitudes of the matrix elements for these processes are then estimated from the experimental data of III.

Note that a numerical discrepancy exists between the potential for nascent rings as calculated by Muirhead *et al.* and by Bowley. This arises from the different approximations used for the structure and energy of the vortex core. In particular, Bowley assumed a hollow core and he explicitly required that the law of conservation of matter was obeyed. Muirhead *et al.*, on the other hand, have used a treatment of the core that is based on solutions of the Ginsburg–Pitaevskii equation by Jones & Roberts (1982).

This, then, concludes our outline description of the two variants of the tunnelling model. Each of the sets of calculations also introduces other novel features which appear to aid comparison with the experimental measurements of III, but we will defer further discussion of the microscopic nucleation mechanism until §6(*e*), after we have seen what additional information can be gained from the study of the ^{3}He effect that forms the main topic of the present paper.

(*b*) *The negative ion in dilute* ^{3}He–^{4}He *solutions*

It has long been known that adding quite small proportions of ^{3}He to He II can greatly increase the propensity of negative ions to create vortex rings. Rayfield (1968) discovered that the maximum observable drift velocity for bare ions (that is the drift velocity above which ring creation occurs in a time that is short compared with the transit time across the cell) in a solution with $x_3 = 1.25 \times 10^{-4}$ was reduced by several metres per second compared to the same quantity in 'pure ^{4}He'. Similar results were also obtained by Neeper & Meyer (1969). (However, in neither case does the ^{4}He seem to have been isotopically purified, so that when these authors mention 'pure ^{4}He' they are probably referring to naturally occurring helium, for which $x_3 \approx 2 \times 10^{-7}$.) Rayfield pointed out that, while the behaviour of the negative ion was markedly altered by the addition of ^{3}He, that of the positive ion remained unchanged. A possible explanation, he suggested, was that the added ^{3}He could lead to modifications in the structure of the negative ion, but not in that of the positive one.

Dahm (1969) proposed that the modifications in question might correspond to the binding of ^{3}He atoms to the surface of the negative ion. Because of its bubble-like structure, the ion presents a free surface quite analogous to that of bulk liquid helium and on which ^{3}He atoms can be trapped in much the same way as that discussed by Andreev (1966) in accounting for the temperature dependence of the surface tension of dilute ^{3}He–^{4}He solutions. The physical origin of the binding arises from the larger zero point energy possessed by a ^{3}He atom, on account of its having a smaller mass than a ^{4}He atom. This energy can be reduced if the ^{3}He

atom moves to a region where the density of the surrounding liquid is relatively small, and it will consequently be attracted to any free surface of the liquid, including that presented by the negative ion. No such considerations apply to the positive ion because, far from being a void, it consists of a region of increased density (and may actually be solid), so that a ^{3}He atom will be repelled rather than attracted. Support for Dahm's suggestion was provided by the experiments of Ketterson *et al.* (1971) and Kuchnir *et al.* (1972), who measured the mobility μ of negative ions in a range of ^{3}He–^{4}He solutions ($7.7\times10^{-5} < x_3 < 3.3\times10^{-3}$) and found clear evidence for a maximum in μ at about 0.4 K, which they attributed to the effect of ^{3}He condensation on the ion. They estimated that the corresponding binding energy was about 2.5 K.

The first direct measurements of ν in dilute ^{3}He–^{4}He solutions ($6.9\times10^{-6} < x_3 < 2.4\times10^{-4}$) were due to Zoll & Schwarz (1973) and Zoll (1976). Consistent with the earlier observations of Rayfield, and Neeper & Meyer, they found that ν was indeed substantially increased by the addition of ^{3}He to natural helium.

In all of the pioneering experiments described above, the possibility that the *ca.* 2×10^{-7} of ^{3}He present in naturally occurring (gas well) helium might be sufficient to affect ν appears to have been overlooked. Yet, as we shall see, even this tiny concentration of ^{3}He can exert a profound influence on the nucleation process, changing ν by an order of magnitude or more. In fact, as discussed in §2(*c*), the *strongest* of the several ^{3}He–^{4}He solutions used in the present experiments, with $x_3 = 1.72\times10^{-7}$, is closely equivalent to what was regarded as 'pure ^{4}He' in that earlier work.

Although, as already indicated, there is good evidence suggesting that the ^{3}He which influences ν is that which is trapped on the outside of the ion, rather than that dissolved in the bulk liquid, the mechanism of the effect has remained a mystery. Dahm made two suggestions. First, he proposed that the condensed ^{3}He would reduce the surface tension and thus cause the ion to expand slightly, which would then be expected to reduce the critical velocity. Such an effect is certainly to be anticipated but, as we shall see, its magnitude would be far too small to account for the extreme sensitivity of ν to tiny values of x_3. Secondly, Dahm suggested that ν might be modified because the presence of even one bound ^{3}He atom would drastically alter the boundary conditions at the surface of the ion. We shall return to consider these ideas, and some other possibilities, in more detail in §6(*e*). For now, we will simply accept as a working hypothesis that the presence of trapped ^{3}He at any given moment increases the probability per unit time that the ion in question will nucleate a vortex ring.

(*c*) *Surface states of* ^{3}He *on the negative ion*

The experimental data to be presented in §3 show that, when ^{3}He is present in the He II, ν varies with temperature T and electric field E in a very much more complicated manner than for the isotopically pure ^{4}He discussed in III. In §§4 and 5 we shall seek to demonstrate that, despite the complexity of $\nu(E, T, x_3)$, almost all of the observed phenomena can be accounted for in terms of two distinct (field-dependent) nucleation rates: one rate characteristic of a bare ion, as has already been discussed in III; and a second rate characteristic of an ion with one trapped ^{3}He atom. We will suggest that the variation of ν with E and T arises in large measure from changes in the average length of time for which a ^{3}He atom remains on the ion, after being trapped, before being re-emitted; and, as already mentioned, we will show in §6(*b*) that the onset of nonlinear effects corresponds to the physical conditions becoming

such that there will be, at any given time, a significant fraction of the ions with two or more trapped ^{3}He atoms. To be able to calculate the average number of bound ^{3}He atoms it is clearly necessary to have detailed information about the ^{3}He surface states in question. In particular, we shall need to know their energies and degeneracies.

Shikin (1973) proposed that bound ^{3}He on the negative ion could be considered as existing in a spherical potential with a hard core. On this basis, the surface states can be characterized by a quantum number l, and have energies

$$\epsilon_l = \epsilon_0 + gl(l+1), \tag{1.1}$$

where

$$g = \hbar^2/2m_s R_s^2, \tag{1.2}$$

the degeneracy of each level is $2(2l+1)$, and l runs from zero up to L, the maximum value for which ϵ_l is negative. Here, ϵ_0 is the depth of the potential well (with a negative absolute value), m_s is the effective mass of the ^{3}He atom in a surface state and R_s is a typical radius for the state, which we may suppose to be greater than the radius R_i of the ion. Shikin was able to demonstrate that the characteristic damping length for the wave-function of the bound state was much smaller than the ionic radius, thereby confirming that the model was self-consistent.

The number n_b of bound ^{3}He atoms on a stationary ion in thermal equilibrium is then given by the usual Fermi sum, so that

$$n_b = \sum_{l=0}^{L} 2(2l+1)\left\{\exp\left(\frac{\epsilon_l - \mu}{k_B T}\right)+1\right\}^{-1}. \tag{1.3}$$

To evaluate n_b we require numerical values of ϵ_0, m_s, and R_s. For any given temperature, the chemical potential, μ, is of course determined by the value of x_3 in the surrounding liquid. No reliable estimates of m_s exist for states on the (spherical) surface of the ion, although Edwards & Saam (1978) have quoted a value of $(1.45\pm0.1)\,m_3$ for ^{3}He states on the (plane) surface of bulk liquid. We may anticipate, however, that m_s for the negative ion at 23 bar† will be larger than this: first because of the increased density of the pressurized liquid; and secondly because the zero point pressure of the trapped electron will cause the ^{3}He atom to lie deeper, on average, in the wall of the ion than it would in a helium surface exposed to a real vacuum. We have therefore made the (somewhat arbitrary) assumption that $m_s = 2.0\,m_3$. Again, it is by no means clear what value we should take for R_s, the radius of the ^{3}He orbit. Noting, however, that the ionic radius at 23 bar (Ellis *et al.* 1983) is 1.15 nm and that the average volume occupied by a ^{3}He atom has a radius of *ca.* 0.15 nm, we have assumed that $R_s = 1.3$ nm. Inserting these values of m_s and R_s into (1.2) we find that $g/k_B \approx 0.024$ K. The well depth ϵ_0 is better known but, once more, most of the calculations refer to the plane surface of bulk liquid. Lekner (1970) showed how to obtain a single-particle Schrödinger equation for the bound states of ^{3}He on both plane and spherical surfaces. His ideas were developed by Saam (1971) and by Chang & Cohen (1973) for plane surfaces, these calculations being reviewed in Edwards & Saam (1978, §11). The theory of Chang & Cohen predicts $\epsilon_0 = -2.353$ K, remarkably close to the value derived from surface tension experiments (Edwards & Saam 1978) of -2.22 ± 0.03 K. No such calculations or experiments have so far been made for the bare surface of the negative ion. To acquire some feeling for the relative magnitudes

† 1 bar $\approx 10^5$ Pa.

PHILOSOPHICAL TRANSACTIONS OF THE ROYAL SOCIETY A MATHEMATICAL, PHYSICAL & ENGINEERING SCIENCES

of the various physical quantities involved, we will take the (zero pressure) plane surface experimental value of -2.22 K, for now (but we will find in §5(*b*) that values of ϵ_0 can in fact be deduced from the experimental data to be presented in §3).

Inserting into (1.1) the numerical values of the constants discussed above we find that the energy level structure for ^{3}He in bound states on the ion should be as shown in figure 2. There are thus ten energy levels to be considered, containing some 200 states in all.

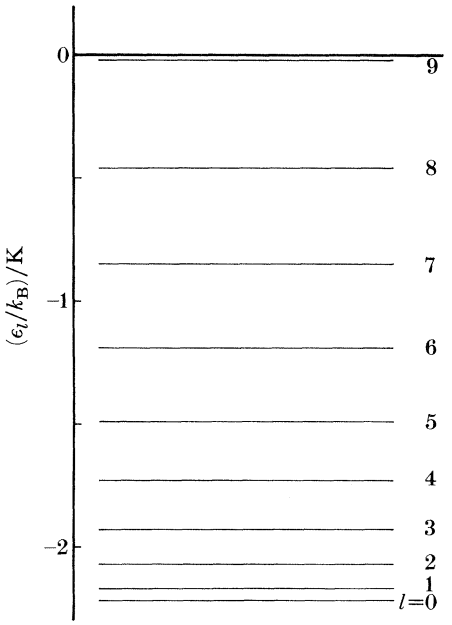

FIGURE 2. Energy levels of the surface states available to a ^{3}He quasiparticle trapped on a stationary negative ion in HeII, according to Shikin (1973) and based on the parameter values discussed in the text.

We must now introduce an important caveat. The discussion so far has centred on the ^{3}He states that exist on a stationary ion, whereas the experiments to be described below refer exclusively to ions which are moving at many tens of metres per second. Fortunately, the resultant departures from Shikin's model are expected to be small. The energy levels will be shifted slightly, owing partly to the inertial mass of the ^{3}He and partly to the existence of a backflow around the moving ion. Furthermore, some of the degeneracy of the states is lifted. States of common l, but different l_z, will be shifted relative to each other by varying amounts.

To estimate the size of the effect, we suppose that the shift $\Delta\epsilon_{l,m}$ in the energy of the bound ^{3}He atom is proportional to the kinetic energy of the fluid that it displaces. Thus, if the ^{3}He atom occupies a volume V_3, then

$$\Delta\epsilon_{l,m} = \int \psi^*_{l,m}(r)\,\frac{\xi\rho_4 V_3 U_B^2}{2}\,\psi_{l,m}(r)\,\mathrm{d}^3r,$$

where ξ is a constant of order unity, U_B is the backflow velocity, m is the usual angular momentum quantum number (such that $l_z = m\hbar$) and ψ is the ^{3}He wave-function specified by l and m. Then, for an ion travelling at velocity U

$$\Delta\epsilon_{l,m} = \frac{\xi\rho_4 V_3 U^2}{4}\int \mathrm{d}^3r\,|\psi_{l,m}(r)|^2\,\frac{R_1^6}{r^6}\{P_0(\cos\theta)+P_2(\cos\theta)\}.$$

The $P_0(\cos\theta)$ term shifts all levels equally and can therefore be accommodated by a redefinition of the binding energy of the ^{3}He. The $P_2(\cos\theta)$ term lifts the degeneracy of the states of different l_z. For example, for $l = 1$, the $l_z = 0$ state is raised in energy by $\xi\rho_4 V_3 U^2 R_1^6 r^{-6}/20$ and the $l_z = \pm\hbar$ states are reduced in energy by half this amount. For $R_1^6 r^{-6} = 1$, $\xi \approx 1$ and $U = 50$ m s^{-1}, this corresponds to a splitting of the levels by *ca.* 0.07 K; and the corresponding shift in all the levels, arising from the $P_0(\cos\theta)$ term, can be estimated at *ca.* 0.045 K. Thus, if the ambient temperature were of order 0.07 K or less, the motion-induced modifications to the energy levels would become noticeable and would need to be taken explicitly into account. For the present experiments, however, all of which were conducted above 0.3 K, the departures from Shikin's energy level structure of figure 2 will be relatively unimportant, provided that we redefine ϵ_0 in such a way as to include the effect of the small velocity-dependent term.

2. Experimental details

The cryogenic arrangements employed in these measurements were essentially the same as those used in I, II and III, and have been described in I. However, the need to maintain and determine accurately the concentration of ^{3}He in each of the dilute solutions has involved the development of a number of novel techniques, which we shall discuss in §2 (*a*). After exploratory measurements of the nucleation rate in dilute solutions had revealed a strong dependence upon temperature below 0.5 K, it was realized that a worthwhile analysis of the effect would require an improvement in the accuracy of temperature determination. To this end we used a calibrated germanium resistor; we shall discuss its use briefly in §2 (*b*).

In §2 (*c*) we shall discuss the validity of our electrostatic induction technique in low electric fields. Previously, the lowest electric field in the drift space was *ca.* 5×10^4 V m^{-1}, whereas our present measurements have involved fields down to *ca.* 10^4 V m^{-1}. The reason for possible doubts about the reliability of the technique in low fields stems from our implicit assumption that an ion which nucleates, and becomes attached to, a vortex ring will instantly stop contributing to the induction current. In high electric fields the vortex rings slow down so quickly that this must indeed be so; in low fields there may, however, be a significant contribution from the current of charged vortex rings, which could lead in turn to an underestimated nucleation rate. We shall attempt to assess the magnitude of this effect.

(*a*) *Measurement and control of the isotopic ratio*

Pressurization of the experimental chamber is effected through use of gas from a pair of standard gas bottles, one of which contains normal commercial ^{4}He ($x_3 \approx 2 \times 10^{-7}$), while the other contains isotopically purified ^{4}He. This nominally pure ^{4}He was the initial product of the continuous-flow purifier described by Ngan *et al.* (1981). It was subsequently found to contain very small residual traces of ^{3}He, but at a level ($x_3 = 1.9 \times 10^{-10}$) which, as we shall see in §3, can be considered negligible as far as the present experiments are concerned. In what follows, therefore, we shall refer to it as pure ^{4}He. (Suspicions that even this minute level of ^{3}He could conceivably affect our nucleation-rate measurements were allayed by comparison with earlier results in a sample for which $x_3 < 10^{-15}$.) Initially, the chamber is pressurized with pure ^{4}He up to the working pressure (usually 23 bar), and then as the measurements progressed, successively stronger ^{3}He concentrations were employed, measurements of $\nu(E, T)$ being repeated for each concentration.

The method by which the concentration is adjusted and controlled was developed from a technique first suggested by Neeper & Meyer (1969), which relies on the 'heat flush' effect in He II. This well known phenomenon occurs whenever He II is subjected to a temperature gradient and results in pure superfluid flowing up the gradient while the normal fluid component, including any impurities that are present, flows down the gradient.

We now consider the length of capillary tubing leading to our experimental chamber. The temperature at the chamber end can be maintained at, say 0.5 K, while the other end of the capillary is thermally anchored to the ^{4}He pot at 1 K, thereby giving rise to a temperature gradient along the capillary. We suppose the chamber (and capillary) to contain a dilute solution of ^{3}He in ^{4}He of isotopic ratio x_3^{i} at a pressure P_{i}. If we reduce the chamber pressure slowly enough, then the heat-flush effect ensures that only pure superfluid will flow from the chamber and out through the capillary, while the normal fluid, containing solute ^{3}He atoms, will remain behind. Next, after the pressure has fallen to some value P_l, we repressurize the chamber with helium of known ^{3}He concentration, x_3^{n}, from our cylinder of natural ^{4}He, the result being that ^{3}He atoms are forced into the chamber. Thus, when we stop repressurizing at a pressure P_{f}, the chamber will contain helium at an increased ^{3}He concentration x_3. It is straightforward (see Appendix C) to demonstrate that this is given by

$$x_3^{\mathrm{f}} = x_3^{\mathrm{i}} \frac{V_{\mathrm{m}}(P_{\mathrm{f}})}{V_{\mathrm{m}}(P_{\mathrm{i}})} + x_3^{\mathrm{n}} \left\{ 1 - \frac{V_{\mathrm{m}}(P_{\mathrm{f}})}{V_{\mathrm{m}}(P_l)} \right\}, \tag{2.1}$$

where V_{m} is the molar volume of liquid ^{4}He at the given pressure.

Values of $V_{\mathrm{m}}(P, T)$ are readily available from a number of sources (we have used the values given by Brooks & Donnelly (1978)); and a sample from our cylinder of natural helium has been analysed by mass spectrometry and found to have an isotopic ratio $x_3^{\mathrm{n}} = 1.64 \times 10^{-7}$. The only other quantity we require is the initial concentration x_3^{i} which, since we pressurize the chamber initially with pure ^{4}He, is zero for the first concentration adjustment.

To ensure the success of this technique some precautions must be observed. First, since the molar volume is a function of T as well as of P, we have taken care to maintain the chamber at *ca.* 0.5 K throughout any concentration adjustments. Secondly, the flow velocity of liquid out through the capillary must not be so high that ^{3}He atoms can get entrained by the flowing turbulent superfluid (in the manner of the operation of a vortex refrigerator) and hence carried towards higher temperatures. Consequently, the cell is depressurized slowly.

Two other precautions must be taken, the need for which is less obvious. We have remarked that a complete set of $\nu(E, T)$ data was recorded at each concentration, with a fixed pressure of 23 bar. Now, this pressure will tend to fluctuate slightly, owing principally to variations in the level of the liquid helium in the main bath and so, to maintain a constant pressure, it is necessary to allow gas to escape from or to enter the top of the capillary. If the tubing leading to the capillary and chamber were left containing natural ^{4}He, then the frequent small adjustments made to maintain a constant pressure would each result in pure ^{4}He leaving the chamber and natural ^{4}He entering, consequently leading to a steady increase of the concentration. Although this effect is small, a significant increase in the concentration could occur over the length of time required to complete the measurements for any given value of x_3. To avoid this potentially large source of error we have adopted the following procedure. After we have reached the final pressure, P_{f}, the chamber is again depressurized to a pressure of *ca.* 10 bar. Although only pure ^{4}He leaves the chamber and capillary, this has the effect of removing any

^{3}He left in the tubes at $T > T_\lambda$. We then repressurize the chamber to P_f with pure ^{4}He so that the tubes and capillary leading to the chamber contain pure ^{4}He. The net effect, of course, is that the chamber concentration is left unchanged.

The other precaution we must take is to ensure that, once the chamber contains a ^{3}He/^{4}He solution, its temperature never exceeds, or even approaches T_λ. If this were allowed to happen then the density anomaly at the λ-point would result in an unpredictable quantity of ^{3}He leaving the chamber. Therefore, the pumped ^{4}He pot had to be maintained at *ca.* 1 K throughout the several weeks of an experimental run.

The values of P_i, P_l, P_f were usually chosen as 23, 2 and 23 bar respectively. The choice of $P_i = P_f = 23$ bar was determined by the fact that this was the pressure we used for most of the nucleation rate measurements, while P_l was chosen to give a suitable concentration change. This gives

$$x_3^f = x_3^i + 0.13\, x_3^n$$

so that each concentration adjustment increases the chamber concentration by $0.13 x_3^n$. In practice, the pressures P_i, P_l, and P_n were not always exactly those quoted, which is the reason for the slight variation (see §3) in the amount by which the concentration increased for each set of $\nu(E, T)$ data.

Assuming that the above techniques are strictly adhered to, we believe that by far the largest source of error in our values at x_3 lies in the determination of x_3^n. Analysis of a sample of our natural helium by mass spectrometry gave $x_3^n = (1.64 \pm 0.05) \times 10^{-7}$, so our quoted values of x_3 are subject to an error of $\pm 3\%$. At the end of each run a sample was taken of the chamber contents and subjected to analysis. Within the accuracy of the analysis we found that, even after as many as eight concentration adjustments, the ^{3}He concentration was identical to that calculated from (2.1), thereby conforming the reliability of the technique.

(*b*) *Thermometry*

In common with the earlier sections of the research programme (I–III), the temperature of the helium sample was measured by means of a carbon resistance thermometer (Speer Carbon Co., nominal 470 Ω), which was glued into a copper jacket soft-soldered to the outside of the sample chamber. Because of the increased importance of the temperature range $0.3 > T > 0.5$ K for the present work, however, compared with that in pure ^{4}He, where ν is almost temperature-independent below 0.5 K, the calibration procedure for the thermometer had to be extended to cover the full range $0.3 > T > 1.0$ K rather than, as previously, simply extrapolating our $T > 0.5$ K ^{3}He vapour pressure calibration downwards in temperature. This was accomplished by comparison of the carbon thermometer with a pre-calibrated germanium resistance thermometer (Lake Shore Cryotronics Inc., model G12-200A-100).

The resistance R_G of the germanium thermometer was determined by means of a d.c. four-terminal technique, the usual precautions being taken to ensure that the measuring current was kept well below the level where self-heating could become a problem, and its polarity being reversed to eliminate the effect of thermal e.m.fs. The resistance R_C of the carbon thermometer was more rapidly and conveniently read by use of a conventional a.c. Wheatstone bridge arrangement. For temperatures in the range $0.3 < T < 1.0$ K, the corresponding resistance ranges were $21708 > R_G > 840$ Ω and *ca.* $8000 > R_C > 2000$ Ω respectively.

The calibration procedure involved obtaining corresponding resistance values for the two thermometers at several temperatures within the range with, where possible, ^{3}He vapour

pressure measurements in addition. The temperatures determined from the germanium resistance and from the ^{3}He vapour pressure invariably agreed within experimental error. Using the germanium derived temperatures we then fitted the empirical relation

$$T^{-1} = A + BR_C + CR_C^{\frac{1}{2}} \tag{2.2}$$

given by Hetzler & Walton (1968) to the resistance values measured for the carbon thermometer. This equation was found to fit at the calibration points, throughout the entire range, to much better than ± 1 mK. Allowing for the errors in the calibration of the germanium thermometer, and for a number of other possible sources of error, we believe that our quoted values of T are accurate to within ± 2 mK.

(c) *Measurement of the nucleation rate in low electric fields*

Our measurements of the vortex nucleation rate rely on the assumption that any ion which nucleates, and becomes attached to, a vortex ring immediately stops contributing to the current induced in the collecting electrode. In high electric fields this is certainly a valid assumption: the bare ions are initially moving with a large drift velocity, whereas a charged vortex ring is subject to an extremely rapid deceleration as soon as it is created.

In our earlier work (III), we restricted our attention to $E \geqslant 5 \times 10^4$ V m^{-1} and no attempt was made to calculate explicitly the effects of the charged-vortex-ring current since we were confident that it would be negligible. For the present measurements, however, we have extended the range of electric fields down to 10^4 V m^{-1}. Although we may still suspect that the vortex current will be negligible, some formal justification for this assumption should now be given. We shall therefore attempt to derive an expression for the errors in our measurements of the nucleation rate resulting from our neglect of the vortex current.

In III it was shown that if we have Q_0 ions at time $t = 0$, then the bare ion current induced in the collector at time t is

$$I_B(t) = \frac{Q_0 \bar{v}}{L} e^{-\nu t}, \tag{2.3}$$

where ν is the vortex nucleation rate, $\bar{v}$ is the average drift velocity of the bare ions, and L is the cell length. We now need to consider the additional contribution to this current due to the charged vortex rings created by the ions. The rate of creation of vortex rings is given by

$$dQ/dt = Q_0 \nu e^{-\nu t} \tag{2.4}$$

so that the number created in the time interval dt' at t' is

$$dQ = Q_0 \nu e^{-\nu t'} dt'. \tag{2.5}$$

At a time $t > t'$, these vortex rings will be moving with a velocity $v_r(t-t')$, and the induced current due to vortex rings will be

$$I_r(t) = \int_0^t \frac{Q_0 v_r(t-t')}{L} e^{-\nu t'} \nu \, dt'. \tag{2.6}$$

The total current is therefore

$$I(t) = I_B(t) + I_r(t) = \frac{Q_0 \bar{v}}{L} e^{-\nu t} \left\{ 1 + e^{\nu t} \int_0^t e^{-\nu t'} \nu \, dt' \frac{v_r(t-t')}{\bar{v}} \right\}. \tag{2.7}$$

It can be shown (see Appendix D) that the second term in the curly brackets leads to the measurement of an apparent nucleation rate ν_a which, to a good approximation, is related to the real nucleation rate by

$$\frac{\nu-\nu_a}{\nu} = 0.0067\left(\frac{\nu}{E}\right)^{\frac{1}{2}}\{4.0+0.5\ln(1+1330Et)\} \tag{2.8}$$

where ν and ν_a are in s^{-1}, E is in V m^{-1} and t is in s. Noting that the ions take typically 10^{-4} s to cross the induction space we find that, for the range of E where we have analysed data ($2\times10^4 < E < 2\times10^5$ V m^{-1}), the experimental measurement of ν_a underestimates ν by a fraction that is always less than 3%, and so we are justified in neglecting the difference. Consequently, in the data reduction leading to the values of ν presented in §3, we have ignored all effects arising from the vortex current.

3. Experimental results

In this section we present a representative selection of the experimental results, and we comment upon them briefly; detailed quantitative analyses of the data, and a discussion of their physical significance, are reserved for §§4–6.

As has already been reported in III, ν is strongly dependent upon each of the four parameters P, E, T and x_3. Unlike that earlier part of the research programme, however, where we held x_3 fixed at zero, in the present work we have, as indicated above, allowed x_3 to vary up to a value approximately equal to that found in naturally occurring helium. The volume of the resultant parameter space is, of course, so huge that it would have been impracticable to attempt a systematic study with a series of equally spaced measurements taking in all of the different permutations of the four variables. For the research to have been completed within a finite period, such measurements would have had to have been too widely spaced in any given variable to reveal in sufficient detail the interesting behaviour that we will describe below. Rather, we have fixed three variables at a time, and then investigated in fine detail the variation of ν with the fourth one; and we have done so for fairly widely spaced triads of fixed variables, while concentrating on those regions of the parameter space which appeared on the basis of preliminary measurements to be potentially the most interesting. In most cases we have either made measurements of $\nu(E)$ for fixed x_3, P, T (which we shall refer to as 'field scans') or we have measured $\nu(T)$ for fixed x_3, P, E ('temperature scans').

Most of the data refer to $P = 23$ bar. We will find that, although the absolute value of ν varies rapidly with P, just as in pure ^{4}He (see III), the variations of ν with E and T are apparently very similar in form at all pressures for which data could be recorded. Measurements were made at $P = 23$ bar, for the same set of values of E and T, in nominally pure ^{4}He and in each of eight different ultra-dilute ^{3}He–^{4}He solutions spanning the range $2.14\times10^{-8} < x_3 < 1.72\times10^{-7}$.

The data to be reported below are presented exactly as measured: no adjustments have been made (see III) to allow for the finite rise time of the collector circuit or for non-idealities in the electrode structure. As we shall see, the analysis of §5 is based on the measured *variation* of ν with x_3, rather than on absolute values, so such corrections (in any case, very small) would serve no useful purpose.

The precision of the measurements varied widely with physical conditions. It can best be

judged from the extent to which individual points deviate from imaginary smooth curves drawn through them on the graphs that follow. The signal magnitude fell with increasing x_3, probably owing to the increased production of charged vortex rings in the emission region. In general, the quality of the data is at its best for the higher electric fields and higher pressures, for temperatures towards the middle of our range $0.3 < T < 0.8$ K. It deteriorates markedly for very low electric fields and in the limits of high and low temperatures, where the signals became very weak, and under conditions such that ν itself lay much outside the range $10^3 < \nu < 2 \times 10^4\ \mathrm{s}^{-1}$.

The individual measurements of ν (*ca.* 3500 in all) that constitute the main body of the data were made in the course of three separate experimental runs starting from room temperature, spread over a period of several months. In the course of each of these, a new series of ^{3}He–^{4}He solutions was prepared by progressive addition of ^{3}He, as described in §2(*c*), and the carbon resistance thermometer was recalibrated (§2(*b*)). On each occasion, some measurements of ν were repeated and carefully compared with data acquired during earlier runs under what were believed to be identical conditions. One example of such a comparison is shown in figure 3. The close agreement of the two sets of $\nu(E)$ data represents reassuring evidence

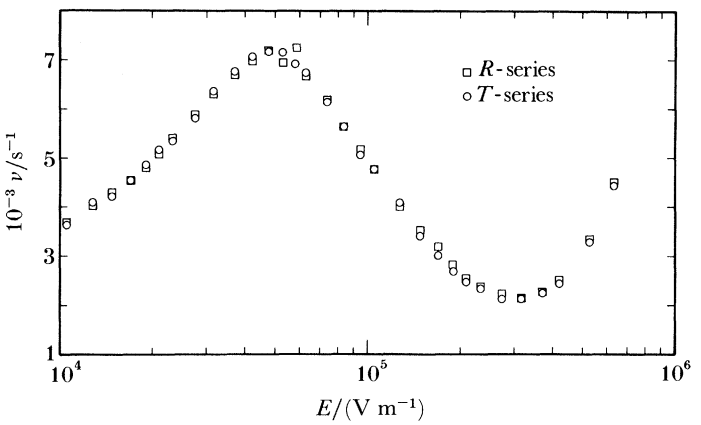

FIGURE 3. A comparison of experimental measurements made during two separate experimental runs (*R*-series data of November 1982, *T*-series data of February 1983; $P = 23$ bar, $x_3 = 1.72 \times 10^{-7}$), demonstrating the reproducibility of the thermometry and of the novel technique (§2(*c*)) developed for adjusting the ^{3}He concentration.

that the thermometry and ^{3}He concentration control are both consistent, within experimental error, from one experimental run to the next since, as reported below, the absolute magnitude of the peak in $\nu(E)$ provides an indication of x_3, and its position gives a measure of T. For the data in figure 3, both of the ^{3}He–^{4}He solutions had been prepared by means of eight separate repressurizations of the cell; and the gratifyingly good agreement obtained demonstrates convincingly the efficacy and precision of the novel techniques for the adjustment of x_3 described in §2(*c*).

The effect on ν of changing the electric field is shown in figure 4. Plots of $\nu(E)$ are given in parts (*a*)–(*d*) for four different values of x_3 and, in each case, the data correspond to several different fixed values of T. Although the points are rather scattered in figure 4(*a*), owing to the relatively small values of ν that are being measured in the most dilute sample

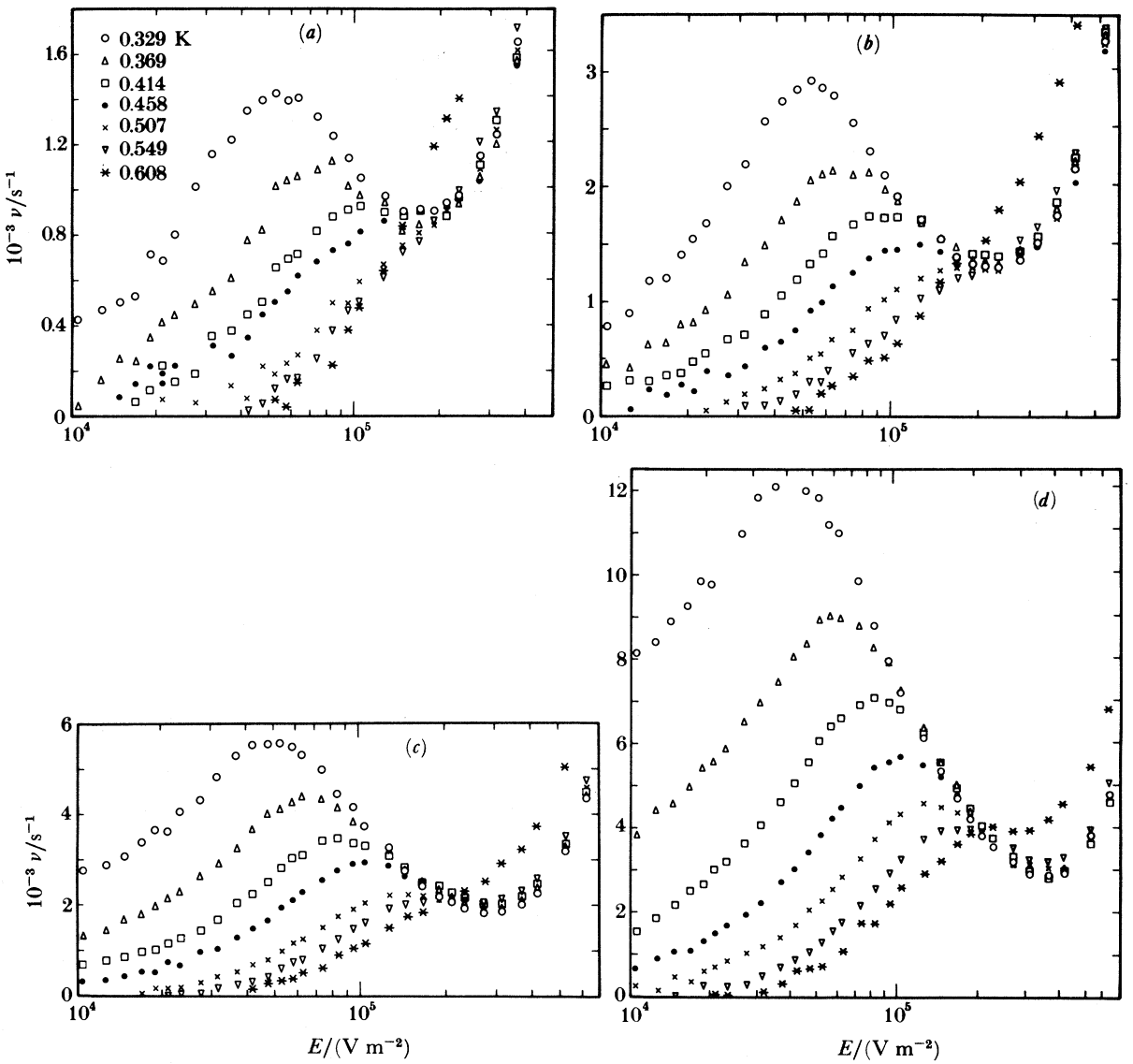

FIGURE 4. Measurements of the nucleation rate ν as a function of electric field E for several different temperatures at 23 bar. A complete set of data is plotted for each of four selected ^{3}He/^{4}He ratios; (*a*) $x_3 = 2.14 \times 10^{-8}$; (*b*) 4.29×10^{-8}; (*c*) 8.58×10^{-8}; (*d*) 1.72×10^{-7}. The key to the symbols given in (*a*) applies equally to (*b*)–(*d*).

($x_3 = 2.14 \times 10^{-8}$), the general form of $\nu(E)$ is clearly very similar for all concentrations. The absolute magnitude of ν changes markedly, however, and the ordinate scales have been adjusted accordingly. For $E \gtrsim 2 \times 10^5$ V m^{-1}, ν is virtually temperature-independent except at the highest temperatures. The temperature-dependent peak in $\nu(E)$ that appears at lower values of E is a feature of particular interest, which was entirely absent in the case of the pure ^{4}He measurements reported in III, and is therefore attributable to the presence of ^{3}He. On the high-E sides of the maxima, the curves traced out by the data at different temperatures coalesce to form an almost temperature-independent envelope, whereas, at low E they remain well separated down to the lowest fields for which reliable measurements could be made. We may infer that the departure of the starred curve at 0.608 K from the other data above 2×10^5 V m^{-1}

occurs in each case because the roton-driven nucleation process described in III has then become important.

In figure 5 (*a*)–(*d*) we plot $\nu(E)$ at each of the eight values of x_3, and for pure ^{4}He, for four selected values of T. It can be seen immediately, first, that the position of the peak is apparently independent of x_3 (provided that due allowance is made for the increasing relative importance

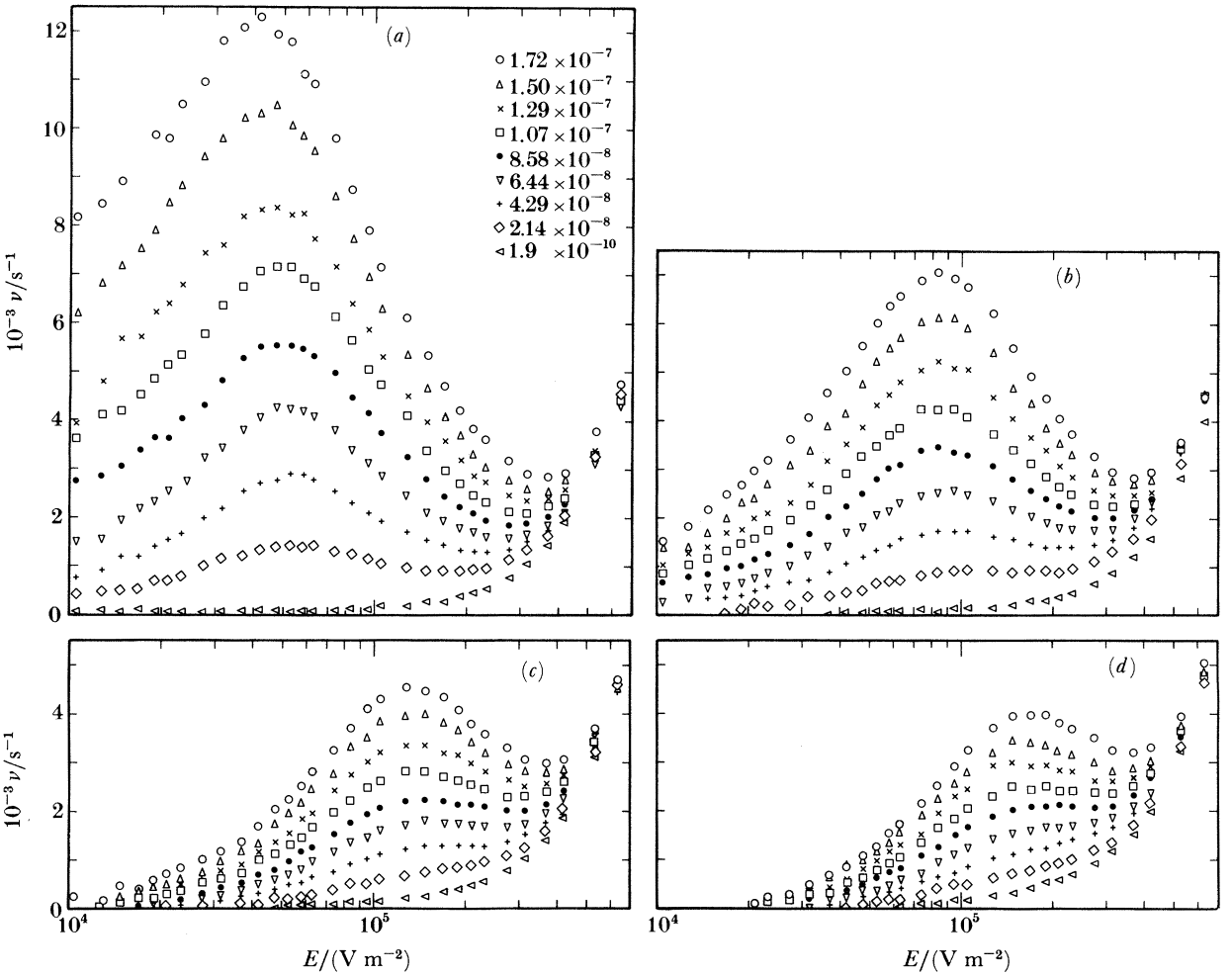

FIGURE 5. Measurements of the nucleation rate ν as a function of electric field E for eight different ^{3}He/^{4}He ratios, and for nominally pure ^{4}He, at 23 bar. A complete set of data is plotted for each of four selected temperatures: (*a*) $T = 0.329$ K; (*b*) 0.414 K; (*c*) 0.507 K; (*d*) 0.549 K. The key to the symbols given in (*a*) applies equally to (*b*)–(*d*).

at the higher temperatures of the intrinsic, pure ^{4}He, nucleation process of III, which, in figure 5 (*d*), can be seen to push the peak slightly towards lower values of E as x_3 decreases and, finally, to eliminate the peak entirely). Secondly, all of the curves appear to tend towards that for pure ^{4}He at high enough E, regardless of the values at which T or x_3 are being held.

Figure 6 (*a*)–(*d*) plots the temperature dependence of ν for four selected values of x_3; T^{-1} is chosen for the abscissa, rather than T, to facilitate comparison with the corresponding pure ^{4}He data of III. For clarity, data are plotted for only four selected electric fields in each part

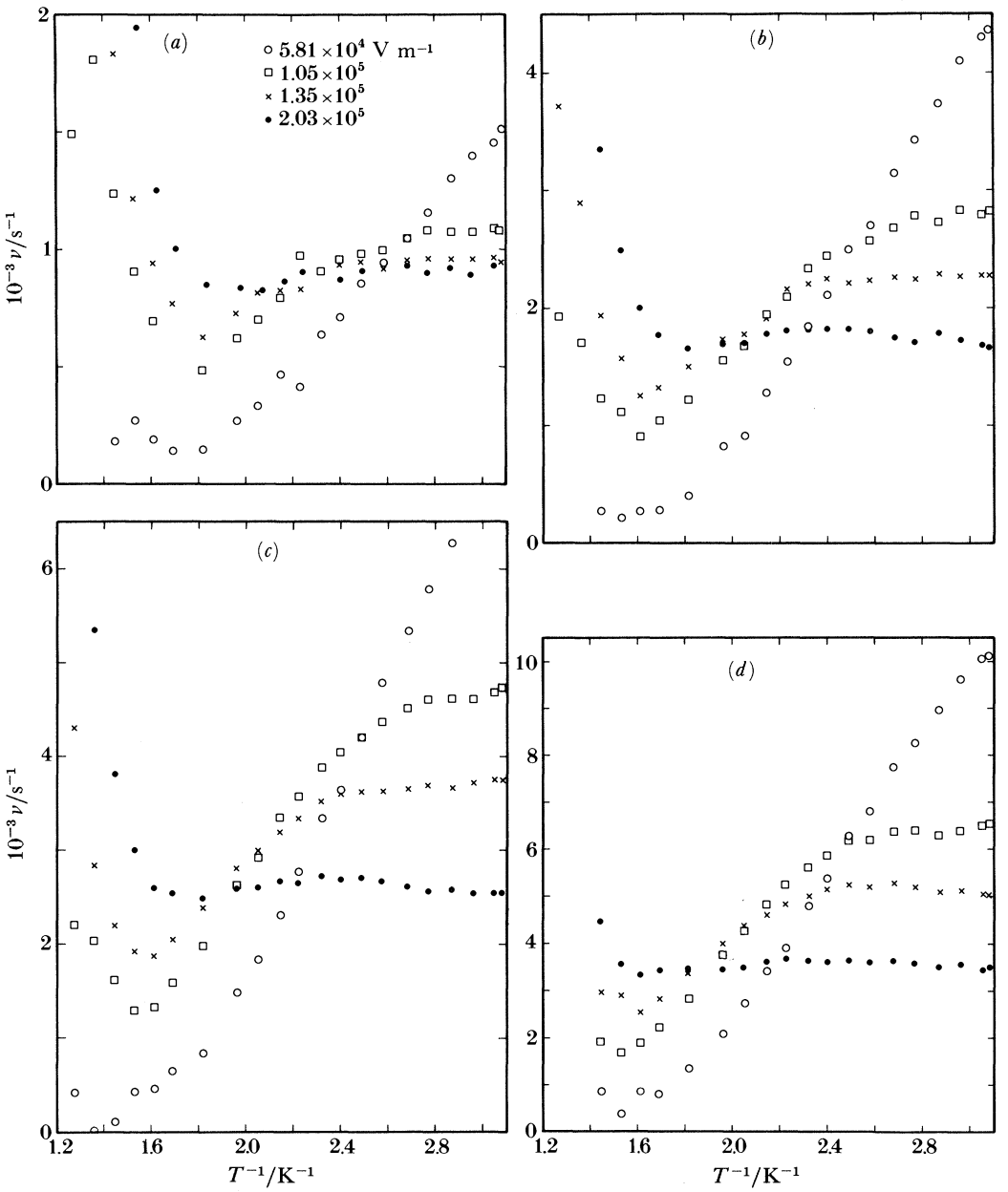

FIGURE 6. Measurements of the nucleation rate ν as a function of reciprocal temperature T^{-1} for four different electric fields at 23 bar. A complete set of data is plotted for each of four selected ^{3}He/^{4}He ratios: (*a*) $x_3 = 2.14 \times 10^{-8}$; (*b*) 6.44×10^{-8}; (*c*) 1.07×10^{-7}; (*d*) 1.50×10^{-7}. The key to the symbols given in (*a*) applies equally to (*b*)–(*d*).

of the figure. As usual, the results for the weakest solution (shown in figure 6 (*a*)) are rather scattered; but it is evident that the general form of the curve is the same for all concentrations. There are large changes, however, in the absolute magnitude of ν, and these are accommodated by making appropriate adjustments to the ordinate scales. All of the curves seem likely to become almost temperature-independent for large enough values of T^{-1}, to pass through a minimum whose position is dependent on E, and to rise again with decreasing T^{-1} at high enough temperatures. The postulated rise in ν could not be observed unambiguously for

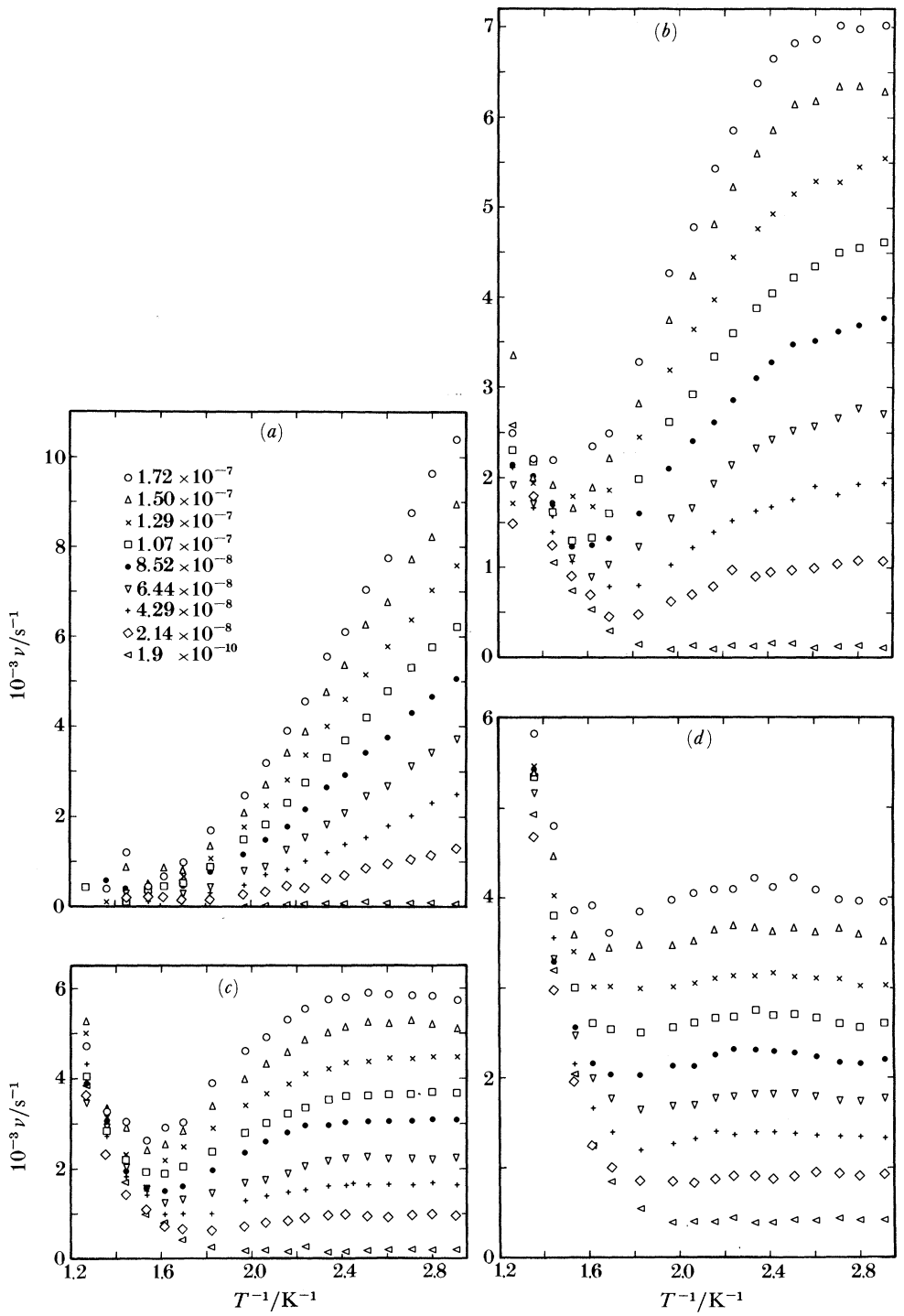

FIGURE 7. Measurements of the nucleation rate ν as a function of reciprocal temperature T^{-1} for eight ^{3}He/^{4}He ratios, and for nominally pure ^{4}He, at 23 bar. A complete set of data is plotted for each of four selected electric fields: (*a*) $E = 5.81 \times 10^4$ V m^{-1}; (*b*) 1.05×10^5 V m^{-1}; (*c*) 1.35×10^5 V m^{-1}; (*d*) 2.03×10^5 V m^{-1}. The key to the symbols given in (*a*) applies equally to (*b*)–(*d*).

PHILOSOPHICAL TRANSACTIONS OF THE ROYAL SOCIETY A MATHEMATICAL, PHYSICAL & ENGINEERING SCIENCES

$E = 5.81 \times 10^4$ V m^{-1}, however, because the signal became too small; and neither could the expected temperature-independent régime be reached, because it lay beyond the (0.3 K) capabilities of the cryostat. The almost temperature-independent sections of the curves at large T^{-1} in figure 6 correspond, of course, to the almost temperature-independent envelope on the high-E side of the maxima in $\nu(E)$ plotted in figure 4.

The variation of ν with T^{-1} is plotted in figure 7 (a)–(d) for four selected values of E, in each case for all eight of the ^{3}He–^{4}He solutions and also for pure ^{4}He. An interesting observation in (c) and (d) is that the plateau regions at large T^{-1} appear, in fact, to be slightly temperature-dependent. The effect is admittedly not very large but, looking at the several curves in figure 7 (d), and particularly at those for intermediate x_3 where measurement conditions were optimal, there seems little doubt that ν is decreasing slightly with falling temperature for low enough temperatures. We shall see in §4 that such an effect is actually to be anticipated because of an expected temperature dependence of the ^{3}He absorption rate by the moving ion.

A cursory inspection of figures 5 and 7 might appear to suggest that the ^{3}He-driven contribution to the nucleation rate (that is, the difference between ν in the ^{3}He–^{4}He solution and the value it would have in pure ^{4}He under the same conditions) was a linear function of x_3. To test this hypothesis, we plot ν directly against x_3 in figure 8 (a) and (b) for two different

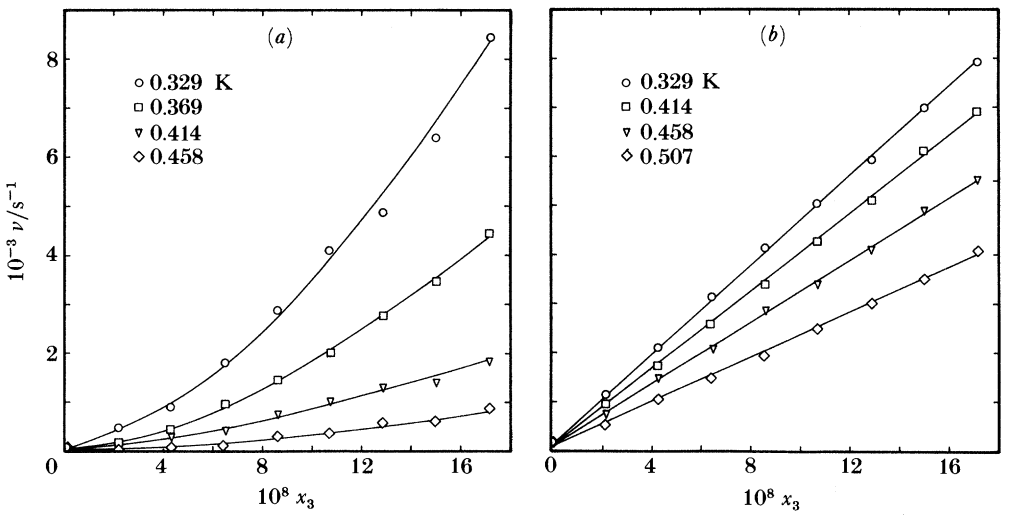

FIGURE 8. Measurements of the nucleation rate ν as a function of the ^{3}He/^{4}He ratio x_3 for various temperatures at 23 bar and two electric fields: (a) $E = 1.27 \times 10^4$ V m^{-1}; (b) 9.5×10^4 V m^{-1}. The full curves in each case are guides to the eye.

values of E. The data in each part of the figure correspond to the same four values of T, and the full curves are merely guides to the eye. It will be noted that, whereas the data of figure 8 (b) are linear in x_3 within experimental error, those of figure 8 (a), for a smaller electric field, definitely curve *upwards* with increasing x_3. Thus, contrary to what one might at first have anticipated, the isotope effect in weak E does not saturate within our present experimental range of x_3 but, rather, varies in the opposite direction such that a given small change in x_3 has an *increasingly* potent effect on ν as more ^{3}He is added. These nonlinearities are at their most evident for small values of T and E. For larger T and E, in fact throughout most of the parameter space studied in these experiments, plots of $\nu(x_3)$ look more like figure 8 (b) than 8 (a).

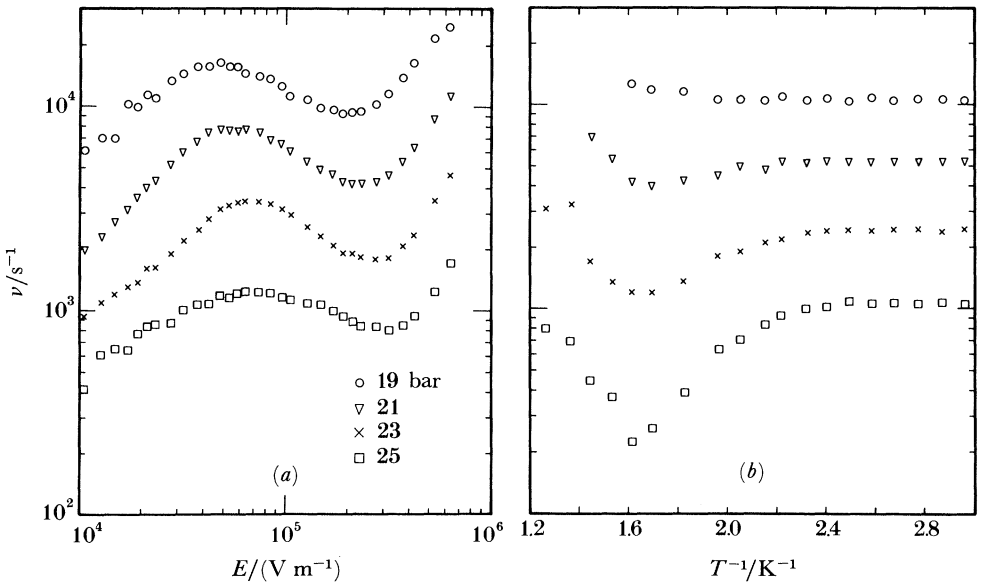

FIGURE 9. Measurements of the nucleation rate ν for a number of pressures, as indicated. There is little qualitative difference between the shapes of the various curves. In (*a*) ν is plotted against electric field E for a temperature $T = 0.369$ K, and in (*b*) ν is plotted against reciprocal temperature for $E = 1.35 \times 10^5$ V m^{-1}. In each case, the ^{3}He/^{4}He ratio $x_3 = 6.44 \times 10^{-8}$.

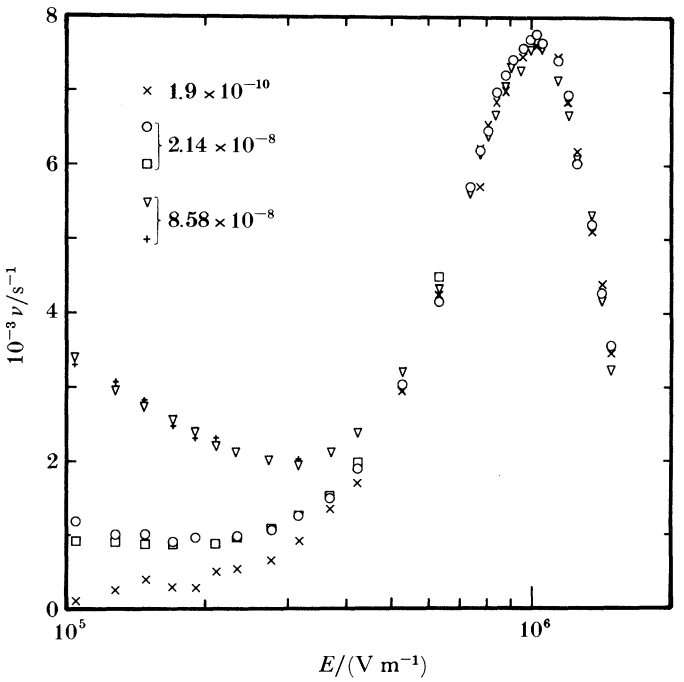

FIGURE 10. Measurements of the nucleation rate ν as a function of electric field E up to a very large E. The data shown are for two ^{3}He/^{4}He ratios x_3, as indicated, and for nominally pure ^{4}He. The circles and triangles refer to data taken in a cell shortened to increase the maximum attainable value of E; and the pluses and squares refer to data acquired in the same cell as was used for all of the other measurements presented in this paper.

In addition to the main body of experimental data at $P = 23$ bar, we have also made a few measurements at 19, 21 and 25 bar. Some of the results are plotted in figure 9 (*a*) and (*b*). We have concluded that there are no obvious qualitative differences between the $\nu(E, T)$ data at different pressures. There are, however, some interesting quantitative changes as P is varied. In particular, the position of the peak in $\nu(E)$ is, weakly but definitely, dependent on P, moving to lower values of E as P is decreased.

Finally, to complete the data set, we reduced the length of the induction space from a nominal 5 mm to a nominal 3 mm, thereby raising the maximum attainable electric field in which ν could be measured to *ca.* 1.5×10^6 V m^{-1}. In doing so we wished, in particular, to ascertain whether or not ν remained independent of x_3 in the region of the high-field maximum (see III) in $\nu(E)$. That this was indeed found to be so is demonstrated by the small sample of high-field data plotted in figure 10. It is reassuring to note, also, the excellent agreement between values of $\nu(E)$ measured in the shorter cell (circles and triangles) with those previously measured in the longer one (squares and crosses).

4. Theory of the linear régime

Having presented the experimental results, we are now in a position to propose a model which, we shall find, is capable of explaining the principal features of the data in quantitative detail. As discussed in §1 (*c*), we proceed on the assumption that the ^{3}He impurities condense on the free surface provided by the negative ion, and that this in some way has the effect of increasing the propensity of an ion to nucleate a vortex ring. We assume, therefore, that there exists a nucleation rate, $\nu_1(E, T, P)$ appropriate to an ion with a bound ^{3}He atom that is larger than the rate $\nu_0(E, T, P)$ for a bare ion. (It is perhaps easier to think of ν_1 as the nucleation rate which would be observed for a group of ions, each of which has one bound ^{3}He atom.) We will suppose (for now) that the ^{3}He concentration, x_3, is such that the average number of bound ^{3}He atoms, n_b, is far less than unity ($n_b \ll 1$). Then we can also interpret n_b as being the probability of finding a bound ^{3}He atom on any one ion and it is then clear that the measured nucleation rate can be expressed as:

$$\nu = (1-n_b)\,\nu_0 + n_b\,\nu_1 = \nu_0 + n_b(\nu_1 - \nu_0) \tag{4.1}$$

or

$$\Delta\nu = \nu - \nu_0 = n_b(\nu_1 - \nu_0). \tag{4.1a}$$

The quantity $\Delta\nu$ represents the additional nucleation rate due to the presence of ^{3}He. In recording the data, great care was taken to ensure that direct comparison between ν and ν_0 was possible by recording $\nu(E, T)$ in pure ^{4}He and in dilute solutions of ^{3}He in ^{4}He under otherwise identical conditions. Some typical graphs of $\Delta\nu(E)$ are presented in figure 11 (*a*) and (*b*) for a variety of temperatures and x_3 values. It should be noted that, while there is some additional scatter in this data (due to the addition of random errors), they should be free from any additive systematic errors in ν (see III), which would have cancelled out in the subtraction.

We shall discuss these data qualitatively in terms of a model to be outlined in §4 (*a*). In §§4 (*b*)–(*e*) we shall develop this model quantitatively; and a detailed comparison with the experimental data is given in §5.

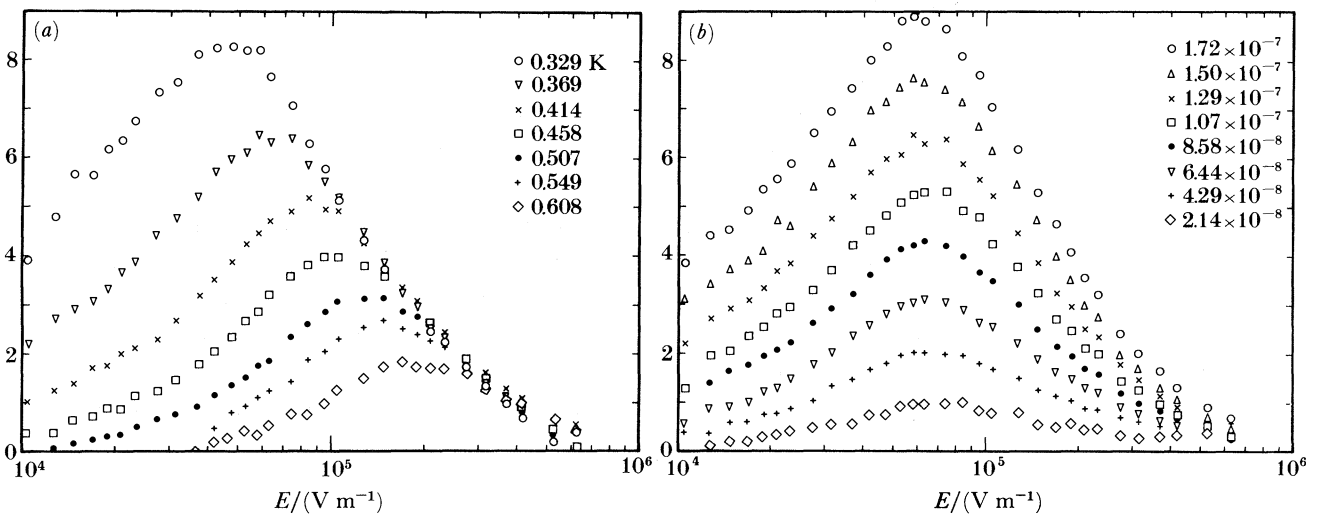

FIGURE 11. The difference $\Delta\nu$ between the nucleation rate measured in a ^{3}He–^{4}He solution, and that measured in isotopically pure ^{4}He under otherwise identical physical conditions, plotted as a function of electric field E: (*a*) for several different temperatures, with $x_3 = 1.29 \times 10^{-7}$; and (*b*) for several different values of x_3, with $T = 0.369$ K.

(*a*) *Outline of the model*

To understand our data we shall need to find expressions for n_b and ν_1. For ν_1 this is difficult since the microscopic mechanism underlying vortex nucleation (§1 (*a*)) is poorly understood even for bare ions, let alone ions with bound ^{3}He. Although we may guess that the form of $\nu_1(E)$ is similar to that of $\nu_0(E)$, we will find that the best approach is to leave ν_1 as an adjustable parameter which we can determine by fitting to the data. This leaves us with the task of determining $n_b(E, T)$, which can be done by considering the rates of absorption and desorption of ^{3}He atoms on to or from an ion. We propose that there are two main processes involved:

1. The absorption of a ^{3}He atom by a negative ion, the binding energy (*ca.* 2 K) being given off as one or more phonons; and the inverse process whereby the absorption of one or more phonons gives rise to the desorption of a bound ^{3}He atom.

2. The emission of a bound ^{3}He atom from the ion together with a pair of rotons, the scarcity of thermal rotons at the temperatures under consideration rendering the inverse process negligible.

That the first process should occur seems only reasonable considering the energies (see §1 (*c*)) involved; the second process requires further consideration.

Originally we attempted to understand the data exclusively on the basis of process 1, but soon found that this approach was untenable: a further emission process was needed to explain the fall in $\Delta\nu$ (figure 11) in high electric fields. It could, of course, be argued that this effect is due to a fall in ν_1 similar to that found for ν_0 in very high electric fields (see III and Nancolas & McClintock 1982). To fit the data, however, the fall in ν_1 would have to occur in a very much lower field than for ν_0. Also, the peak in $\Delta\nu$ is dependent on temperature, which implies that ν_1 would have to be dependent on temperature, whereas, for $T \lesssim 0.5$ K, ν_0 is independent of temperature.

We have concluded that, even if a suitable form of $\nu_1(E, T)$ could be found to fit the data

without recourse to an additional emission process, its use would still be difficult to justify on physical grounds. On the other hand, we believe that we can offer some justification for the inclusion of process 2 even though it inevitably remains somewhat speculative. It has been well established (I) that an ion, travelling at a mean velocity in excess of the Landau velocity, can dissipate energy via the emission of a pair of rotons; and it is not inconceivable, therefore, that this process could sometimes have the effect of dislodging a bound ^{3}He atom. As in the case of ordinary roton-pair emission we expect that there will be a critical velocity for this process due to the need for energy conservation, and that this is bound to be higher than v' (see I). We would therefore expect that the rate at which process 2 occurs increases rapidly with electric field. Before attempting to develop our model further, let us see if we can, on the basis of the discussion so far, offer a qualitative explanation of our results.

In low fields few ions will travel fast enough to undergo process 2 and so the number of bound ^{3}He atoms will depend largely on absorption and desorption via the first process. In this régime n_b will be strongly temperature dependent and, in agreement with our results (figure 11), we would expect $\Delta\nu$ to fall with increasing T. The field dependence of $\Delta\nu$ can, of course, be understood in terms of the field dependence of ν_1.

In higher fields the emission of ^{3}He atoms via the second process will start to dominate. Since this process is independent of temperature we would expect $\Delta\nu$ to become independent of temperature, as is indeed observed. We would also expect to see $\Delta\nu$ fall to zero once E is large enough for ^{3}He atoms to be stripped from the ions almost immediately after absorption and, again, this is exactly what we observe.

Apparently then, our model is at least capable of providing a qualitative explanation of the experimental data and so we shall now attempt to develop it in quantitative detail. We shall start by analysing process 1 to determine the way in which the number of bound ^{3}He atoms varies with temperature in low electric fields. We will find it necessary to introduce a temperature-dependent absorption cross-section, which we shall discuss in §4 (*c*). In §4 (*d*) we shall analyse process 2 and obtain a general formula for n_b which can be applied over the whole range of fields under consideration. Finally, in §4 (*e*) we shall generalize this model to take into account the likelihood (see §1 (*c*)) that there are a number of excited states for a ^{3}He atom on the ion.

(*b*) *Process* 1: '*thermal equilibrium*'

To simplify matters we suppose that only one phonon is emitted when a ^{3}He atom is absorbed. For this to occur there must be an interaction of the form

$$\hat{V}_1 = \sum_{\boldsymbol{p}} \sum_{\boldsymbol{q}} \sum_{\boldsymbol{k},\sigma} T^{\boldsymbol{p}}_{\boldsymbol{k},\boldsymbol{q}}\, \hat{a}^\dagger_{\boldsymbol{p}+\boldsymbol{k}-\boldsymbol{q}}\, \hat{b}^\dagger_{\boldsymbol{q}}\, \hat{d}^\dagger_\sigma\, \hat{c}_{\boldsymbol{k},\sigma}\, \hat{a}_{\boldsymbol{p}} + \text{hermitian conjugate}. \tag{4.2}$$

Here $\hat{c}^\dagger_{\boldsymbol{k},\sigma}$ is the creation operator for a ^{3}He quasiparticle of momentum $\hbar\boldsymbol{k}$ and spin $\boldsymbol{\sigma}$ and $\hat{d}^\dagger_\sigma$ is the creation operator of the bound state of the ^{3}He on the ion. We assume here that there is only one such state. The results we obtain can readily be generalized for the case where there are many such bound states; and we do so in §4 (*e*). The operator $\hat{b}^\dagger_{\boldsymbol{q}}$ creates a phonon of momentum $\hbar\boldsymbol{q}$ and energy $E_{\boldsymbol{q}}$. The operator $\hat{a}^\dagger_{\boldsymbol{p}}$ creates the ion in a state of momentum $\hbar\boldsymbol{p} = m_i\boldsymbol{v}$.

The rate of absorption of ^{3}He by the ion is given by Fermi's golden rule:

$$r_a = \frac{2\pi}{\hbar} \sum_{\boldsymbol{k},\sigma} \sum_{\boldsymbol{p}} \sum_{\boldsymbol{q}} |\, T^{\boldsymbol{p}}_{\boldsymbol{k},\boldsymbol{q}}|^2\, f(\boldsymbol{v})\, n_{\boldsymbol{k}}(1+f_{\boldsymbol{q}})\,(1-n_0)\,\delta\left\{\epsilon_{\boldsymbol{k}} + \frac{\hbar^2 p^2}{2m_i} - \frac{\hbar^2(\boldsymbol{p}+\boldsymbol{k}-\boldsymbol{q})^2}{2m_i'} - E_{\boldsymbol{q}} - E_b\right\}. \tag{4.3}$$

PHILOSOPHICAL TRANSACTIONS OF THE ROYAL SOCIETY A MATHEMATICAL, PHYSICAL & ENGINEERING SCIENCES

Here, the energies ϵ_k and E_b are the energies of the ^{3}He quasiparticle and of the bound states, m_i' is the effective mass of the ion with one bound ^{3}He atom, and the distribution functions $f(\boldsymbol{v})$, f_q, n_k and n_0 refer to the ion, the phonon, the ^{3}He quasiparticle and the bound state, respectively. Thus

$$n_k = \exp\{\beta(\epsilon_k - \mu) + 1\}^{-1} \tag{4.4}$$

where $\beta = 1/k_B T$. The chemical potential

$$\mu = -k_B T \ln\left\{\frac{2}{n_3}\left(\frac{m_3^* k_B T}{2\pi\hbar^2}\right)^{\frac{3}{2}}\right\} \tag{4.5}$$

where n_3 is the ^{3}He number density and m_3^* ($\approx 2.8 m_3$) is the ^{3}He effective mass (i.e. $\epsilon_k = \hbar^2 k^2/2m_3^*$).

The distribution function of the phonons

$$f_q = \{\exp(\beta E_q) - 1\}^{-1} \tag{4.6}$$

and the distribution function of the ionic velocities $f(\boldsymbol{v})$ have already been calculated by Bowley & Sheard (1977) as a function of the electric field.

The quantity n_0 is the occupancy of the bound state, and for a given ion it can be zero or one at any given time. We are interested in the average rate of absorption of ^{3}He by the ion. This average can be the time average for a single ion or the average over an ensemble of ions: in the steady state the two averages are, of course, equivalent. We replace n_0 by n_b, the average occupancy of the bound state, to obtain the average absorption rate, $\bar{r}_a$,

$$\bar{r}_a = \frac{2\pi}{\hbar}\sum_{k,\sigma}\sum_{p}\sum_{q} |T^{p}_{k,q}|^2 f(\boldsymbol{v})\, n_k(1+f_q)\,(1-n_b)\,\delta\left\{\epsilon_k + \frac{\hbar^2 p^2}{2m_i} - \frac{\hbar^2(\boldsymbol{p}+\boldsymbol{k}-\boldsymbol{q})^2}{2m_i'} - E_q - E_b\right\}.$$

Now let us examine the desorption of ^{3}He atoms via the inverse process. This occurs at an average rate

$$\bar{r}_e = \frac{2\pi}{\hbar}\sum_{k,\sigma}\sum_{p}\sum_{q} |T^{p}_{k,q}|^2 f_b(\boldsymbol{v}_3')\,(1-n_k)\, f_q\, n_b\,\delta\left\{\epsilon_k + \frac{\hbar^2 p^2}{2m_i} - \frac{\hbar^2(\boldsymbol{p}+\boldsymbol{k}-\boldsymbol{q})^2}{2m_i'} - E_q - E_b\right\} \tag{4.7}$$

where $f_b(\boldsymbol{v}_3')$ is the distribution function for ions with a bound ^{3}He atom and

$$\boldsymbol{v}_3' = (\boldsymbol{p}+\boldsymbol{k}-\boldsymbol{q})/m_i'. \tag{4.8}$$

Both n_k and f_q are equilibrium distribution functions at the same temperature. We can write

$$f_q = (1+f_q)\exp(-\beta E_q) \tag{4.9a}$$

$$1 - n_k = n_k \exp\{\beta(\epsilon_k - \mu)\}. \tag{4.9b}$$

This enables us to rewrite equation (4.7) as

$$\bar{r}_e = \frac{2\pi}{\hbar}\sum_{k,\sigma}\sum_{p}\sum_{q} |T^{p}_{k,q}|^2 f_b(\boldsymbol{v}_3')\, n_k(1+f_q)\, n_b \exp\{\beta(\epsilon_k - \mu - E_q)\}$$
$$\times\,\delta\left\{\epsilon_k + \frac{\hbar^2 p^2}{2m_i} - \frac{\hbar^2(\boldsymbol{p}+\boldsymbol{k}-\boldsymbol{q})}{2m_i'} - E_q - E_b\right\}. \tag{4.10}$$

We can now obtain the *net* rate of absorption of ^{3}He by the ion, $\bar{R}_a$:

$$\left.\begin{aligned}\bar{R}_a &= \bar{r}_a - \bar{r}_e \\ &= \frac{2\pi}{\hbar}\sum_{k,\sigma}\sum_{p}\sum_{q} |\, T^{p}_{k,q}\,|^2 f(v)\, n_k(1+f_q) \\ &\quad\times[1-n_b-n_b\exp\{\beta(\epsilon_k-\mu-E_q)\}f_b(v_3')/f(v)] \\ &\quad\times\delta\left\{\epsilon_k+\frac{\hbar^2p^2}{2m_i}-\frac{\hbar^2(\boldsymbol{p}+\boldsymbol{k}-\boldsymbol{q})^2}{2m_i'}-E_q-E_b\right\}.\end{aligned}\right\} \tag{4.11}$$

If we were considering a massive ion ($m_i \to \infty$) which was stationary, then this expression would simplify considerably: the factor in square brackets would become

$$[1-n_b-n_b\exp\{\beta(E_b-\mu)\}].$$

When $\bar{R}_a = 0$ one would find that n_b was given by the formula

$$n_b = [\exp\{\beta(E_b-\mu)\}+1]^{-1}, \tag{4.12}$$

indicating that the system was in thermal equilibrium. In our case, however, we need to consider an ion moving with a velocity of *ca.* 55 m s^{-1}, whose effective mass is *ca.* $80m_4$, where m_4 is the mass of a ^{4}He atom. This alters the situation.

For temperatures of *ca.* 0.5 K the average magnitude of $\boldsymbol{k}$ is about 5 nm^{-1} for the ^{3}He quasiparticle. The wave-vector of the emitted phonon is about 0.009 nm^{-1} if it is assumed to have an energy of 2.5 K. Consequently we can ignore terms involving q as being small in comparison with k. (Of course, p is very much larger, being about 2.8 nm^{-1} for $\bar{v} = 55$ m s^{-1}.)

If a ^{3}He atom collides 'head on' with an ion, then the velocity of the ion is reduced by *ca.* 1 m s^{-1}. Usually, of course, the ^{3}He atom will collide with the ion at some other angle and the change in the velocity will be very much smaller. However, even this change is very much less than the width of $f(v)$, which is determined by the recoil of the ion when it emits a pair of rotons. This width is about 9 m s^{-1} at 23 bar (see I and Bowley & Sheard, 1977). Consequently, the ratio $f_b(v_3')/f(v)$ can be taken to be unity to an excellent approximation. Making these two approximations, we find

$$\begin{aligned}\bar{R}_a &\approx \frac{2\pi}{\hbar}\sum_{k,\sigma}\sum_{p}\sum_{q} |\, T^{p}_{k,q}\,|^2 f(v)\, n_k(1+f_q) \\ &\quad\times[1-n_b-n_b\exp\{\beta(\epsilon_k-\mu-E_q)\}] \\ &\quad\times\delta\left\{\epsilon_k+\frac{\hbar^2p^2}{2m_i}-\frac{\hbar^2(\boldsymbol{p}+\boldsymbol{k})^2}{2m_i'}-E_q-E_b\right\}.\end{aligned} \tag{4.13}$$

We need to average over $\boldsymbol{k}$, the wave-vector of the quasiparticle. It is helpful to rewrite the δ-function appearing in equation (4.13) in the following way:

$$\delta\left\{\frac{\hbar^2}{2m_3'}\left(\boldsymbol{k}-\frac{m_3'}{m_i'}\boldsymbol{p}\right)^2-E_q-E_b-\frac{\hbar^2p^2}{2}\left(\frac{1}{m_i'-m_3^*}-\frac{1}{m_i}\right)\right\},$$

where

$$\frac{1}{m_3'} = \frac{1}{m_3^*}-\frac{1}{m_i'}. \tag{4.14}$$

We can also redefine the binding energy for an ion of momentum $\hbar p$ as

$$E_{\mathrm{B}} = E_{\mathrm{b}} - \frac{\hbar^2 p^2}{2}\left(\frac{1}{m_{\mathrm{i}}} - \frac{1}{m_{\mathrm{i}}' - m_3^*}\right) \tag{4.15}$$

and define a new wave vector $\boldsymbol{k}'$ by

$$\boldsymbol{k}' = \boldsymbol{k} - (m_3'/m_{\mathrm{i}}')\,\boldsymbol{p}. \tag{4.16}$$

The δ-function then becomes

$$\delta\,(\hbar^2 k'^2/2m_3' - E_q - E_{\mathrm{B}}).$$

This δ-function can best be used in calculating the integral over the phonon momentum q. With

$$E_q = \hbar c_1 q, \tag{4.17}$$

one finds for a unit volume

$$\bar{R}_{\mathrm{a}} = \frac{1}{\pi\hbar^4 c_1^3}\sum_{\boldsymbol{p}}\sum_{\boldsymbol{k},\boldsymbol{\sigma}} |\,T^{\boldsymbol{p}}_{\boldsymbol{k},\boldsymbol{q}}\,|^2 \left\{-E_{\mathrm{B}} + \frac{\hbar^2 k'^2}{2m_3'}\right\}^2 f(\boldsymbol{v})\, n_{\boldsymbol{k}}\left[1 - n_{\mathrm{b}} - n_{\mathrm{b}}\exp\left\{\beta\left(\epsilon_k - \mu + E_{\mathrm{B}} - \frac{\hbar^2 k'^2}{2m_3'}\right)\right\}\right]. \tag{4.18}$$

Here, we have ignored the factor f_q, which is very small compared to one if $-E_{\mathrm{B}}$ is about 2.5 K and the temperature is about 0.5 K. We have also assumed that $T^{\boldsymbol{p}}_{\boldsymbol{k},\boldsymbol{q}}$ does not vary with $\boldsymbol{q}$. Now we can do the sum over $\boldsymbol{k}$ and $\boldsymbol{\sigma}$. The factor $n_{\boldsymbol{k}}$ is always given by the formula

$$n_{\boldsymbol{k}} = \exp\{-\beta(\epsilon_{\boldsymbol{k}} - \mu)\} = \frac{n_3}{2}\left(\frac{2\hbar^2}{m_3^* k_{\mathrm{B}} T}\right)^{\frac{3}{2}} \exp\,(-\beta\epsilon_{\boldsymbol{k}}) \tag{4.19}$$

for the low concentrations we are considering. Consequently, the absorption term, which is proportional to $1 - n_{\mathrm{b}}$, gives

$$\frac{n_3}{\pi\hbar^4 c_1^3}\sum_{\boldsymbol{p}} |\,T^{\boldsymbol{p}}_{\boldsymbol{k},\boldsymbol{q}}\,|^2 \overline{\left(-E_{\mathrm{B}} + \frac{\hbar^2 k'^2}{2m_3'}\right)^2} f(\boldsymbol{v})\,(1 - n_{\mathrm{b}}).$$

The emission term (proportional to n_{b}) is best considered as an integral over $\boldsymbol{k}'$, since the factor $\exp\,(\beta\epsilon_{\boldsymbol{k}})$ cancels out. Here the bar indicates the value when averaged over k. This gives

$$\frac{n_3}{\pi\hbar^4 c_1^3}\left(\frac{m_3'}{m_3^*}\right)^{\frac{3}{2}}\sum_{\boldsymbol{p}} |\,T^{\boldsymbol{p}}_{\boldsymbol{k},\boldsymbol{q}}\,|^2 \overline{\left(-E_{\mathrm{B}} + \frac{\hbar^2 k'^2}{2m_3'}\right)^2} f(\boldsymbol{v})\, n_{\mathrm{b}} \exp\{\beta(E_{\mathrm{B}} - \mu)\}.$$

The averages of $\hbar^2 k'^2/2m_3'$ are different in each case; here, the average is over $\boldsymbol{k}'$, not $\boldsymbol{k}$. However, since E_{B} is larger than $\hbar^2 k'^2/2m_3'$, these two averages are almost equal. Moreover, the ratio m_3'/m_3^* is very nearly equal to none. Consequently a fair approximation, after averaging over $\boldsymbol{p}$, is

$$\bar{R}_{\mathrm{a}} \approx \frac{n_3}{\pi\hbar^4 c_1^3} |\,T^{\boldsymbol{p}}_{\boldsymbol{k},\boldsymbol{q}}\,|^2 \overline{\left(-E_{\mathrm{B}} + \frac{\hbar^2 k'^2}{2m_3'}\right)^2}\,[1 - n_{\mathrm{b}} - n_{\mathrm{b}}\exp\{\beta(E_{\mathrm{B}} - \mu)\}], \tag{4.20}$$

where E_{B} must now be calculated at the average velocity of the ion. When $\bar{R}_{\mathrm{a}} = 0$ one finds that n_{b} is given by its equilibrium value

$$n_{\mathrm{eq}} = [\exp\{\beta(E_{\mathrm{B}} - \mu)\} + 1]^{-1}, \tag{4.21}$$

which shows that a sort of 'thermal equilibrium' can be achieved. The binding energy is shifted from E_{b} to E_{B}.

PHILOSOPHICAL TRANSACTIONS OF THE ROYAL SOCIETY A MATHEMATICAL, PHYSICAL & ENGINEERING SCIENCES

Let us try to estimate the size of the effect. To do so, we need to know $m_i' - m_i$, the change in the ion's effective mass when a ^{3}He atom is bound to it. Let us assume that it is

$$m_i' - m_i = m_3,$$

where m_3 is the bare ^{3}He mass. The correction to E_b is about 1 K for a velocity of 55 m s^{-1}, a sizeable quantity. However, we are interested here mainly in the *variation* in E_B with the average velocity of the ion, which we may take to be ± 5 m s^{-1}. The corresponding variation in E_B is then about 0.1 K. This is slightly smaller than the uncertainty in the value of E_B which we will obtain below from the experimental data; which implies, in turn, that with the present data we are unable to detect the predicted variation of E_B with change in the mean velocity of the ion as given by equation (4.15).

We can rewrite equation (4.20) in the following way:

$$\bar{R}_a = n_3(1 - n_b/n_{eq})\, K(\bar{v}, T), \tag{4.22}$$

where we have lumped the unknown parameters into a rate constant $K(\bar{v}, T)$, a function of the average velocity of the ion and of the temperature. This equation tells how the distribution of ions with bound ^{3}He atoms reaches equilibrium. The constant $K(\bar{v}, T)$ depends on the process by which ^{3}He atoms are absorbed on the ion. The factor $1 - n_b/n_{eq}$ tells us that a sort of thermal equilibrium can exist even for such fast ions.

The more cautious reader may be inclined to object to the cavalier way in which we have made approximations. Accordingly, we list them below and comment on the validity of each.

(1) We have ignored q by comparison with k. This is a good approximation for the temperature we are considering, but it breaks down at temperatures below *ca.* 0.02 K.

(2) We have ignored any dependence of the matrix element on k, q or p. We cannot justify this step, which is, however, discussed further in the next section, although from a different viewpoint. Our main conclusion, however, that $\bar{R}_a$ depends linearly on $1 - n_b/n_{eq}$, does not depend on this particular approximation.

(3) The rates of both absorption and emission depend on the average value of q^2, where

$$q = \frac{1}{\hbar c_1}\left(-E_B + \frac{\hbar^2 k'^2}{2m_3'}\right), \tag{4.23}$$

this average being different, however, in the two cases. For absorption one averages over k and this gives

$$q_{abs} = \frac{1}{\hbar c_1}\left(-E_B + k_B T + \frac{m_3' \bar{v}^2}{2}\right). \tag{4.24}$$

For emission one averages over k' and this gives

$$q_{em} = \frac{1}{\hbar c_1}(-E_B + k_B T). \tag{4.25}$$

Consequently, the values of q to be used in evaluating the emission and absorption rates are not equal. This modifies the formula for n_{eq} to

$$n_{eq} = [\eta \exp\{\beta(E_B - \mu)\} + 1]^{-1}, \tag{4.26}$$

where η is a number close to one which varies slowly with temperature.

In practice we only need consider situations in which $n_{eq} \ll 1$ so that the presence of the

extra factor η only has the effect of changing the *magnitude* of n_{eq}, not its temperature dependence. The size of η depends on whether the matrix elements are constant, or whether there is some q dependence. For example, if $T^{p}_{k,q}$ varied as q^{-1}, then the factor η would be exactly equal to unity.

We have chosen to put $\eta = 1$ for convenience. This means that when we obtain values of the nucleation rate with a ^{3}He atom bound to the ion, these values may be in error due to overestimating (or underestimating) η.

(4) We have assumed that the ratio $f_b(v')/f(v)$ is equal to unity. This has been based on the belief that the distribution function for ions each with a bound ^{3}He atom is almost the same as that for bare ions. This would appear to be a reasonable assumption: the ionic effective mass is changed only marginally by the presence of a bound ^{3}He atom, so the critical velocity for emission of rotons will be almost the same as for a bare ion.

(c) *The absorption cross-section*

We now present a discussion of the quantity $K(\bar{v}, T)$ introduced in our expression (4.22) for the average net ^{3}He absorption rate $\bar{R}_a$. Although the formal definition of $K(\bar{v}, T)$ above is rather complicated, its physical significance immediately becomes clear if we note that the factor $1-n_B/n_{eq}$ in (4.22) simply represents the fractional departure of n_b from its equilibrium value. Thus $K(\bar{v}, T)$ must represent the product of an effective cross-section for the absorption process with the average relative velocity $\bar{v}_{rel}$ between the ^{3}He atom and the ion. We therefore write (4.22) in the form

$$\bar{R}_a = n_3 \bar{v}_{rel} \sigma_g \Pi (1 - n_b/n_{eq}), \tag{4.27}$$

where we have set

$$K(\bar{v}, T) = \bar{v}_{rel} \sigma_g \Pi. \tag{4.28}$$

The quantity σ_g is the geometrical cross-section and Π represents the probability that a ^{3}He atom striking the ion will actually be absorbed.

We can now examine the way in which we expect K to vary with $\bar{v}$ and T, through its dependence on $\bar{v}_{rel}$ and Π. First, the relative velocity between the ion and incident ^{3}He atom obeys the relation

$$\bar{v}^2_{rel} = \bar{v}^2 + \bar{v}^2_3, \tag{4.29}$$

where $\bar{v}_3$ is the average thermal velocity of the ^{3}He atoms. We then have,

$$\bar{v}_{rel} = (\bar{v}^2 + \bar{v}^2_3)^{\frac{1}{2}} = \bar{v}(1 + 3k_B T/m^*_3 \bar{v}^2)^{\frac{1}{2}} \tag{4.30}$$

or

$$\bar{v}_{rel} \approx \bar{v}(1 + 0.9T)^{\frac{1}{2}} \tag{4.31}$$

for an ion travelling at 55 m s^{-1}. If the temperature were to rise from 0.32 to 0.5 K we would therefore expect $\bar{v}_{rel}$, and hence K, to increase by 6%.

However, this is not the only effect of temperature upon K: we must now examine the nature of the factor Π, the temperature dependence of which we believe can be understood in terms of the following simple model. It has been suggested (Bowley & Lekner 1970) that a ^{3}He atom will suffer a long range-repulsive interaction with an ion due to a polarization interaction and the fact that the ^{3}He atom, with its larger zero point energy, occupies a larger volume than a ^{4}He atom. The potential for this interaction is

$$V(r) = \alpha\gamma e^4/8\pi\epsilon_0 r^4 \tag{4.32}$$

where γ is the polarizability of the ^{4}He atom and α is the excess fractional volume occupied by the ^{3}He atom. Near the surface of the ion this potential has a maximum value, V_p, of about 0.22 K. Beyond this potential barrier the ^{3}He is attracted by the relative vacuum of the electron bubble and forms a bound state on the ion, as discussed in §1 (*c*).

To arrive at the surface of the ion the ^{3}He atom must have sufficient energy to overcome the potential barrier. For an ion moving with velocity $\boldsymbol{v}$, this is possible if

$$\hbar^2k^2/2m_3^* - \hbar\boldsymbol{k}\cdot\boldsymbol{v} > V_p \tag{4.33}$$

where V_p is the barrier height. We have assumed that the probability of the ^{3}He tunnelling through the barrier is negligible.

Clearly, the number of ^{3}He atoms capable of overcoming the barrier will increase with temperature and we can say that the proportion of ^{3}He atoms with sufficient thermal energy to reach the surface of the ion is,

$$p(T) = \sum_{\boldsymbol{k}} n_{\boldsymbol{k}}\,\theta\left(\frac{\hbar^2k^2}{2m_3^*} - \hbar\boldsymbol{k}\cdot\boldsymbol{v} - V_p\right)\Big/\sum_{\boldsymbol{k}} n_{\boldsymbol{k}} \tag{4.34}$$

where θ is the unit step function.

Values of $p(T)$ for three values of V_p are plotted in figure 12, where we have taken $v = \bar{v} = 55$ m s^{-1}. The factor Π in equation (4.28) now becomes

$$\Pi = \lambda p(T),$$

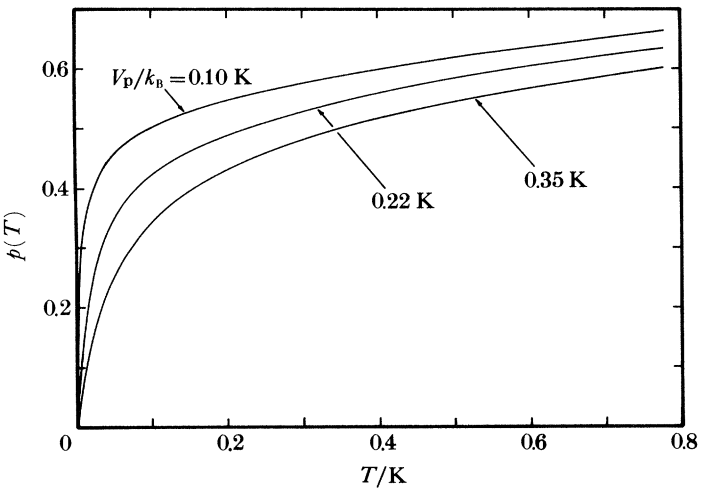

FIGURE 12. The proportion $p(T)$ of ^{3}He quasiparticles which have sufficient energy to overcome the potential barrier V_p that impedes their capture by negative ions in He II, plotted as a function of temperature T for three possible values of V_p.

where the constant λ is the capture probability for a ^{3}He atom which has succeeded in reaching the surface of the ion. Strictly speaking, λ will depend on temperature since it is likely to vary with the ^{3}He thermal wave vector, $\boldsymbol{k}$. We expect that this effect will be small and so, for simplicity, it is neglected.

Finally, then, equation (4.28) becomes

$$K = \bar{v}_{\mathrm{rel}}\,\sigma_g\,\lambda p(T) = \bar{v}_{\mathrm{rel}}\,\sigma p(T) \tag{4.35}$$

where we have introduced an effective absorption cross-section, σ ($= \lambda\sigma_g$), which we take as being a constant.

(*d*) *Process 2: Roton-assisted* ^{3}He *emission*

In §4(*a*) we discussed the need for an additional ^{3}He emission process, which we suggested might be linked to the two-roton emission mechanism that is known to occur for ions travelling at $v > v'$ (see I). A bare ion emits pairs of rotons at a rate of *ca.* 10^{10} s^{-1} when it travels at 10 m s^{-1} above the critical velocity; it seems plausible, therefore, that a bound ^{3}He atom may sometimes be emitted together with a roton pair. As we shall see, it is possible for energy and local momentum to be conserved during such an emission event (which would *not* be so if the ^{3}He atom were being emitted by itself). We shall now attempt to derive an expression for the critical velocity above which this process can occur.

Suppose that the ion with a bound ^{3}He atom has a momentum $\hbar\boldsymbol{p}'$, that it emits rotons of momentum $\hbar\boldsymbol{\omega}$ and $\hbar\boldsymbol{\omega}'$ and that it emits a ^{3}He quasiparticle of momentum $\hbar\boldsymbol{k}$. For energy and momentum to be conserved,

$$E_{\mathrm{b}}+\frac{\hbar^2p'^2}{2m_{\mathrm{i}}'}=\frac{\hbar^2}{2m_{\mathrm{i}}}(\boldsymbol{p}'-\boldsymbol{k}-\boldsymbol{\omega}-\boldsymbol{\omega}')^2+\epsilon_{\boldsymbol{k}}+E_{\boldsymbol{\omega}}+E_{\boldsymbol{\omega}'}. \tag{4.36}$$

For a bare ion emitting a pair of rotons one would have

$$\frac{\hbar^2p^2}{2m_{\mathrm{i}}}=\frac{\hbar^2}{2m_{\mathrm{i}}}(\boldsymbol{p}-\boldsymbol{\omega}-\boldsymbol{\omega}')^2+E_{\boldsymbol{\omega}}+E_{\boldsymbol{\omega}'}, \tag{4.37}$$

and it would then be straightforward to solve for the lowest velocity $(\hbar\boldsymbol{p}/m_{\mathrm{i}})$ which satisfies (4.37),

$$\begin{aligned} v'=\left(\frac{\hbar\boldsymbol{p}}{m_{\mathrm{i}}}\right)_{\min}&=\frac{E_{\boldsymbol{\omega}}+E_{\boldsymbol{\omega}'}}{\hbar(\boldsymbol{\omega}+\boldsymbol{\omega}')}+\frac{\hbar(\boldsymbol{\omega}+\boldsymbol{\omega}')}{2m_{\mathrm{i}}}\\ &\approx\frac{\Delta}{\hbar k_0}+\frac{\hbar k_0}{m_{\mathrm{i}}} \end{aligned} \tag{4.38}$$

where $\hbar k_0$ is the momentum at the roton minimum in the dispersion curve and Δ is the corresponding energy.

For an ion with a bound ^{3}He atom, however, we have to find the lowest velocity $\hbar\boldsymbol{p}'/m_{\mathrm{i}}'$ which satisfies equation (4.36): to do so we have to find the appropriate value of $\boldsymbol{k}$. Equation (4.36) can be rewritten using

$$\frac{1}{m_3''}=\frac{1}{m_3^*}+\frac{1}{m_{\mathrm{i}}} \tag{4.39}$$

as

$$\begin{aligned} \frac{\hbar^2}{m_{\mathrm{i}}}\boldsymbol{p}'\cdot(\boldsymbol{\omega}+\boldsymbol{\omega}')=E_{\boldsymbol{\omega}}+E_{\boldsymbol{\omega}'}+\frac{\hbar^2}{2m_{\mathrm{i}}}(\boldsymbol{\omega}+\boldsymbol{\omega}')^2-E_{\mathrm{b}}-\frac{\hbar^2p'^2}{2m_{\mathrm{i}}'}+\frac{\hbar^2p'^2}{2m_{\mathrm{i}}}\\ +\frac{\hbar^2}{2m_3''}\left\{k-\frac{m_3''}{m_{\mathrm{i}}}(\boldsymbol{p}'-\boldsymbol{\omega}-\boldsymbol{\omega}')\right\}^2-\frac{\hbar^2m_3''}{2m_{\mathrm{i}}^2}(\boldsymbol{p}'-\boldsymbol{\omega}-\boldsymbol{\omega}')^2. \end{aligned} \tag{4.40}$$

The minimum value of $\boldsymbol{p}'$ will occur when

$$\boldsymbol{k}=\frac{m_3''}{m_{\mathrm{i}}}(\boldsymbol{p}'-\boldsymbol{\omega}-\boldsymbol{\omega}'), \tag{4.41}$$

which clearly minimizes the right-hand side of equation (4.40). With this choice of $\boldsymbol{k}$ the equation for $\boldsymbol{p}'/m_i'$ is

$$\frac{\hbar^2}{m_i}\boldsymbol{p}'\cdot(\boldsymbol{\omega}+\boldsymbol{\omega}')\left(1-\frac{m_3''}{m_i}\right)=E_\omega+E_{\omega'}+\frac{\hbar^2}{2m_i}(\boldsymbol{\omega}+\boldsymbol{\omega}')^2\left(1-\frac{m_3''}{m_i}\right)-E_b-\frac{\hbar^2p'^2}{2}\left(\frac{1}{m_i'}-\frac{1}{m_i}+\frac{m_3''}{m_i^2}\right). \tag{4.42}$$

The velocity we want is the minimum value of $\hbar\boldsymbol{p}'/m_i'$. To a very good approximation this is given by

$$v_{c3}=\left(\frac{\hbar p'}{m_i'}\right)_{\min}=\min\left\{\frac{(E_\omega+E_{\omega'})}{\hbar(\omega+\omega')}\left(\frac{m_i}{m_i'}\right)\left(\frac{m_i}{m_i-m_3''}\right)+\frac{\hbar(\omega+\omega')}{2m_i'}\right\}-\frac{E_B}{\hbar(\omega+\omega')}\left(\frac{m_i}{m_i'}\right)\left(\frac{m_i}{m_i-m_3''}\right)$$

$$\approx v_L\frac{m_i^2}{m_i(m_i-m_3'')}+\frac{\hbar k_0}{m_i'}-\frac{E_B}{2\hbar k_0}. \tag{4.43}$$

If $m_i'=m_i+m_3''$, then the increase in the critical velocity is

$$\delta v=v_{c3}-v'\approx -E_B/2\hbar k_0.$$

If $-E_B/k_B=2.5$ K, then the change in the critical velocity is *ca.* 8 m s^{-1}, so only those ions travelling faster than *ca.* 58 m s^{-1} will be able to emit a ^{3}He atom together with a pair of rotons. Very few ions will travel as fast as this in low electric fields. As the field is increased, however, the process occurs more and more frequently until, for $E\gtrsim 10^5$ V m^{-1}, it becomes the dominant influence on the number of bound ^{3}He atoms.

Let us suppose that the average rate of two-roton emission together with a ^{3}He atom is $R_e(E)$. Then, in the steady state, the net rate of absorption of ^{3}He atoms by the ion must equal the rate of loss of such ions due to vortex nucleation. Thus

$$n_3K(\bar{v},T)(1-n_b/n_{eq})-n_bR_e(E)=n_b(\nu_1-\nu_0). \tag{4.44}$$

The quantity $\nu_1-\nu_0$ is the increase in the nucleation rate due to the presence of a ^{3}He atom on the ion. Rearrangement of (4.44) then gives the average number of bound ^{3}He atoms as

$$n_b=n_{eq}(1+n_{eq}R'/n_3K)^{-1} \tag{4.45}$$

with

$$R'=R_e(E)+\nu_1-\nu_0.$$

Consequently, when the term involving R'/K is very small, n_b tends to the equilibrium value n_{eq}. In the opposite limit when R'/K is large, n_b tends to n_3K/R'. The number of bound ^{3}He atoms is then governed by the ratio of the rate of ^{3}He absorption to the rate of emission via the two-roton process.

(*e*) *Generalization of the model for many bound states*

So far it has been assumed that there is only one bound state into which the ^{3}He can be absorbed. However, according to Shikin's model (see §1 (*c*)) there will actually be several bound states, and any realistic model of the absorption and emission processes must make explicit allowance for this fact. Although the assumption of a single bound state is inherent in the arguments of §4 (*b*)–(*d*), the generalization to many bound states does not render these arguments void; we can simply say that they now refer to a particular bound state, which we can label by the quantum number, l. Thus, the main conclusion of the previous section (4.45), becomes

$$n_l=n_l^{eq}(1+n_l^{eq}R_l'/n_3K_l)^{-1} \tag{4.46}$$

where n_l is the average number of ^{3}He atoms in the state l; n_l^{eq} is the equilibrium number of ^{3}He atoms in the state l; and the other terms have similar interpretations. The energies of the bound states are given by a modified version of (1.1) and (1.2), which now become

$$\epsilon_l = E_{\mathrm{b}} + (\hbar^2/2m_{\mathrm{s}} R_{\mathrm{s}}^2)\, l(l+1), \tag{4.47}$$

where E_{B} is the effective binding energy defined by (4.15). As discussed in §1 (*c*), we propose to ignore any splittings in the energy levels due to effects associated with the backflow around the moving ion.

Equation (4.1) now gives

$$\begin{aligned} \nu &= \nu_0 + n_{\mathrm{b}}(\nu_{1l} - \nu_0) \\ &= \nu_0 + \sum_{l=0}^{L} \frac{2(2l+1)\,(\nu_{1l}-\nu_0)\, n_l^{\mathrm{eq}}}{(1+n_l^{\mathrm{eq}}\, R_l'/n_3\, K_l)}, \end{aligned} \tag{4.48}$$

where we also allow ν_1 to vary with l. Unfortunately, this has made the situation rather complex; we now have to determine R_l', K_l and ν_{1l} for each of the $L+1$ values of l. Clearly, we cannot hope to do this with each one of them as an adjustable parameter, and we therefore need to make some simplifying assumptions.

We shall, in fact, proceed on the basis of two models. Model A is the simplest, employing the assumption that all three of these parameters are independent of l, i.e. $R_l' = R'$, $K_l = K$, $\nu_{1l} = \nu_1$. In model B we shall choose to allow the roton-induced emission rate R_l to vary realistically with l, but we will retain the assumption $K_l = K$ and $\nu_{1l} = \nu_1$. It must be admitted, however, that the reasons for this choice are based as much on our lack of knowledge of the processes affecting ν_{1l} and K_l as they are on any physical grounds: in the current state of our understanding, there is no reason to suppose that ν_{1l} or K_l will in fact vary with l; but on the other hand, it seems inevitable that the emission rate, R_l', will vary with the energy of the bound state, and hence will exhibit a dependence on l, this effect being due to a lowering of the critical velocity for the emission process.

In the previous section we demonstrated that the critical velocity for ^{3}He emission from the ion is

$$v_{\mathrm{c3}} = v' - E_{\mathrm{B}}/2\hbar k_0, \tag{4.49}$$

where E_{B} is the ground-state energy. If the ^{3}He atom is in an excited state, then the binding energy is reduced and we have

$$v_{\mathrm{c}l} = v' - \frac{1}{2\hbar k_0}\{E_{\mathrm{B}} + gl(l+1)\} = v_{\mathrm{c3}} - \frac{gl(l+1)}{2\hbar k_0} = v_{\mathrm{c3}} - \delta v_{\mathrm{c}l}, \tag{4.50}$$

where g is given by (1.2).

It is now necessary to make some assumptions about the way in which the emission rate of ^{3}He with rotons increases with velocity when $v > v_{\mathrm{c}l}$. For convenience, we will suppose that it does so in a similar manner to the ordinary two-roton emission process for which, as discussed in (I), the rate varies as $(v-v')^2$. We note, however, that this assumption clearly cannot be quite correct because the phase space restrictions governing the emission of a pair of rotons plus a ^{3}He atom will certainly differ from those governing the emission of a pair of rotons on their own. An explicit calculation of the ^{3}He plus roton pair emission rate would, of course, be possible but we have felt it to be unjustified, for two reasons. First, there is in any case no justification *a priori* for our assumption that the ^{3}He will be emitted with pairs of rotons, rather

than with single rotons. For the latter type of process the critical velocity would be smaller and its velocity dependence would be different. Secondly, we may note that the main distinguishing feature of model B is that the critical velocity for ^{3}He emission decreases as the ^{3}He atom occupies successively higher energy levels on the ion: the precise velocity dependence of the emission rate above the threshold for any given value of l is of secondary importance. We will therefore suppose that the emission rate of ^{3}He atoms from the state l is given by

$$R_l = \int_{v_{cl}}^{\infty} R_r (v - v_{cl})^2 f_b(v, E)\, dv \tag{4.51}$$

where $f_b(v, E)$ is the distribution function for ions with bound ^{3}He atoms, which, as was argued in §4 (*b*), we believe to be essentially the same as the distribution function for bare ions.

We could in principle now determine R_l by performing a numerical integration of (4.51). For low fields, however, $f(v, E)$ is known analytically (Bowley & Sheard 1977) and, considering the number of approximations we have already made, little harm would seem to result from using the analytic form of $f(v, E)$ over all fields. We then have

$$R_l = R_e \exp\left[\left\{\frac{m_i R_r (v_{cl} - v')^2}{eE} + \frac{6}{v_{cl} - v'}\right\} \delta v_{cl}\right] \tag{4.52}$$

where R_e is the ^{3}He emission rate from the ground state. With the exception of R_e, all the quantities in this equation are known. Consequently, allowance for the variation of R_l with l has not introduced any undetermined parameters additional to those of model A.

5. Data analysis for the linear régime

Each of the models we have developed contains three undetermined parameters, the binding energy, E_b; the nucleation rate for ions with single bound ^{3}He atoms, $\nu_1(E)$; and the ratio $R'(E)/K(E, T)$. Our first task, then, is to determine these parameters by fitting both models to the experimental data. Although we may hope that model B will give a superior fit, we shall also retain model A. The advantage of doing so is that, should model B turn out to provide a significantly better fit than model A, then this may reasonably be regarded as positive evidence in favour of the premises on which it is based including, particularly, the type of energy-level structure sketched in figure 2.

We cannot, however, fit either model immediately to the raw data. The reason for this stems from the fact that both models were developed on the assumption that a maximum of one ^{3}He atom would condense on any ion; whereas we believe (see §6) that, for the higher concentrations, a significant number of ions with two or more bound ^{3}He atoms may exist. This problem can, however, be avoided simply. We have found that the measured concentration dependence of the nucleation rate, $\nu(x_3)$, can be expressed as a power series,

$$\nu = \nu_0 + \nu' x_3 + \nu'' x_3^2 + \ldots, \tag{5.1}$$

where ν_0 is the nucleation rate in pure ^{4}He. For data such as those of figure 8 (*b*), however, terms beyond the linear one are unnecessary; whereas, for those of figure 8 (*a*), the inclusion of higher terms in x_3 is clearly essential. Over much of the parameter range that we have studied, however, the most appropriate fitting procedure is less obvious. For example, although the 0.369 K data of figure 13 are clearly better fitted by a very shallow curve than by a straight

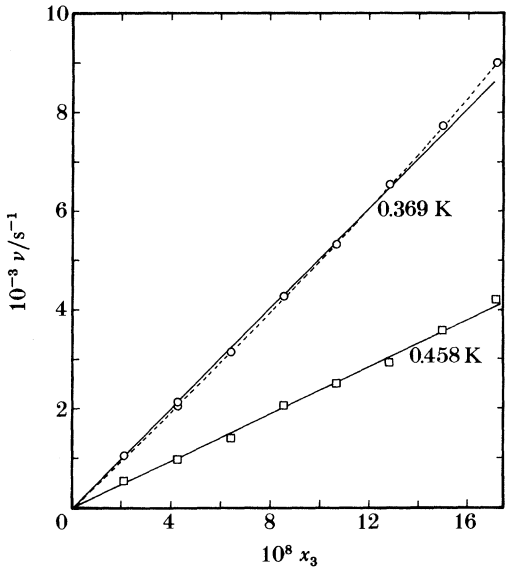

FIGURE 13. The measured nucleation rate ν plotted as a function of the ^{3}He/^{4}He ratio x_3 at 23 bar and $E = 5.81 \times 10^4$ V m^{-1} for two temperatures. The data at the higher temperature (squares) appear to be linear within experimental error, whereas those at the lower temperature (circles) show slight signs of upward curvature as indicated by the dashed line.

line, that the same thing is also true of the results at the higher temperature of 0.458 K is far from clear. A statistical analysis confirms, however, that the latter data are, in fact, (slightly) better fitted by a curve.

The quantity $\nu' x_3$ is the nucleation rate for ions with bound ^{3}He atoms in the limit $x_3 \to 0$, that is, the *linear régime* for which our theory has been developed. Comparison with (4.1) then yields

$$\nu' = (n_b/x_3)\,(\nu_1 - \nu_0). \tag{5.2}$$

In §5 (*a*) we shall discuss the evaluation of ν' and also of ν'', the latter coefficient being related to the *non-linear régime* to be discussed in §6.

Having found values of $\nu'(E, T)$ we shall be able to fit both models A and B. Rather than use all our data in this fitting procedure we shall only use those recorded at lower temperatures. The reasons for this are twofold. First, we shall see that the analysis of higher-temperature data involves complicating factors which could perhaps distort the accuracy of the fitted parameters; and second, we wish to judge the ability of our theory to predict values of $\nu'(E, T)$. We believe that using the low temperature data to fix the unknown parameters in our model, and then using the model to predict the high temperature data, should provide a stringent test of the theory.

In §5 (*b*) we shall evaluate the binding energy, E_b, and then, in §5 (*c*), we will use this in our fit to the data, thereby obtaining values of $\nu_1(E)$ and $R'(E)/K(E, T)$. Our attempts to predict the higher-temperature data will be discussed in §5 (*d*). Finally, in §5 (*e*), we shall examine some of the consequences of our results for the theory of vortex nucleation.

(*a*) *Values of ν' and ν''*

Equation (5.1) has been fitted to the data (figures 8 and 13) with the aid of a computer programme (Bevington 1969) designed to calculate the values of ν_0, ν' and ν'' giving the best fit as determined by the χ^2-test, and to evaluate the standard errors in these quantities.

Values of $\nu'(E, T)$ and $\nu''(E, T)$ derived on this basis are shown in figures 14 and 15 respectively. The values of ν' have an error of about $\pm 15 \times 10^8$ s^{-1} and values of ν'' have an error of about 10^{16} s^{-1}. Note that any errors in these quantities will be correlated; if, for example, a particular value of ν'' is 2×10^{16} s^{-1} higher than it should be, the corresponding value of ν' will be 35×10^8 s^{-1} too low. This effect is particularly unfortunate for the high field region, where it seems likely (figure 14) that the values of ν' should lie on a common curve independent of temperature.

We have found that within experimental error all the data we have analysed are in excellent accord with (5.1) if we take terms up to x_3^2. This suggests that the neglect of cubic and higher-order terms is justified for the range of concentrations and temperatures that we have used. In fact, we have found that for high fields or high temperatures, $\nu(x_3)$ can be fitted quite acceptably by a linear equation. We have therefore chosen to analyse the data where $E \geqslant 1.5 \times 10^5$ V m^{-1} or $T \geqslant 0.55$ K as if $\nu'' = 0$.

We shall find that, particularly for the higher temperatures, it is more useful to study the

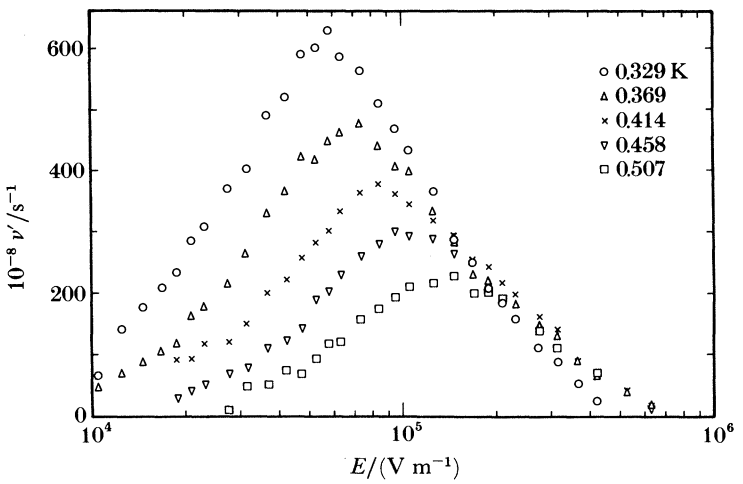

FIGURE 14. The coefficient ν' plotted as a function of electric field E for various temperatures.

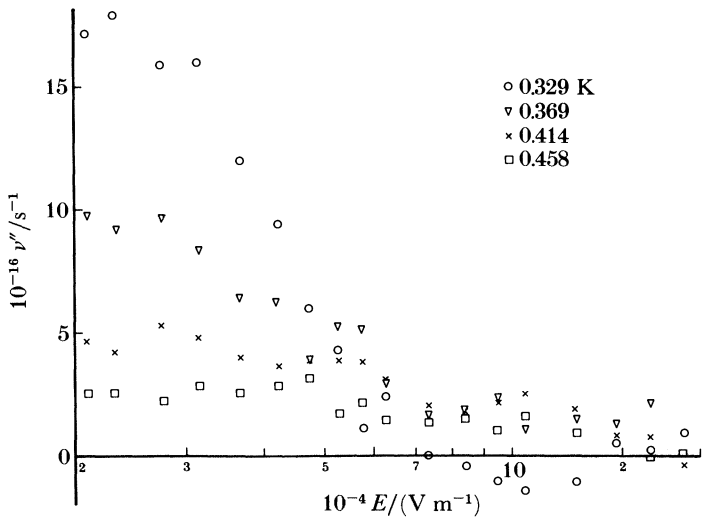

FIGURE 15. The coefficient ν'' plotted as a function of electric field E for various temperatures.

temperature dependence of ν' for constant drift velocity than for constant field. Figure 16 shows ν' plotted as a function of $\bar{v}$ for several temperatures. The values of $\bar{v}$ are obtained by averaging over the values recorded for the lowest six concentrations at each field; data from the higher concentrations were not used in determining $\bar{v}$ since they exhibit a small but noticeable reduction in $\bar{v}$ due to ion-^{3}He scattering. We have indicated by the dashed lines data taken

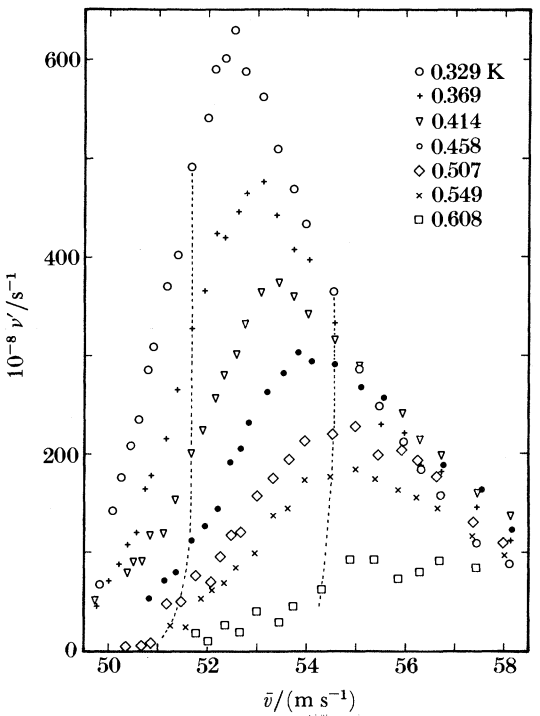

FIGURE 16. The coefficient ν' plotted as a function of the ionic drift velocity $\bar{v}$. At low temperatures $\bar{v}$ is temperature independent, whereas at high temperatures it is reduced by roton scattering. The dashed lines indicate the velocities corresponding to constant electric fields, as described in the text.

at fields of 1.26×10^5 V m^{-1} and 3.69×10^4 V m^{-1}. For temperatures below *ca.* 0.5 K, $\bar{v}$ appears to be independent of temperature but above this temperature the velocity is reduced owing to the effect of roton scattering. This effect is particularly pronounced at lower fields.

To obtain values of $\nu'(\bar{v})$ we have adopted the procedure of taking the drift velocity at the lowest temperature for any given field, and then, for higher temperatures, reading off the value of ν' given by smooth curves drawn through the data at each temperature. In practice, this procedure was necessary only for $T > 0.507$ K.

There is, however, a further source of complication involving the higher-temperature data. In our earlier studies (III) of $\nu(E, T)$ in pure ^{4}He we suggested that the observed increase in ν with temperature is due to vortex rings being nucleated with the aid of roton interactions. We cannot discount *a priori* the possibility either that this process may occur with enhanced vigour when a bound ^{3}He atom is present or, on the contrary, that it may be blocked by the presence of a bound ^{3}He atom. Either situation could lead to a distortion of the data above *ca.* 0.55 K where the roton-drive mechanism becomes important in pure ^{4}He. Accordingly we restrict our attention, for the moment, to the data recorded below 0.53 K.

(*b*) *Determination of the binding energy* E_b

One of the more important parameters we can determine by fitting our model to the data is the binding energy, E_b, of a ^{3}He atom on the free He II surface provided by the negative ion. We believe that the present work provides the first reliable determination of this quantity under pressure although, as discussed in §1 (*c*), the binding energy (on a plane surface) under the saturated vapour pressure (s.v.p.) is well established from surface tension measurements.

As stated in the previous section, we have been forced to restrict our attention to a narrow range of temperature, $0.329 < T < 0.507$ K, incorporating just five field scans. This is unfortunate since, to determine E_b, we need to fit $\nu'(T)$. However, we do have a wide range of fields, $2\times10^4 \leqslant E \leqslant 10^5$ V m^{-1}, over which ν' is strongly temperature-dependent, which gives us the opportunity of using the data for each field to obtain a number of independent estimates of E_b. From (4.48) we have

$$\nu' = \frac{1}{x_3}\sum_{l=0}^{L}\frac{2(2l+1)\,(\nu_1-\nu_0)\,n_l^{eq}}{(1+n_l^{eq}\,R_l'/n_3\,K)} \tag{5.3}$$

where, for model A, $R_l' = R'$. By fitting to the data, we obtain estimates of ν_1, the ratio R_l'/K, and n_l^{eq} for each field. Values of E_b can now be found explicitly by using equations (4.15), (4.21) and (4.47).

In figure 17 (*a*) and (*b*) we show the values of $-E_b$ and associated error bars for models A and B respectively, for a range of electric fields. In low fields the scatter in the data is relatively

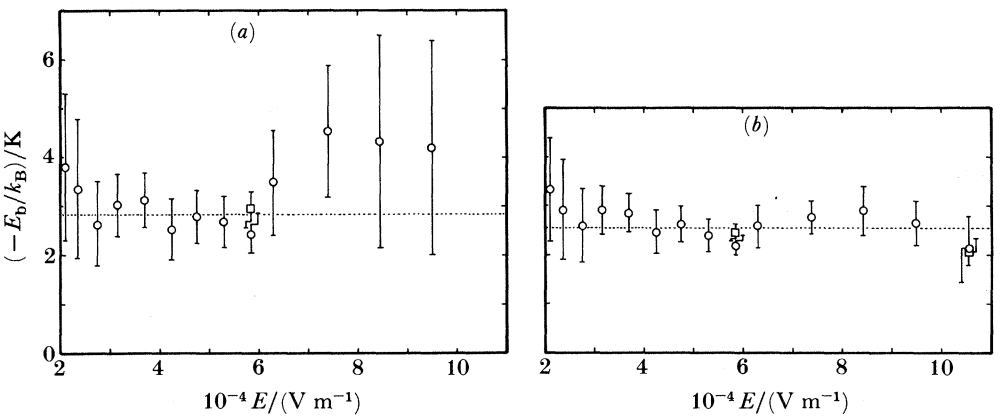

FIGURE 17. Values of $-E_b$ obtained from data recorded at different electric fields E: (*a*) on the basis of model A; and (*b*) on the basis of model B. In each case, the dashed line indicates the (weighted average) best value of $-E_b$.

large and consequently there are large errors in the derived values of E_b. There are also large errors in the values of E_b in high fields, owing to the relatively weak variation of ν' with T. A window of electric fields exists, ranging from 3×10^4 to 6×10^4 V m^{-1} for model A, and from 3×10^4 to 7.5×10^4 V m^{-1} for model B, where relatively accurate values of E_b can be obtained. We have also been able to use the data from the temperature scans at 5.8×10^4 V m^{-1} and 1.05×10^5 V m^{-1}. The values of $-E_b$ obtained in this way (indicated by squares) are probably more reliable since they include more temperatures.

We can see that the results are consistent with $-E_b$ being independent of field, although drawing a horizontal line through the data of figure 17 (*b*) is, perhaps, more plausible than it is for the data of figure 17 (*a*). Since we would, of course, expect E_b to be constant for all fields, this result provides strong support for both models and particularly for model B.

The weighted average over all the points in figure 17 (*a*) and (*b*) gives final 'best fit' values of $-E_b$ for models A and B respectively. These values, which will be used in all the following analyses, are shown in table 1 and are indicated by the dashed lines in the figures.

TABLE 1

data used in fitting	binding energy, $-E_b/k_B$ model A	model B
field scans (○ in figure 17)	2.80 ± 0.19	2.54 ± 0.11
temperature scans (□ in figure 17)	2.93 ± 0.36	2.45 ± 0.18
weighted mean (– – – in figure 17)	2.83 ± 0.17	2.52 ± 0.09

(*c*) *Fitting the model to the data*

Having obtained a value for the binding energy for each of the two models, we can then refit the data using the average values of E_b given in table 1. In the hope of being able to decide which model gives the best fit we have determined the total χ^2 for each; with 53 degrees of freedom we find $\chi^2 = 26.97$ for model A and 26.86 for model B, the data used being the five field scans for $T \leqslant 0.503$ K and two temperature scans at 5.8×10^4 V m^{-1} and 1.05×10^5 V m^{-1}. Apparently, therefore, we cannot discriminate between the two models on the basis of this particular test. In figure 18 (*a*) and (*b*) we show curves for both models fitted to the data from the two temperature scans. In each case, agreement with the data is excellent.

We can also generate curves for both models, using the fitted parameter values already obtained, for comparison with the data from the temperature scans at 1.35×10^5 V m^{-1} and 2.03×10^5 V m^{-1}, yielding the results shown in figure 18 (*c*) and (*d*) respectively. Except at the highest field discriminating between the models is still difficult. If anything, model A appears to give slightly better agreement but the scatter in the data makes this suggestion far from conclusive. For the data at 2.03×10^5 V m^{-1} (figure 18 (*d*)), however, model B clearly gives the superior curve in that it is able to reproduce the peak in $\nu'(T)$, whereas model A does not fit these high-field data at all. Note that the experimental values of $\nu'(T)$ in figure 18 (*d*) were derived on the assumption that $\nu'' = 0$. If this requirement is removed, the scatter in the points becomes larger, but the conclusion still remains the same: that ν' increases with T at low temperatures.

The effect described can, we believe, only be understood in terms of the temperature dependence of $K(T)$. Not surprisingly, our generated $\nu'(T)$ curve is extremely sensitive to details of our theory of the absorption cross-section, and whether a better fit could be obtained with a modified form of $K(T)$ would seem to be a pertinent question. For model A, the answer is probably no; after several attempts we have concluded that model A lacks the 'flexibility' to give the relatively sharp maximum seen in figure 18(*d*). Model B would be in better agreement with the data if the temperature dependence of $K(T)$ was increased. This could arise if, for example, the potential barrier, V_p, rose to about 0.35 K, rather than the 0.22 K we originally chose. However, the model that we have proposed for $K(T)$ is rather crude, and improved agreement with the data could probably only meaningfully be achieved on the basis of a more refined theory.

Finally, we come to consider the values of ν_1 and R'/K that we have obtained by fitting

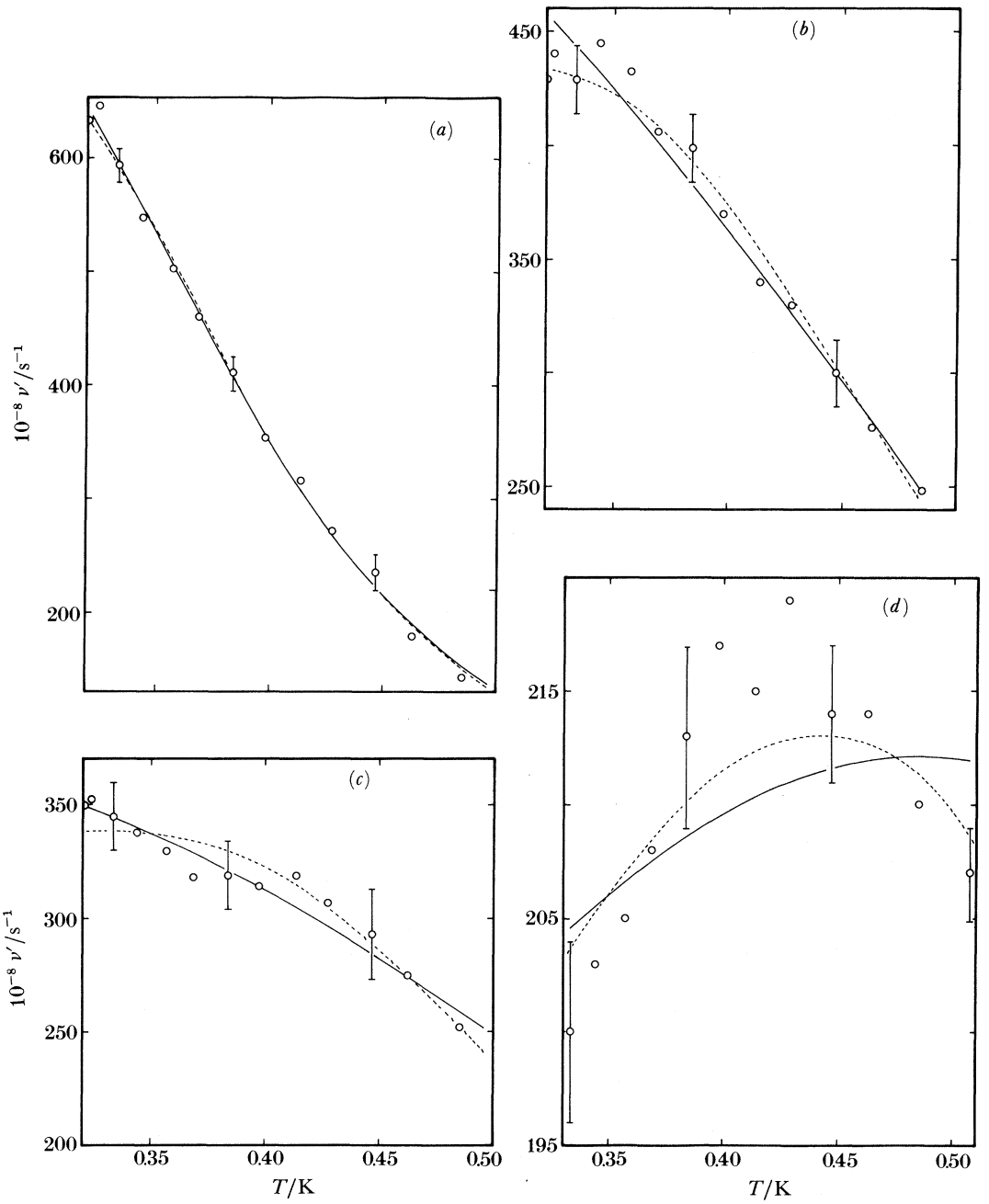

FIGURE 18. The measured variation of the coefficient ν' with temperature T (points) compared with the theoretical curves for model A (full curves) and model B (dashed curves) at four different electric fields; (*a*) $E = 5.81 \times 10^4$ V m^{-1}; (*b*) 1.05×10^5 V m^{-1}; (*c*) 1.35×10^5 V m^{-1}; (*d*) 2.03×10^5 V m^{-1}. The theoretical curves in (*a*) and (*b*) represent best-fits to the data shown, generating the values of E_b plotted as squares in figure 17. The curves in (*c*) and (*d*), on the other hand, are *predictions* of $\nu'(T)$ for higher values of E, based on the weighted average value of E_b shown by the dashed lines in figure 17. Note also that the data in (*d*) are derived from an analysis based on the assumption that the quadratic coefficient ν'' is zero. Model B evidently fits the observed form of $\nu'(T)$ in (*d*) better than model A.

to the five low-temperature field scans. In figures 19 and 20, respectively, we have plotted $\nu_1(E)$ and the quantity

$$\frac{R'p(T)}{2K(T)}\left(\frac{2\pi\hbar^2}{m_3^* k_B}\right)^{\frac{3}{2}},$$

which is both dimensionless and (see § 4 (*c*)) independent of T. The behaviour of these quantities is seen to be qualitatively the same for both models, but model B gives higher values of ν_1, whereas model A gives higher values of $R'p(T)/K(T)$.

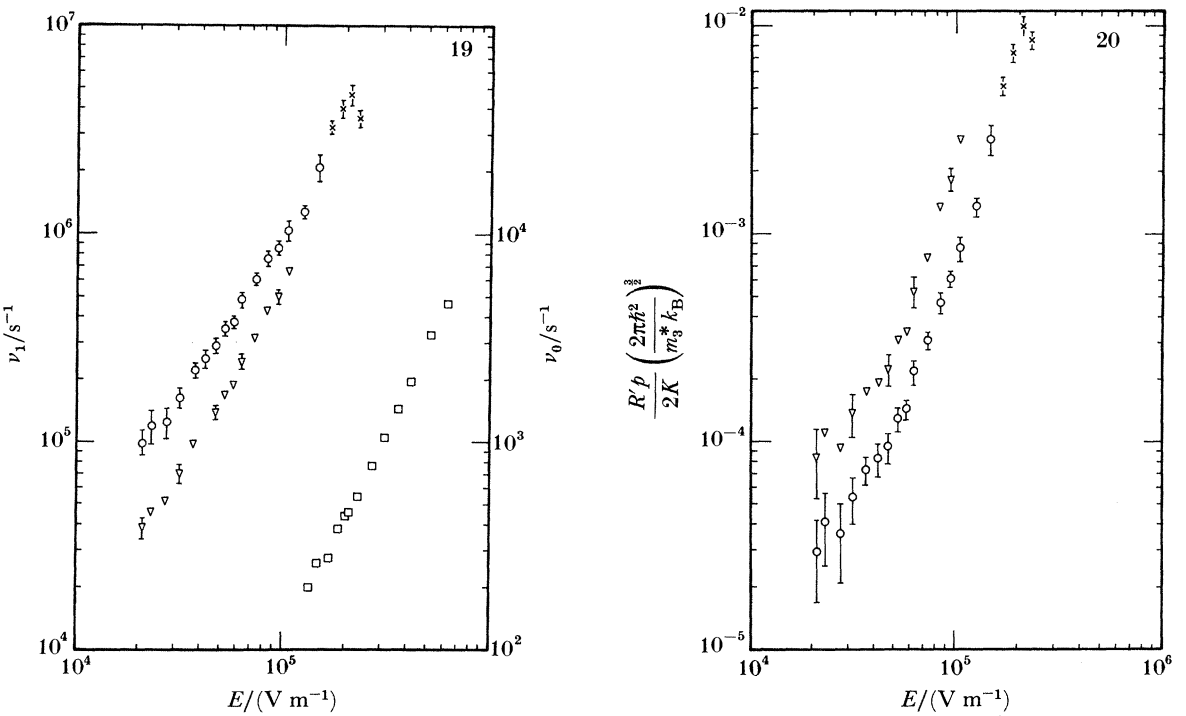

FIGURE 19. Values of ν_1 obtained by fitting to the experimental data model A (triangles) and model B (circles), plotted as a function of electric field E. The squares show, for comparison, values of ν_0 increased by a factor of 100 (see right-hand ordinate scale). Interestingly, $\nu_1/\nu_0 \approx 10^4$. The crosses represent values of ν_1 obtained from model B in high electric fields on the assumption that the coefficient ν'' is zero, that is, the linear approximation.

FIGURE 20. Values of $(R'p/2K)\,(2\pi\hbar^2/m_3^* k_B)^{\frac{3}{2}}$ plotted as a function of electric field E. This quantity is proportional to the ratio of the ^{3}He emission rate (with rotons) to the temperature-dependent part of the ^{3}He capture cross section. The triangles refer to model A and the circles to model B. The crosses represent values obtained from model B in high electric fields on the assumption that the coefficient ν'' is zero, that is, the linear approximation.

In low fields the error is relatively large owing to the large scatter in the experimental data. At high fields the data are more accurate and, although we are able to determine the product $(\nu_1-\nu_0)\,K(T)/R'p(T)$ very accurately, the individual values of ν_1 and $R'p(T)/K(T)$ are less accurately known. This is because they are determined by the variation of ν' with T, and in high fields this variation is relatively weak.

Clearly, both ν_1 and $R'p(T)/K(T)$ can be fitted by smooth curves, which could then be used to generate values of these parameters at other fields. In practice, however, we have found that plotting graphs of $(\nu_1-\nu_0)/E$ and

$$\frac{R'p(T)}{2K(T)}\left(\frac{2\pi\hbar^2}{m_3^* k_B}\right)^{\frac{3}{2}}(\nu_1-\nu_0)^{-1}$$

as functions of E is preferable, as shown in figures 21 and 22 respectively, since these quantities vary less rapidly with E. By drawing smooth curves through the points of figures 21 and 22 we acquire a basis for predicting the values of ν' which should be observed at any given temperature (values of $p(T)$ being given in figure 11) and field. In figure 23 (a)–(d), we compare values of ν' predicted in this way (curves) with the experimental data (points). As we would expect, since we used these data to fit the model, the agreement is excellent. The dashed extensions of the curves are based not on figures 21 and 22 as illustrated, but on reasonable extrapolations of the curves in those figures.

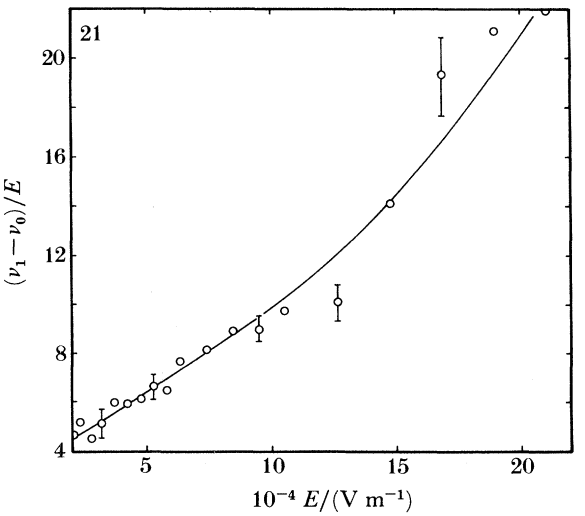

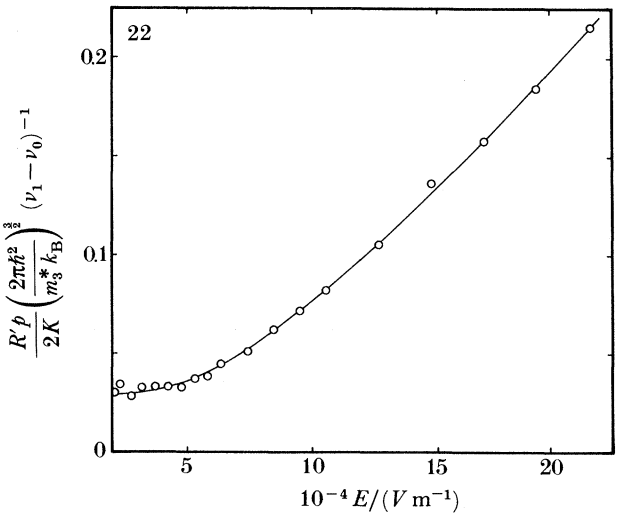

FIGURE 21. Values of $(\nu_1-\nu_0)/E$ for model B. The full curve drawn through the data has been used, together with that from figure 22, to generate the curves shown in figures 23 and 24.

FIGURE 22. The quantity $(R'p/2K)\,(2\pi\hbar^2/m_3^* k_B)^{\frac{3}{2}}(\nu_1-\nu_0)^{-1}$ plotted as a function of electric field E. The full curve drawn through the data has been used, together with that from figure 21, to generate the curves shown in figures 23 and 24.

(d) *Extension to higher temperatures*

A more stringent test of our model is to see how well it can cope with data at higher temperatures. Before we can do this, however, two additional matters require consideration: the effects of roton scattering on the velocity distribution; and the possible influence of roton-assisted vortex nucleation (see III) on ions that possess a bound ^{3}He atom.

The effects of roton scattering on the velocity distribution have been treated previously (III). It was found that they could be compensated for by introducing an effective electric field,

$$E' = E - k(T)\,\bar{v}, \tag{5.4}$$

where $k(T)$ is a temperature-dependent drag factor. We can use the values of $k(T)$ given in III to calculate the effective field, E', and then find interpolated values of ν_1 and R'/K from figures 21 and 22.

In relation to possible problems with roton-assisted vortex nucleation, we may expect that, because so few ^{3}He atoms are bound to the ion at higher temperatures, any such effects will be of negligible importance. To illustrate this, we may consider a field of 2.03×10^5 V m^{-1} at a temperature of 0.69 K, where the value of ν_1 is about 4×10^6 s^{-1} and the value of ν' is about 9.5×10^9 s^{-1}. Even at the highest concentration, $x_3 = 1.7\times10^{-7}$, we find that n_b is only

PHILOSOPHICAL TRANSACTIONS OF THE ROYAL SOCIETY A MATHEMATICAL, PHYSICAL & ENGINEERING SCIENCES

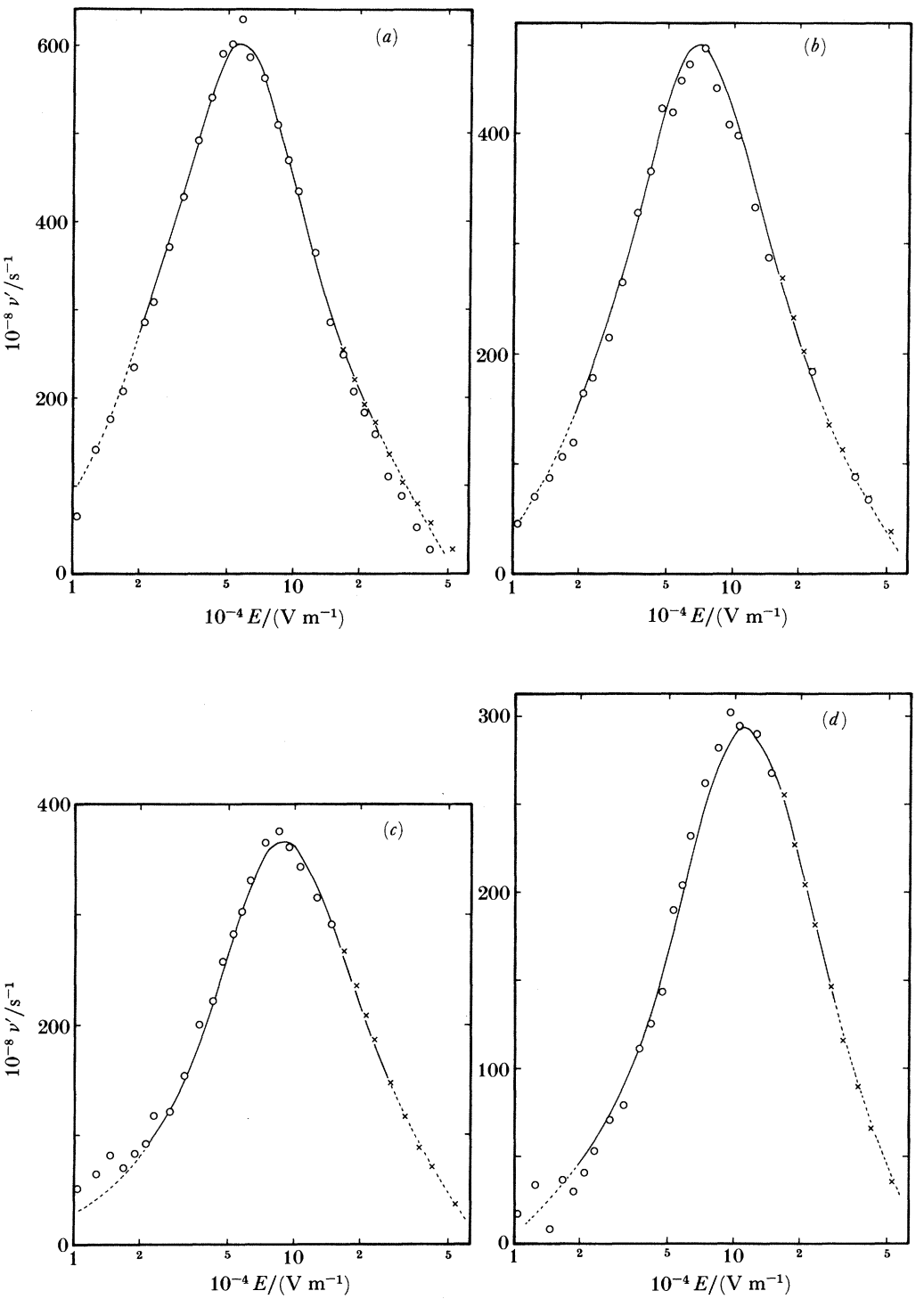

FIGURE 23. Values of the coefficient ν' as a function of electric field E generated from the curves of figures 21 and 22 (full curves) compared with those derived from an analysis of experimental field scan data (points). The crosses were obtained on the assumption that ν'' is zero for $E > 1.5 \times 10^5$ V m^{-1}. The dashed lines represent values of ν' calculated from plausible extensions made to the curves shown in figures 21 and 22. The four temperatures at which the comparisons are made are: (*a*) $T = 0.329$ K; (*b*) 0.369 K; (*c*) 0.414 K; (*d*) 0.458 K.

ca. 4×10^{-4}. Now, the magnitude of ν_r, the roton-assisted nucleation rate for this temperature, is *ca.* 2800 s^{-1}. If this process were completely blocked by the presence of a ^{3}He atom on the ion, the observed fall in the measured nucleation rate would be only about 1 s^{-1}; that is, very much less than the random error in the data. Of course, the bound ^{3}He atom might conceivably have the opposite effect and actually promote the roton-assisted process, but such an effect would clearly have to be extremely large to affect the data noticeably.

Apparently, then, although we cannot rule out the possibility of bound ^{3}He atoms affecting the roton-assisted process, it is extremely unlikely that we would need to make any explicit allowance for it. In the light of these considerations, it is reasonable to feel some confidence that our model should also be capable of accounting for the higher temperature data and that, if so, this will provide a reassuring demonstration of its validity. First we look at the field scans taken at 0.508, 0.549 and 0.608 K (figure 24), where the crosses refer to values of ν' calculated on the assumption that $\nu'' = 0$ and the dashed extension curves have the same significance as before. The predicted curves for $T = 0.508$ and 0.549 K can be seen to fit excellently over the whole range of fields. However, the curve for $T = 0.608$ K exhibits a rather curious discrepancy in that much better agreement is obtained with values of ν' obtained from linear fits to (5.1), even at the lower fields. This may be due simply to the fact that ν'' will be small for all fields at this high a temperature and consequently highly susceptible to any random errors in the data. However, the way in which allowance for finite ν'' in the determination of ν' leads to values which fall consistently below the predicted curve is surprising and the reasons are not understood at present.

Another test we can apply to our model is to produce predicted curves for $\nu'(T)$ at the four fields used in our temperature scans. Of course, we have already seen the fits at low temperature (figure 18), but we are now able to extend these so as to cover the whole temperature range in each case.

To predict values of $\nu'(T)$, we have worked out E' for each data point, obtained values of $R'(E')/K$ and $\nu_1(E')$ from figures 21 and 22, and then used these to give $\nu'(T)$. The results are shown in figure 25, where once again we have indicated by crosses the value of ν' obtained by using a linear fit at higher temperatures. (For $E = 2.03 \times 10^5$ V m^{-1} only the linear fit is indicated.) Agreement is excellent except at the highest field, where the predicted curve does not fall quite rapidly enough. As before, we interpret this discrepancy as being due to deficiencies in our simplistic model of $K(T)$. Bearing in mind, however, that we have now extended our comparison to cover the entire experimental temperature range, we believe that the high level of agreement obtained can be construed as providing strong support for our model.

(*e*) *Critical velocity for the creation of the vortex rings*

One of our principal motivations for studying the concentration dependence of the nucleation rate has been the hope that this will provide some clues to the nature of the microscopic processes involved in vortex-ring creation. We shall include some speculative remarks on this topic in §6 (*e*) but, first, we need to illustrate how our model, explaining the influence of ^{3}He impurities, can provide what may turn out to be highly relevant information.

In III it was suggested that the measured nucleation rate, ν, in pure ^{4}He is given by

$$\nu(E) = \int_0^\infty \mathscr{R}_v(v) f(v, E)\, \mathrm{d}v, \tag{5.5}$$

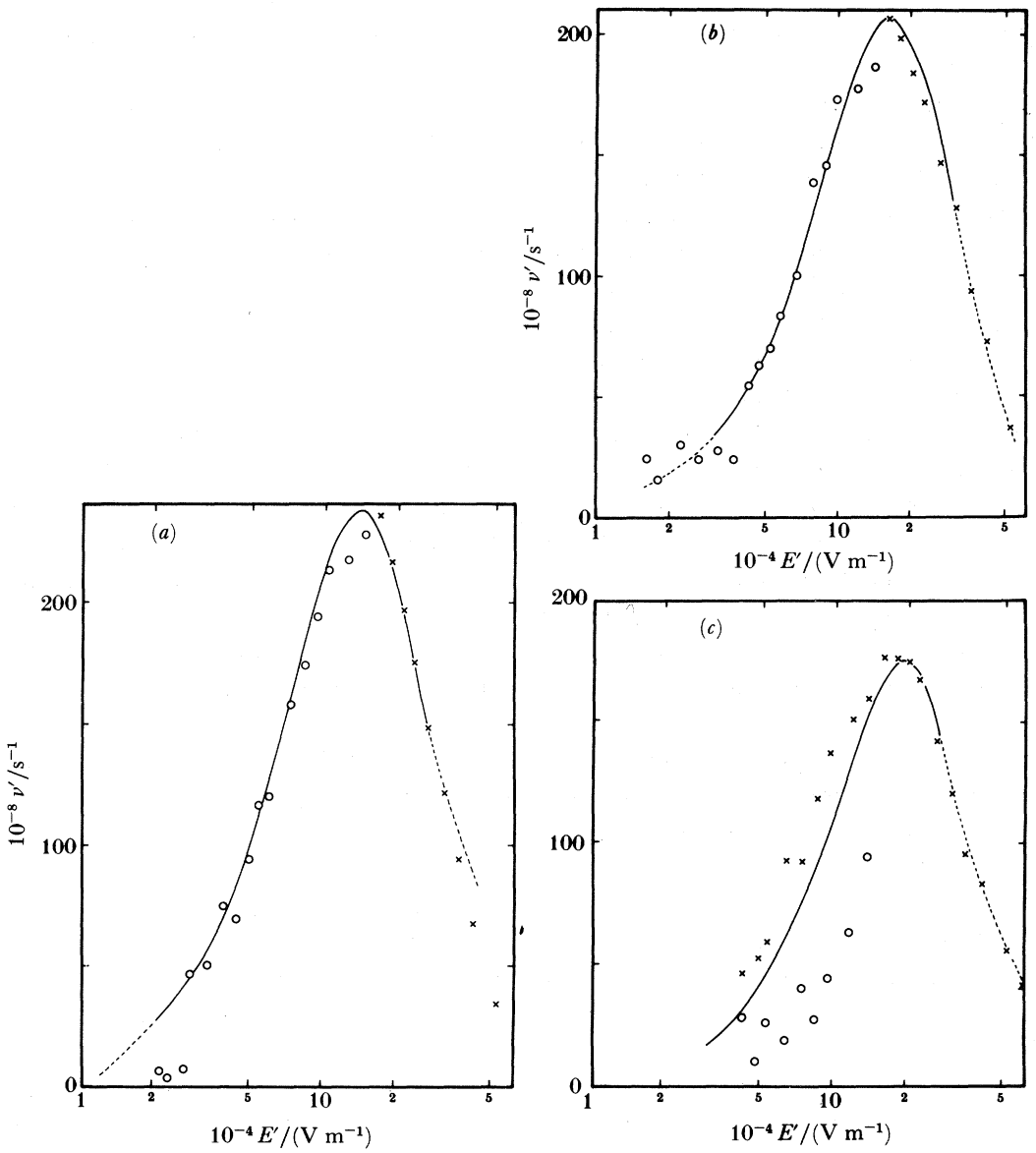

FIGURE 24. Values of the coefficient ν' as a function of the reduced electric field E', as discussed in the text. The full curves, generated from those in figures 21 and 22, are compared with values of ν' derived from experimental field scan data (points). The crosses were obtained on the assumption that ν'' is zero, that is, the linear approximation. The dashed lines represent values of ν' calculated from plausible extensions made to the curves shown in figures 21 and 22. The three temperatures at which the comparisons are made are: (*a*) $T = 0.508$ K; (*b*) 0.549 K; (*c*) 0.606 K.

where $f(v, E)$ is the ionic distribution function, and $\mathscr{R}_{\mathrm{v}}(v)$ is the intrinsic nucleation rate,

$$\mathscr{R}_{\mathrm{v}}(v) = \mathscr{R}_0\,\theta(v - v_{\mathrm{c}}). \tag{5.6}$$

Here, v_{c} is a critical velocity for the nucleation process, $\mathscr{R}_0$ is a characteristic rate, and θ is the unit step function.

In fitting our model of the ^{3}He-influenced process we have been able to derive values of the

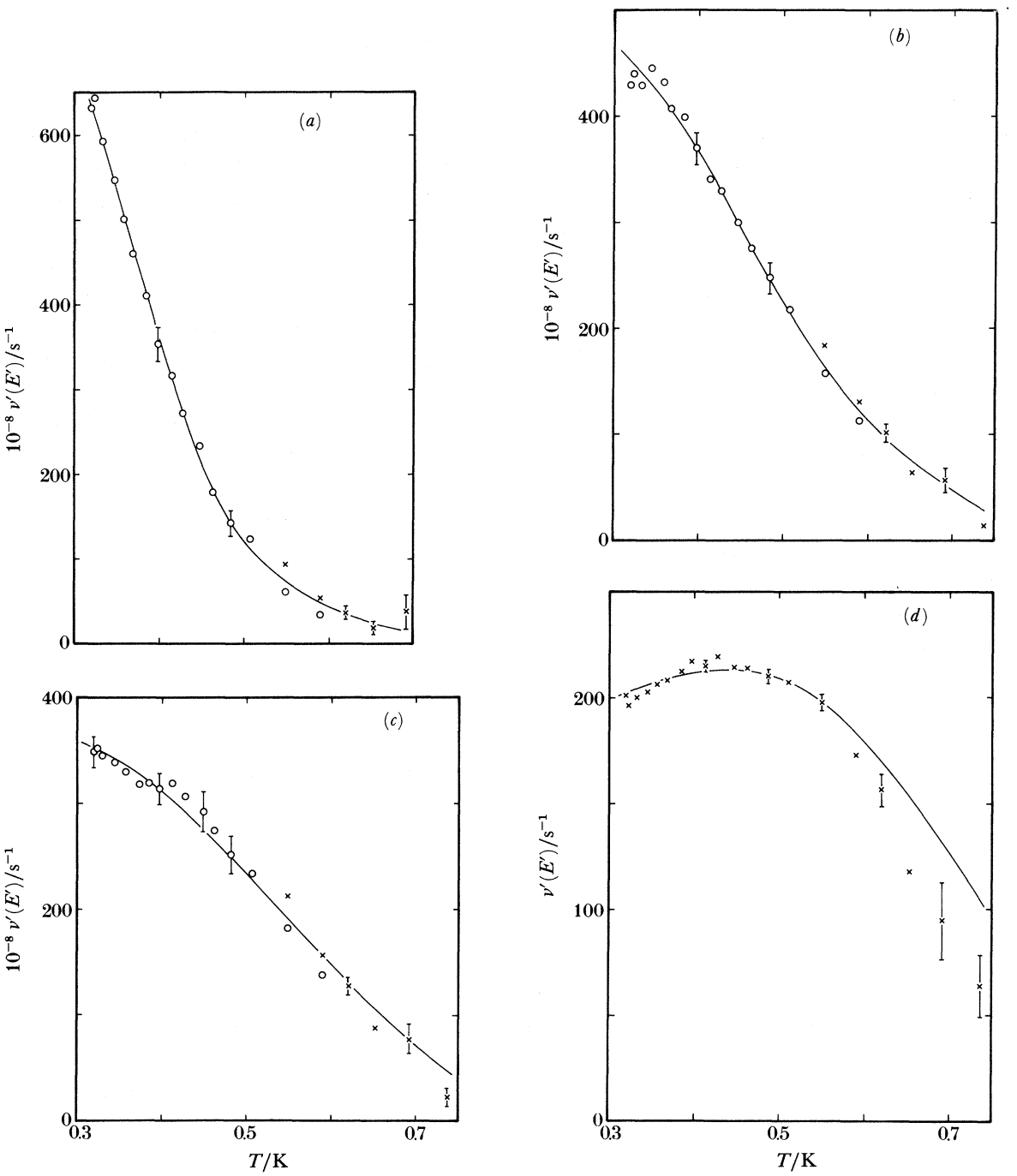

FIGURE 25. Values of the coefficient ν' predicted for temperatures T of up to 0.7 K (full curves) compared with experimental values (points). The theoretical values were calculated through use of the reduced electric field E' in conjunction with the curves shown in figures 21 and 22. The crosses were derived from experimental measurements on the assumption that ν'' was zero, that is, the linear approximation. The electric fields for which the comparisons are made are; (*a*) $E = 5.81 \times 10^4$ V m^{-1}; (*b*) 1.05×10^5 V m^{-1}; (*c*) 1.35×10^5 V m^{-1}; (*d*) 2.03×10^5 V m^{-1}. The deviations between theory and experiment at high temperatures in (*d*) are believed to arise because of a deficiency in the model used for $K(T)$.

quantity $\nu_1(E)$, the nucleation rate for ions with a bound ^{3}He atom. By analogy, therefore, it seems natural to write,

$$\nu_1(E) = \int_0^\infty \mathscr{R}_{v1}(v) f_b(v_3', E)\, dv \tag{5.7}$$

where

$$\mathscr{R}_{v1} = \mathscr{R}_1 \theta(v - v_{c1}), \tag{5.8}$$

v_{c1} being the critical velocity for vortex nucleation in the presence of a bound ^{3}He atom, $f_b(v_3', E)$ is the distribution function for ions with a bound ^{3}He atom, and $\mathscr{R}_1$ is the corresponding rate.

We can attempt to fit (5.7) to the data shown in figure 19. The best fitting curves give a value of *ca.* 57 m s^{-1} for v_{c1} (57.3 m s^{-1} for model A and 56.8 m s^{-1} for model B), whereas for a bare ion the corresponding critical velocity is 60.7 m s^{-1}. We have assumed here that $f_b(v_3', E)$ is the same as for bare ions. The quantity governing the size of the nucleation rate, $\mathscr{R}_1$, is found to be more sensitive to the model used; we find $\mathscr{R}_1 = 3.6 \times 10^6$ s^{-1} for model A and $\mathscr{R}_1 = 4.8 \times 10^6$ s^{-1} for model B. In either case, the value is very much larger than the corresponding quantity, $\mathscr{R}_0$, for bare ions, which (see III) is *ca.* 2.6×10^3 s^{-1}. Although these figures cannot be taken as being wholly reliable, since we have had to guess at the form of $f_b(v, E)$, they do at least indicate that the presence of a bound ^{3}He atom has the dual effect of lowering the critical velocity for vortex creation *and* of increasing the characteristic rate. In §6 (*e*) we will offer some tentative suggestions as to why this may occur.

Another interesting quantity that appears in our model is the rate of emission R', of a ^{3}He atom with a pair of rotons. Although knowledge of this quantity would not in itself appear to shed very much light on the vortex creation process it should be of assistance in checking the consistency of our model since, on account of the higher critical velocity required for this process, we would expect R' to be smaller than the corresponding rate for ordinary two-roton emission. Knowledge of the emission rate would also enable us to judge which of our models is superior as this quantity, in particular, responds to the distinctions between them. Unfortunately, however, the analysis we have so far presented only provides us with information regarding the ratio R'/K, and does not enable us to extract values of the individual quantities from the data.

In the next section we shall see how analysis of the quadratic term in (5.1) allows us to evaluate R' and K separately. We shall therefore defer further discussion of the emission rate until §6 (*d*).

6. Further discussion

The discovery that $\nu(x_3)$ curves *upwards* (figure 8 (*a*)) came as a considerable surprise. Physical intuition had suggested that the presence of the first bound ^{3}He atom would provide the greatest modification to the system whereas the addition of a second ^{3}He atom would be of relatively minor consequence. On the contrary, however, the experimental results can be taken to indicate that the presence of a second ^{3}He atom has a disproportionately large effect.

In this section we extend our model so as to be able to accommodate effects arising from the presence of the second ^{3}He atom; and we fit it to the measured values of ν'', thereby obtaining explicit values of K and R'. We conclude with a brief speculative discussion of the results in the general context of the theories of vortex nucleation summarized in §1 (*a*).

(*a*) *Nonlinear behaviour*

The quantity which characterizes the nonlinearity of $\nu(x_3)$ is ν'', the coefficient of x_3^2 in (5.1). We illustrated in figure 15 some of the values of $\nu''(E)$ from the four lowest-temperature field

scans. In figure 26 we show values of $\nu''(E)$ for the three lowest temperatures over the complete range of fields. The scatter in the data is quite large, particularly at low fields, and it increases with temperature until, above 0.414 K, the measured values of ν'' are of little use and consequently have not been plotted.

For all three temperatures it appears that $\nu''(E)$ falls with increasing field, reaching zero for $E \geqslant 5\times10^4$ V m^{-1}; although, for $T = 0.329$ K, there is evidence for a possible minimum, with $\nu''(E)$ increasing slightly again at high fields. It is also possible that in high fields $\nu''(E)$ sometimes takes negative values, but the large scatter in the data precludes a definite conclusion on this point. Finally, we note that, at low fields, $\nu''(E)$ seems to have reached a plateau region, where it becomes independent of E.

(*b*) *Theory of the nonlinear terms*

To account for the observed form of $\nu''(E)$ we shall need to extend our model slightly to allow for multiple occupation of the bound states (§1 (*c*)) for ^{3}He atoms on the ion. We start by considering how we should interpret the quantity ν'' in relation to the occupation numbers of these states.

In §4 (*a*) we pointed out that for low concentrations, where $n_b \ll 1$, n_b could be regarded as being the probability that any given ion will have a bound ^{3}He atom. Clearly, since we are now considering ions with two bound ^{3}He atoms, this point of view is no longer tenable and we need to start with a more fundamental approach.

It would appear, at first sight, that the correct way to calculate the probabilities for finding an ion with 0, 1, 2 or more bound ^{3}He atoms is to use the Poisson distribution. If we correctly define n_b as the average number of bound ^{3}He atoms/ion, then the relevant probabilities are

$$P(0) = \mathrm{e}^{-n_b} \approx 1-n_b+\tfrac{1}{2}n_b^2, \tag{6.1}$$

$$P(1) = n_b\,\mathrm{e}^{-n_b} \approx n_b-n_b^2, \tag{6.2}$$

$$P(2) = \frac{n_b^2}{2!}\mathrm{e}^{-n_b} \approx \tfrac{1}{2}n_b^2, \tag{6.3}$$

where we have ignored terms beyond n_b^2. (For $n_b \ll 1$ we have $P(0) \approx 1-n_b$ and $P(1) \approx n_b$, justifying the approach we took earlier.) The measured nucleation rate is then given as

$$\begin{aligned}\nu &= (1-n_b+\tfrac{1}{2}n_b^2)\,\nu_0+(n_b-n_b^2)\,\nu_1+\tfrac{1}{2}n_b^2\,\nu_2\\ &= \nu_0+n_b(\nu_1-\nu_0)+\tfrac{1}{2}n_b^2(\nu_2-2\nu_1+\nu_0),\end{aligned} \tag{6.4}$$

where ν_2 is the instantaneous nucleation rate for an ion with two bound ^{3}He atoms. This equation may be compared with (5.1):

$$\nu = \nu_0+\nu' x_3+\nu'' x_3^2.$$

Since we are considering ions with more than one bound ^{3}He atom we are clearly dealing with relatively large values of n_{eq}. In this case (4.45) becomes

$$n_b \approx \frac{n_3 K}{R'} = x_3\frac{N_A}{V_m}\frac{K}{R'} \tag{6.5}$$

where V_m is the molar volume of ^{4}He and N_A is Avogadro's Number. Thus n_b^2 is proportional to x_3^2 and comparison of (6.4) with (5.1) then gives

$$\nu' x_3 = n_b(\nu_1-\nu_0) \tag{6.6}$$

and

$$\nu'' x_3^2 = \tfrac{1}{2}n_b^2(\nu_2-2\nu_1+\nu_0). \tag{6.7}$$

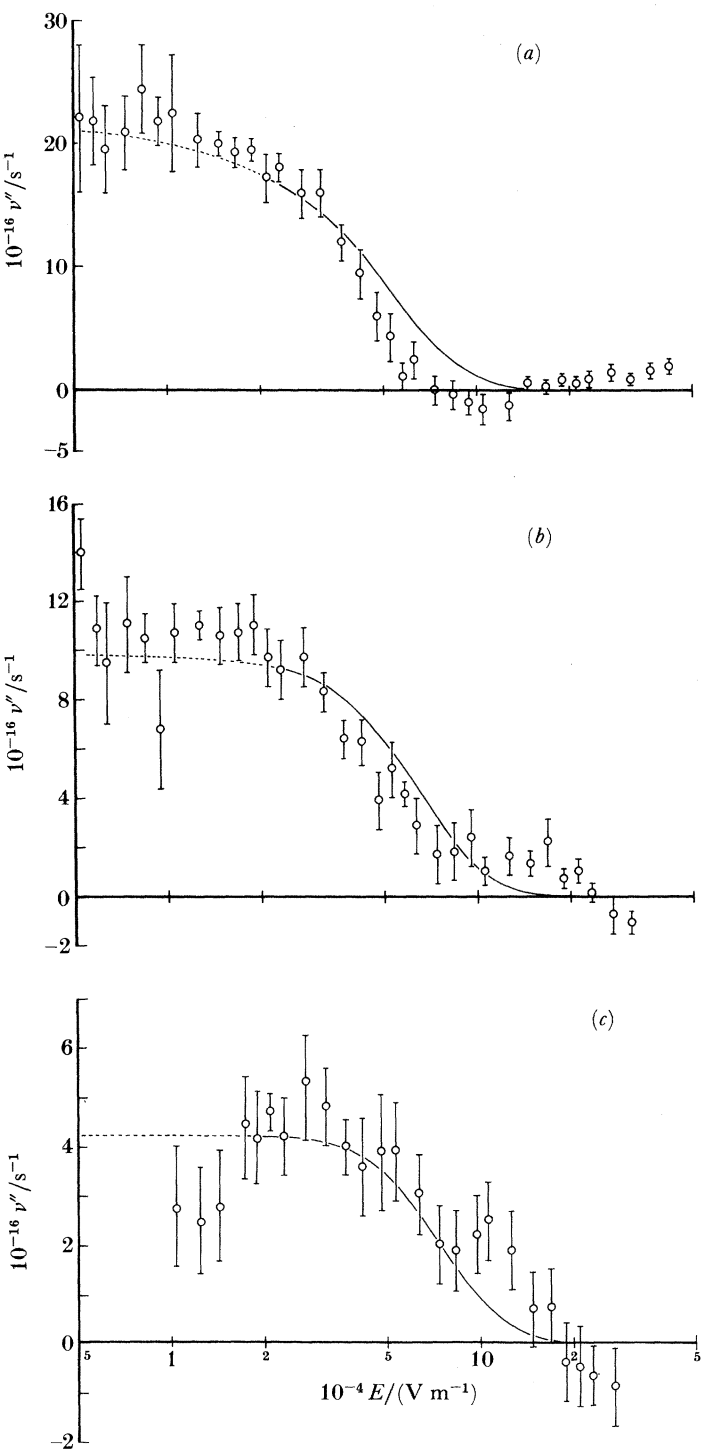

FIGURE 26. Values of the coefficients ν'' from equation (5.1), plotted as a function of the electric field E, for three different temperatures; (*a*) 0.329 K; (*b*) 0.369 K; (*c*) 0.414 K. The curves represent fits of the theory to the data. The dashed sections are based on values of ν_1 and R'/K obtained from extrapolations of the curves in figures 21 and 22.

PHILOSOPHICAL TRANSACTIONS OF THE ROYAL SOCIETY A MATHEMATICAL, PHYSICAL & ENGINEERING SCIENCES

If we now eliminate n_b between (6.6) and (6.7) we find

$$\frac{\nu''}{\nu'^2} = \frac{\nu_2 - 2\nu_1 + \nu_0}{2(\nu_1 - \nu_0)},$$

which should be independent of temperature. In table 2 we give values of ν''/ν'^2 for two fields at four temperatures. It is clear that this ratio is *not* temperature independent and that consequently our approach is, for some reason, unsound.

TABLE 2. VALUES OF ν''/ν'^2

T/K...	0.329	0.369	0.414	0.458
E/(V m^{-1})				
2.74×10^4	$(1.16 \pm 0.33) \times 10^{-4}$	$(2.10 \pm 0.65) \times 10^{-4}$	$(3.6 \pm 2.0) \times 10^{-4}$	$(4.4 \pm 4.4) \times 10^{-4}$
4.21×10^4	$(0.32 \pm 0.10) \times 10^{-4}$	$(0.47 \pm 0.13) \times 10^{-4}$	$(0.73 \pm 0.33) \times 10^{-4}$	$(1.8 \pm 0.9) \times 10^{-4}$

The fallacy in our reasoning stems from the use of the Poisson distribution in determining the probabilities of finding an ion with the appropriate number of bound ^{3}He atoms. By using this probability distribution we have implicitly assumed that the probabilities are independent. We can conceive of three reasons why this might not be so. First, the presence of a single ^{3}He atom on the ion could alter the energy levels for another ^{3}He atom: we could envisage such a phenomenon by analogy with the exchange interaction for atomic electrons. The second possibility is that the emission rate R_1 is affected in some way. In fact, in model B, the emission rate is allowed to vary with the energy of the bound state, so the existence of an 'exchange interaction' could also account for a variation in the emission rate. However, thirdly, there is a simpler explanation as to why R_1 should depend on the number of bound ^{3}He atoms: when there are n bound ^{3}He atoms there are n ways in which the emission of a single ^{3}He atom can take place and hence the emission rate becomes nR. In what follows we shall only consider this effect on the emission rate since there are reasons to believe that other effects, such as a shift in the energy levels, will be small.

We can now return to our original problem. Instead of trying to determine the probability of an ion possessing m bound ^{3}He atoms, let us simply suppose that the fraction of ions with m bound ^{3}He atoms is N_m and that their vortex nucleation rate is ν_m. We then have

$$\nu = \sum_{m=0}^{\infty} N_m \nu_m, \tag{6.8}$$

where the quantities N_m satisfy the constraint

$$\sum_{m=0}^{\infty} N_m = 1. \tag{6.9}$$

The quantity N_0, the fraction of ions which are bare, is of order unity, whereas $N_1 \approx n_b$, which is linear in n_3. We shall now show that a self-consistent approximation is to take the term N_m to be of leading order n_3^m. The advantage of this approach is that it will enable us to expand (6.8) in a power series in n_3. We can then identify the term varying as n_3^2 as being proportional to $\nu''(E)$.

We now need to consider the rates of creation of ions with m bound ^{3}He atoms. In §4 (b) we found that the total rate of absorption, via process 1, of single bound ^{3}He atoms on to bare ions was given by

$$\bar{R}_a = n_3 K(1 - n_b/n_{eq}),$$

where

$$n_{eq} = [1 + \exp\{\beta(E_B - \mu)\}]^{-1}$$

and it was assumed that $n_b \ll 1$, an assumption which in the circumstances now being considered is no longer tenable.

The origin of the term $1-n_b/n_{eq}$ lies (see equation (4.20)) with the factor $1-n_b-n_b \exp\{\beta(E_B-\mu)\}$, which is proportional to $\bar{R}_a$. In our present notation we can replace $1-n_b$ with N_0, the fraction of bare ions, and n_b with N_1, the fraction of ions with one bound ^{3}He atom. We then have

$$\bar{R}_{a1} \propto N_0 - N_1 \exp[\beta(E_B-\mu)] \tag{6.10}$$

for the rate of absorption of single ^{3}He atoms onto bare ions. In general this will become

$$\bar{R}_{am} \propto N_m - (m+1)\, N_{m+1} \exp\{\beta(E_B-\mu)\} \tag{6.11}$$

for the absorption of single ^{3}He atoms onto ions with m bound ^{3}He atoms; the factor $m+1$ expresses the fact that there is a choice of which ^{3}He atom is emitted in the desorption process.

Some important assumptions are involved here. First, we have assumed that the energy levels are unaltered by the presence of m bound ^{3}He atoms and, in fact, that the binding energy is the same for all the bound atoms. According to the discussion of §1 (*c*), such an assumption is obviously unjustified but, as we shall soon see, in the final analysis, we only need to consider up to two bound ^{3}He atoms, in which case the assumption is not unreasonable. Secondly, we are assuming that the absorption rate per unit number density, K, is independent of the number n_b of bound ^{3}He atoms. We have effectively done this already in §4 (*e*), where we assumed that K was independent of the energy level, l, of the bound state, so again, this is not unreasonable. Thirdly, we shall also be assuming in what follows that processes involving the simultaneous absorption or desorption of two or more ^{3}He atoms can be neglected.

Let us now consider the total rate of ^{3}He trapping, involving the absorption of single ^{3}He atoms onto ions that already possess 0, 1, 2 etc. bound ^{3}He atoms. This is just the sum over the individual processes involving m bound ^{3}He atoms and so (6.11) becomes:

$$\begin{aligned}\bar{R}_{aT} &\propto \sum_{m=0}^{\infty} [N_m - (m+1)\, N_{m+1} \exp\{\beta(E_B-\mu)\}] \\ &\propto \sum_{m=0}^{\infty} N_m - \exp\{\beta(E_B-\mu)\} \sum_{m=1}^{\infty} m N_m .\end{aligned} \tag{6.12}$$

Now, we know $\sum_{m=0}^{\infty} N_m = 1$, (6.9), and it is clear that $\sum_{m=1}^{\infty} m N_m$ is just the average number of bound ^{3}He atoms per ion. In the steady state this is simply the equilibrium number of bound ^{3}He atoms, i.e. n_{eq}. Since in equilibrium we must have $\bar{R}_{aT} = 0$, we have

$$\bar{R}_{aT} \propto 1 - n_{eq} \exp\{\beta(E_B-\mu)\} = 0, \tag{6.13}$$

which gives us a new expression for n_{eq}:

$$n_{eq} = [\exp\{\beta(E_B-\mu)\}]^{-1}. \tag{6.14}$$

We have neglected to allow for the exclusion principle in deriving this expression and consequently it is only valid in the non-degenerate limit. Since we shall not need to consider more than two bound ^{3}He atoms on the ion, this is probably a reasonable approximation. If we were to allow for degeneracy then we would find

$$n_{eq} = [1 + \exp\{\beta(E_B-\mu)\}]^{-1},$$

i.e. the expression we originally derived for $n_b \ll 1$. For the lowest temperature of 0.32 K and the highest concentration of 1.7×10^{-7} the error produced in using equation (6.14) is found to be only *ca.* 1% and hence we shall use equation (6.14) for n_{eq} in all that follows.

Equation (4.22) for the absorption of a single ^{3}He atom onto a bare ion now becomes:

$$\bar{R}_{a1} = n_3 K(N_0 - N_1/n_{eq}) \tag{6.15}$$

or, in general, $$\bar{R}_{am} = n_3 K\{N_m - (m+1)\, N_{m+1}/n_{eq}\}.$$

Having derived an expression for the rate of absorption of a ^{3}He atom onto an ion with m bound ^{3}He atoms, we can now consider the processes involved in the creation of an ion with m bound ^{3}He atoms. We need to consider four processes: two involving the creation of the state, and two involving its destruction. An ion with m bound ^{3}He atoms can be created via the absorption of a ^{3}He atom onto an ion with $m-1$ bound ^{3}He atoms, this process occurring at a rate $n_3 K(N_{m-1} - mN_m/n_{eq})$, and also by emission (with rotons, as in §4 (*d*)) of a ^{3}He atom from an ion with $m+1$ bound ^{3}He atoms, this occurring at a rate $(m+1)\, N_{m+1} R_{m+1}$, where the emission rate, R_e, is allowed to vary with the number of bound ^{3}He atoms, and the factor $m+1$ expresses the choice of which of the $m+1$ bound ^{3}He atoms is to be emitted. The two ways in which an ion with m bound ^{3}He atoms can be lost are: first, the absorption of a further ^{3}He atom, this process occurring at a rate $n_3 K\{N_m - (m+1)\, N_{m+1}/n_{eq}\}$; and, second, the emission of a bound ^{3}He atom, this occurring at a rate $mN_m R_m$.

In the steady state, the net rate of creation will be equal to the loss via vortex ring creation and we therefore have

$$n_3 K(N_{m-1} - mN_m/n_{eq}) + (m+1)\, N_{m+1} R_{m+1} - n_3 K\{N_m - (m+1)\, N_{m+1}/n_{eq}\} - mR_m N_m = N_m \nu_m. \tag{6.16}$$

We have set out to show that N_m is of leading order n_3^m. Rearrangement of (6.16) gives

$$N_m = \frac{z_m}{m}\left[N_{m-1} + \frac{(m+1)\, N_{m+1} R_{m+1}}{n_3 K} - \left\{N_m - \frac{(m+1)\, N_{m+1}}{n_{eq}}\right\}\right], \tag{6.17}$$

where $$z_m = \left(\frac{1}{n_{eq}} + \frac{R_m + \nu_m/m}{n_3 K}\right)^{-1}. \tag{6.18}$$

Now, z_m is linear in n_3 regardless of m and so (6.17) shows that N_m is of leading order n_3^m, provided N_{m-1} is of leading order n_3^{m-1}. However, we know that N_1 is of leading order n_3^1, so the result we require follows by induction.

After a little algebra, and making appropriate comparisons with (5.1), we find (Appendix E) that, for the order of approximation within which we are working,

$$\nu' x_3 = (\nu_1 - \nu_0)\, z_1 \tag{6.19}$$

and

$$\nu'' x_3^2 = \frac{n_3 K z_1}{1 + 2n_3 K/z_1 \nu_2} - 2z_1^2(\nu_1 - \nu_0). \tag{6.20}$$

(*c*) *Fit to the data*

To fit (6.20) to the experimental data, we need to obtain values of z_1. We can do so with the aid of (6.19) and the values of ν' and ν_1 obtained from fitting model B to the $\nu'(E)$ data. Substitution of (6.19) into (6.20) and use of $K = \sigma \bar{v} p(T)$ gives, after rearrangement,

$$\frac{p(T)\, \nu'}{(\nu_1 - \nu_0)\, \nu'' + 2\nu'^2} = \frac{1}{G} + \frac{2p(T)}{\nu_2}\frac{(\nu_1 - \nu_0)}{\nu'}, \tag{6.21}$$

where $G = n_4 \bar{v} \sigma$.

By plotting $p(T)\,\nu'/[(\nu_1-\nu_0)\,\nu''+2\nu'^2]$ against $p(T)\,(\nu_1-\nu_0)/\nu'$, we then obtain a straight-line graph with an intercept, $1/G$, from which we can calculate the effective absorption cross-section, $\lambda\sigma_g$, and a slope $2/\nu_2$. The intercept G^{-1} should be essentially temperature-independent and only weakly dependent on field, whereas the slope should decrease if, as may be expected by analogy with ν_0 and ν_1, ν_2 increases with field.

Unfortunately, only a very limited range of data are worth plotting in this way, we believe. For low fields, the errors in ν'' are large, whereas, for higher fields, ν'' falls sharply towards zero so that although the absolute errors may be small, the relative errors are quite large. We have therefore restricted our attention to just four electric fields in the range 2×10^4 to 4×10^4 V m^{-1}, where ν'' is reasonably large and the errors, in consequence, are relatively small. The available range of temperatures is also severely restricted: we find that large enough values of ν'' are available only at the three lowest temperatures of 0.329, 0.369 and 0.414 K. The data in question have been plotted in figure 27. For each temperature it should in principle be possible

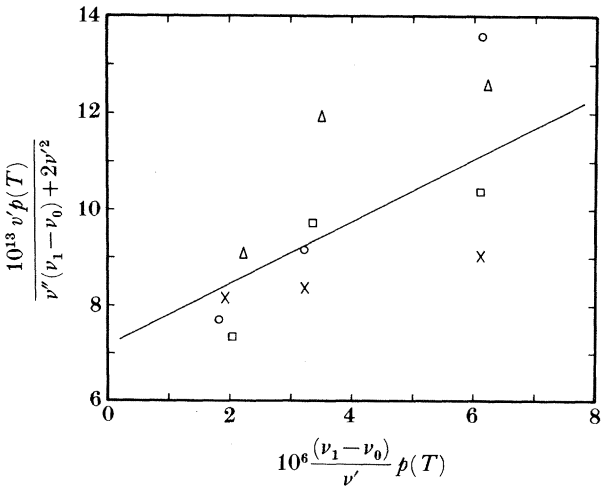

FIGURE 27. Data plotted so as to enable a value of σ to be derived from equation (6.21), as described in the text. The circles, crosses, squares and triangles correspond, respectively, to measurements made in electric fields of 2.32×10^4, 2.74×10^4, 3.16×10^4 and 3.69×10^4 V m^{-1}.

to draw a best-fitting straight line to obtain four values of $\nu_2(E)$. In fact, however, the scatter is such that this exercise would be fruitless. Instead, we have chosen to fit a single straight line to all the data, thereby obtaining a value of ν_2 averaged over the four fields. We find $\nu_2 = 3\times10^7$ s^{-1}, with an estimated error of 50 %.

For the intercept, on the other hand, only a weak variation with field is to be expected: an average value for this quantity is therefore far more acceptable and can be determined with much greater accuracy. For model B we find for the effective absorption cross-section, $\sigma = 1.06\pm0.5$ nm^2 which, as anticipated, is considerably smaller than the geometric cross-section of *ca.* 3.50 nm^2.

We can use these values of ν_2 and σ to predict values of $\nu''(E)$. We do not know for certain how, or even if, ν_2 varies with field; but we shall proceed on the assumption that ν_2 is independent of field and take the average value we have obtained in the range $2\times10^4 < E < 4\times10^4$ V m^{-1}. The real test of our model is how well we are able to predict the data at higher and lower fields. Theoretical curves, based on model B, are shown in

figure 26 (*a*)–(*c*). The dashed line indicates the expected behaviour (extrapolated by extending the curves of figures 21 and 22) in low fields where we have no accurate values of $\nu_1(E)$ or $\nu'(E)$. It can be seen that relatively poor agreement is obtained with the lowest-temperature data (figure 26 (*a*)) for fields around 7×10^4 V m^{-1}. The reason for this discrepancy is not clear. However, if we remember, first, that we have had to rely on a two-parameter fit over a narrow range of fields, and, secondly, that we have assumed (probably unjustifiably) that ν_2 is independent of field, the agreement can actually be regarded as being surprisingly good.

In §5 we obtained values of ν' for high temperatures and/or high fields on the assumption that $\nu''=0$. We can now see that this assumption was entirely justified. For fields above 1.5×10^5 V m^{-1}, ν'' is typically *ca.* 0.17×10^{16} s^{-1}; so the assumption of $\nu''=0$ would lead to an overestimate of ν' by *ca.* 3×10^8 s^{-1}, which is much less than the experimental error. Similarly, it can be seen from figure 26 (*a*)–(*c*) that ν'' falls rapidly with increasing temperature. The effect of ignoring ν'' for temperatures above 0.55 K is to overestimate ν' by, at the most, 7×10^8 s^{-1}, which is again well within the experimental error.

(*d*) *Rate of emission of* ^{3}He *with a pair of rotons*

We found in §5 that it was possible only to determine the ratio R'/K, rather than the two quantities by themselves. Now that we have determined σ, and hence K, we are in a position to obtain absolute values of the ^{3}He emission rate $R_e(E)$.

Before discussing these values let us return to consider some of the assumptions we made concerning $R_e(E)$ in §4. In particular, we assumed that this emission rate has the same form as that for two-roton emission,

$$R(v) = R_r(v-v')^2 \tag{6.22}$$

and hence that

$$R(E) = \int_0^\infty f_b(v,E)\, R_r(v-v')^2\, \mathrm{d}v, \tag{6.23}$$

where $f_b(v,E)$, the distribution function for ions with bound ^{3}He atoms, is identical to $f(v,E)$, the distribution function for bare ions. We are now in a position to test this hypothesis but, before we do so, we shall find it helpful to make one further assumption. We shall take the rate constant, R_r, to be the same for ^{3}He emission as it is for ordinary roton-pair emission. Consequently, the difference between the two processes arises only through their different critical velocities.

Using the value of σ obtained for model B together with the values of R'/K deduced in §5, we are able to extract values of $R_e(E)$. These are shown in figure 28, divided by $eE/2\hbar k_0$, the average rate of roton pair emission, as a function of E. It is encouraging to note, first, that the ratio is less than unity (implying that ^{3}He emission is less frequent than roton-pair emission), and secondly, that it is an increasing function of E, both results being entirely in accord with our expectations.

If the rather bold assumptions we have made are correct, then it should be possible to predict values of $R_e(E)$. In low fields the distribution function can be determined analytically (Bowley & Sheard 1977) as

$$f(v,E) = \frac{m_i}{2\hbar k_0}\exp\left\{-\frac{R_r\, m_i (v-v')^3}{3eE}\right\};\quad v>v'. \tag{6.24}$$

We then expect to find

$$R_e(E) = \int_{v_{c3}}^\infty \mathrm{d}v\, \frac{R_e\, m_i}{2\hbar k_0}(v-v_{c3})^2 \exp\left\{-\frac{R_r\, m_i (v-v')^3}{3eE}\right\}. \tag{6.25}$$

PHILOSOPHICAL TRANSACTIONS OF THE ROYAL SOCIETY A MATHEMATICAL, PHYSICAL & ENGINEERING SCIENCES

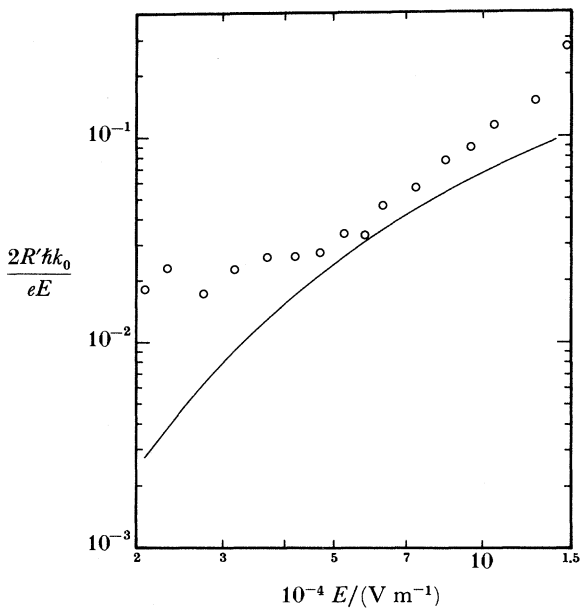

FIGURE 28. Ratio of the ^{3}He emission rate to the roton pair creation rate, plotted as a function of electric field E. The full curve represents a theoretical prediction, based on the assumptions described in the text.

Putting $y = (v - v_{c3})\ (R_r\, m_i/eE)^{\frac{1}{3}}$, we then have

$$R_e(E) = \frac{eE}{2\hbar k_0}\int_0^\infty \mathrm{d}y\, y^2 \exp\{-\tfrac{1}{3}(y+d)^3\}, \tag{6.26}$$

where

$$d = \left(\frac{R_r\, m_i}{eE}\right)^{\frac{1}{3}}(v_{c3} - v') \approx \left(\frac{R_r\, m_i}{eE}\right)^{\frac{1}{3}}\frac{|E_B|}{2\hbar k_0},$$

using the result of §4. All the parameters in (6.26) are known, so it is possible to evaluate $R_e(E)\ 2\hbar k_0/eE$ as a function of field, as shown by the solid line in figure 28.

Bearing in mind the crudity of the model, the level of agreement obtained is acceptable. The discrepancy in high fields is to be expected since the analytic formula for $f(v, E)$ is then no longer applicable. In low fields the experimental values of $R_e(E)$ are likely to be subject to large errors since the emission rate has little effect on the number of bound ^{3}He atoms, and $\nu(E)$ is consequently rather insensitive to $R_e(E)$. For fields of *ca.* 6×10^4 V m^{-1}, the predicted curve gives values lying within 20% of the experimental data. This level of agreement is actually far better than we had any right to expect; and it suggests that our simple model does, in fact, bear a fairly close resemblance to reality.

(*e*) *Implications for the microscopic mechanism of vortex nucleation*

The excellent fit that has been obtained between the model (particularly version B) and the data can be taken as constituting strong support both for its premises and for the conclusions that arise from it. Thus, we may now regard the following two points, among several others, as having been reasonably well established; first, that ^{3}He influences ν through the action of (for the present experimental ranges of x_3 and T) one, or sometimes two, ^{3}He atoms trapped on the surface of the ion; and, secondly, that the presence of a single trapped ^{3}He atom has

the dual effect of reducing the critical velocity for vortex nucleation by *ca.* 4 m s^{-1}, while simultaneously increasing the relevant rate constant by a factor of *ca.* 10^3. It is interesting to speculate on the implications of these findings for the microscopic models of the vortex nucleation mechanism that were discussed in §1 (*a*).

Before doing so, we may note immediately that we can set aside any suggestion that the changes in ν arise purely, or even mainly, from changes in the ionic radius: the effect of a single ^{3}He atom on the surface tension, and hence on the radius of the ion, would clearly be negligible.

A possible explanation (W. F. Vinen, personal communication) for the decrease in the critical velocity for an ion with an adsorbed ^{3}He atom is that the vortex ring or loop can then form with the ^{3}He atom trapped on its core, thereby reducing its energy, and consequently also reducing the critical velocity needed for its creation. The magnitude of such an effect would presumably be a good deal larger for a loop than it would be for a ring, where the core length of the initial vortex is considerably longer. Detailed calculations are urgently required, therefore, to determine the change in critical velocity to be expected in each case; one may reasonably hope that comparison with the experimental value reported above will then throw light on whether the threshold nucleating configuration is the loop of Donnelly & Roberts (1971) and Muirhead *et al.* (1984), or the ring of Schwarz & Jang (1973) and Bowley (1984) that our earlier experiments in pure ^{4}He (III) appeared to favour.

The change in the rate constant caused by a trapped ^{3}He atom may be accounted for in several ways, not all of which are mutually exclusive. First, if one regards vortex nucleation as an example of quantum tunnelling (Muirhead *et al.* 1984), then the tunnelling rate will, of course, be critically dependent on the height and width of the barrier; and, as discussed above, the barrier is likely to be modified, perhaps to a significant extent, if a ^{3}He atom is available for incorporation into the initial vortex.

Secondly, as originally pointed out by Dahm (1969), the presence of ^{3}He on the surface of the ion modifies fundamentally the nature of the interface between the superfluid and the ion. For a bare ion, the interface is with a vacuum whereas, in the case we are now considering, the interface is with what effectively consists of a layer of ^{3}He. Although Dahm envisaged a surface layer consisting of many ^{3}He atoms, even a single ^{3}He atom can perhaps be considered to behave like a layer coating the entire ion, if it is occupying a surface state of the type suggested by Shikin (see §1 (*c*)). Thus, the moving ion may be perceived by the superfluid not as a void, but as a thin spherical shell of ^{3}He; and there would then be a sense in which the ion could be regarded as having taken on some of the character of a *positive* ion for which, again, the interface is believed to consist of a spherical layer of helium, moving with the ion (although for the positive ion in He II it is a surface of ^{4}He rather than ^{3}He, and probably solid rather than mobile). The nucleation rate for positive ions is, of course, very much larger than for negative ones, for reasons that are still not properly understood.

On the other hand, we may note, thirdly, that any concept of a ^{3}He atom behaving as a continuous (quantum mechanically smeared) layer on the ion must break down in relation to events that occur on a time scale that is shorter than the orbital period, which is of order $2\pi m_3 R_s^2/h$ (*ca.* 1 ns), which may very well prove to be longer than the time scale of the transition. It is, for example, somewhat longer than the characteristic tunnelling time envisaged by Muirhead *et al.* The possibility remains, therefore, that, at least as far as the vortex transition is concerned, the ^{3}He atom may be viewed more realistically as a localized excrescence on the outside of the ion, rather than as the layer of ^{3}He suggested above. An excrescence of this nature

PHILOSOPHICAL TRANSACTIONS OF THE ROYAL SOCIETY A MATHEMATICAL, PHYSICAL & ENGINEERING SCIENCES

would be expected to constitute a very substantial perturbation of the cylindrical symmetry of the system and, in a purely qualitative sense, it would not be in the least surprising if one consequence was an increase in the rate constant, for the nucleation process.

The last viewpoint appears to imply, however, that the addition of the second ^{3}He atom would be expected to alter the critical velocity and rate constant by increments approximately equal to those caused by the trapping of the first ^{3}He atom on a bare ion. This does not, in fact, appear to be so. Although the precision with which $\nu_2(E)$ can be measured at present is insufficient to allow any conclusion concerning the corresponding critical velocity, it is immediately evident that the second bound ^{3}He atom exerts an enormously greater influence than the first one. Indeed, a comparison of our derived value of $\nu_2 \approx 3 \times 10^7$ s^{-1} at $E \approx 3 \times 10^4$ V m^{-1} with the $\nu_1(E)$ values of figure 19 suggests that the rate constant may well increase by a *factor* of *ca.* 10^2 on the trapping of the second ^{3}He atom. This observation appears to contradict any suggestion that the ^{3}He atoms act as individual localized nucleating sites for the nascent vortex.

In the light of these various considerations, to try to reach any definite conclusion about the nature of the microscopic mechanism of vortex nucleation would clearly be premature. Our experiments have, however, contributed some further items of information, particularly those relating to the changes in the critical velocity and rate constant, which any satisfactory theory will need to be able to encompass. The most desirable next step is, as indicated above, the undertaking of some explicit calculations, within the general philosophy of the models of Schwarz and Jang (1973), Muirhead *et al.* (1984) and Bowley (1984), to determine the effect of one or two trapped ^{3}He atoms on the critical velocities to be expected, respectively, for vortex rings or vortex loops.

7. Conclusions

The principal conclusions to be drawn from the experiments described here and their analysis may be summarized as follows.

(1) The remarkably potent influence exerted by tiny proportions of ^{3}He on the rate at which negative ions nucleate quantized vortex rings in He II arises through the influence of ^{3}He adsorbed in surface trapping states on the ions.

(2) The observed (highly complicated) dependence of ν upon E and T can be understood in terms of the variation with these parameters of n_b, the average number of adsorbed ^{3}He atoms per ion, averaged over the ensemble of ions.

(3) The value of n_b is itself determined by a balance between the competing processes of: ^{3}He absorption onto the ion, with emission of a phonon; and ^{3}He emission from the ion, either in response to an incoming phonon or, spontaneously, together with rotons so as to ensure conservation of energy and momentum. By fitting the data to a model (in two variants) based on these ideas it has been possible to deduce numerical values of E_b, $\nu_1(E)$, $K(T)$ and $R'(E)$.

(4) The deduced binding energy E_b/k_B (given in table 1) is slightly larger than the accepted low temperature value (-2.22 ± 0.03 K) for a plane surface of He II at s.v.p.

(5) The temperature dependence of the ^{3}He absorption cross-section, as specified by the fitted form of $K(T)$, appears to confirm the existence of a small energy barrier separating ^{3}He surface states on the ion from the free-particle-like states of ^{3}He in the bulk liquid.

(6) The magnitude and functional form of $\nu_1(E)$ indicate that the presence of a single adsorbed ^{3}He atom has the dual effect of reducing the critical velocity for vortex nucleation

(by *ca.* 4 m s^{-1}) and simultaneously increasing the corresponding rate constant (by a factor of *ca.* 10^3). The physical mechanism through which these remarkable effects occur remains a mystery. Further calculations and developments in the theory will be required before a choice can be made between the possibilities tentatively discussed in §6(*e*), or a decision taken that some quite different process is involved.

It is a pleasure to acknowledge stimulating discussions with R. J. Donnelly, F. E. Moss, C. M. Muirhead, K. W. Schwarz and P. C. E. Stamp. We are greatly indebted to W. F. Vinen for reading in detail and for making a number of perceptive and extremely helpful comments upon an earlier version of this paper. We are grateful to Mr D. E. Emerson of the U.S. Bureau of Mines for several speedy and efficient isotopic analyses of our samples of helium. The research programme has been supported by the Science and Engineering Research Council to whom one of us (G.G.N.) is also indebted for the support of a research associateship.

Appendix A. Glossary of symbols

For the convenience of the reader, we list below brief explanations of the main symbols used in this paper. The place where each quantity is used for the first time is indicated by the equation or subsection number given in parentheses. The significance of symbols that have more than one meaning should in all cases be clear from the context in which they are being used.

a_0	vortex core radius, (D 1)
$\hat{a}^\dagger$ $(\hat{a})$	creation (annihilation) operator for ion, (4.2)
$\hat{b}^\dagger$ $(\hat{b})$	creation (annihilation) operator for phonon, (4.2)
$\hat{c}^\dagger$ $(\hat{c})$	creation (annihilation) operator for ^{3}He quasiparticle, (4.2)
c	low field correction to bare ion current, (D 14)
c_1	velocity of first sound
$\hat{d}^\dagger$ $(\hat{d})$	creation (annihilation) operator for bound state, (4.2)
e	electronic charge, (D 2)
E	electric field (§1(*c*))
E'	effective electric field, (5.4)
E_b	^{3}He-ion binding energy, (4.3)
E_B	effective ^{3}He-ion binding energy, (4.15)
E_q	phonon energy, (4.3)
$E_\omega, E_{\omega'}$	roton energy, (4.36)
ΔE	increase in energy upon creation of vortex ring (§1(*a*))
$f(\boldsymbol{v}), f(v, E)$	distribution function of bare ions, (4.3), (5.5)
$f_b(\boldsymbol{v}'_3), f_b(\boldsymbol{v}'_3, E)$	distribution function of ions with bound ^{3}He, (4.7), (5.7)
f_q	phonon distribution function, (4.3)
$F(x)$	Dawson's integral, (D 10)
g	energy quantum for orbital states of ^{3}He on ion, (1.2)
G	$= n_4 \bar{v}\sigma$, (6.33)
$\hbar$	Planck's constant/2π, (1.2)
I	impulse of vortex ring, (D 2)
I_B	bare ion current, (2.3)
I_r	charged vortex ring current, (2.6)

$k(T)$	ionic drag factor, (5.4)
k_0	roton wave vector, (4.38)
$\boldsymbol{k}$	^{3}He wave-vector, (4.2)
$\boldsymbol{k}'$	vector defined by (4.16)
k_B	Boltzmann's constant, (1.3)
$K(\boldsymbol{v}, T)$	^{3}He absorption rate per unit number density, (4.22)
K_l	^{3}He absorption rate per unit number density into orbital state l, (4.46)
l	orbital quantum number for ^{3}He on ion (§1)
l_z	z-component of orbital angular momentum for ^{3}He on ion (§1 (*c*))
L	largest value of l for which ϵ_l is negative (§1 (*b*)); and induction cell length, (2.3)
m	quantum number for z-component of angular momentum of ^{3}He on ion (§1 (*c*)); and number of ^{3}He atoms bound to ion, (6.12)
m_i	bare ion mass, (4.3)
m_i'	mass of ion with bound ^{3}He, (4.3)
m_s	effective mass of ^{3}He on ion, (1.2)
m_3	^{3}He atomic mass (§4 (*b*))
m_3'	parameter defined by (4.14)
m_3''	parameter defined by (4.39)
m_4	^{4}He atomic mass (§4 (*b*))
m_3^*	^{3}He quasiparticle mass, (4.5)
M	effective mass of vortex ring per unit length (§1 (*a*))
n_b	number of bound ^{3}He atoms, (1.3)
n_{eq}	equilibrium number of bound ^{3}He atoms, (4.21)
$n_{\boldsymbol{k}}$	^{3}He distribution function, (4.3)
n_l	number of ^{3}He atoms in orbital state l, (4.46)
n_l^{eq}	equilibrium value of n_l, (4.46)
n_0	occupancy of bound state on ion, (4.3)
n_3	^{3}He number density, (4.5)
n_4	^{4}He number density, (6.33)
N_A	Avogadro's constant, (C 1)
N_m	fraction of ions with m bound ^{3}He atoms, (6.8)
$\boldsymbol{p}$	ion wave-vector, (4.2)
$\boldsymbol{p}'$	ion-^{3}He wave-vector, (4.36)
$p(T)$	probability of ^{3}He reaching surface of ion, (4.43)
P	pressure (§3)
$P_n(\cos\theta)$	Legendre polynomial (§1 (*c*))
$\boldsymbol{q}$	phonon wave-vector, (4.2)
Q_0	initial bare ion charge, (2.3)
r	vortex ring radius, (D 1)
r_a	absorption rate of ^{3}He atoms with emission of phonons, (4.3)
r_e	emission rate for ^{3}He atoms with absorption of phonons, (4.7)
R	roton pair emission rate, (6.22)
R'	effective emission rate for ^{3}He with rotons, (4.45)
$\bar{R}_a$	average net ^{3}He absorption rate via process 1, (4.11)
$\bar{R}_{am}$	average rate of absorption of ^{3}He onto ion with m bound ^{3}He atoms, (6.11)
$\bar{R}_{aT}$	average net rate of ^{3}He absorption, (6.12)

R_C resistance of carbon thermometer (§2(*b*))
R_e rate of emission of ^{3}He with rotons, (4.44)
R_G resistance of germanium thermometer (§2(*b*))
R_i ionic radius (§1(*a*))
R_l emission rate, with rotons, for ^{3}He from orbital state l, (4.51)
R'_l effective emission rate, with rotons, for ^{3}He from orbital state l, (4.46)
R_m ^{3}He emission rate with rotons, from ion with m bound ^{3}He atoms (§6(*b*))
R_r roton-pair emission rate constant, (4.51)
R_s radius for ^{3}He surface state, (1.2)
$\mathscr{R}_v$ intrinsic vortex nucleation rate, (5.5)
$\mathscr{R}_{v'}$ intrinsic vortex nucleation rate for ion with bound ^{3}He, (5.7)
$\mathscr{R}_0$ characteristic rate for vortex nucleation, (5.6)
$\mathscr{R}_1$ characteristic rate for vortex nucleation from ion with bound ^{3}He, (5.8)
t time, (2.8)
T temperature (§1(*c*))
T_λ temperature of the lambda transition
$T^p_{k,q}$ matrix element for ^{3}He absorption process, (4.2)
U ionic velocity (§1(*c*))
U_B backflow velocity around moving ion (§1(*c*))
$\boldsymbol{v}$ bare ion velocity (§1(*a*))
$\boldsymbol{v}'$ critical ion velocity for roton emission (§4(*d*))
v_c critical velocity for vortex nucleation (5.6)
v_{cL} critical velocity for nucleation of vortex loop (§1(*a*))
v_{cR} critical velocity for nucleation of vortex ring (§1(*a*))
v_{c1} critical velocity for vortex nucleation from ion with bound ^{3}He, (5.8)
v_{cl} critical velocity for emission of ^{3}He with rotons from orbital state l, (4.50)
v_{c3} critical velocity for emission of ^{3}He with rotons, (4.43)
v_i velocity of ion at moment of vortex nucleation (§1(*a*))
v_r vortex ring velocity, (2.6)
$\bar{v}_{rel}$ average relative velocity between ion and free ^{3}He atom, (4.27)
v_{v1} first critical velocity for vortex nucleation (as in III) (§1(*a*))
$\bar{v}_3$ average thermal velocity of ^{3}He, (4.29)
v'_3 velocity of ion with bound ^{3}He, (4.8)
δv_l shift in critical velocity when ^{3}He emitted from orbital state l, (4.50)
$V(r)$ potential for ^{3}He-ion interaction, (4.32)
V_m molar volume of ^{4}He, (C 1)
V_p height of potential barrier opposing ^{3}He reaching ion's surface, (4.33)
V_3 volume occupied by ^{3}He atom (§1(*c*))
x_3 ratio of ^{3}He–^{4}He number densities (§1)
z_m quantity defined by (6.18)
α parameter defined by (D 4); and excess volume of ^{3}He atom in bulk ^{4}He, (4.32)
β $1/k_B T$, (4.4)
γ polarizability of ^{4}He atom, (4.32)
Δ roton energy gap, (4.38)
δ Dirac δ-function (§4(*b*))
ϵ_k energy of free ^{3}He atom, (4.3)

PHILOSOPHICAL TRANSACTIONS OF THE ROYAL SOCIETY A MATHEMATICAL, PHYSICAL & ENGINEERING SCIENCES

ϵ_l	energy of bound ^{3}He atom (§1)
ϵ_0	depth of potential well for ^{3}He atom bound to ion, (1.1); and permittivity of free space, (4.32)
η	a constant of order unity, (4.26)
κ	quantum of circulation (§1 (*a*))
λ	probability of capture of ^{3}He at surface of ion (§4 (*c*))
μ	chemical potential of ^{3}He, (1.3)
ν	measured vortex nucleation rate (§1)
ν', ν''	coefficients of power series expression of $\nu(x_3)$, (5.1)
ν_a	apparent nucleation rate, (D 18)
ν_r	roton-assisted vortex nucleation rate (§5 (*d*))
ν_0	vortex nucleation rate for bare ions, (4.1)
ν_1	vortex nucleation rate for ions with one bound ^{3}He atom, (4.2)
ν_m	vortex nucleation rate for ions with m bound ^{3}He atoms, (6.8)
ν_{1l}	vortex nucleation rate for ions with a ^{3}He atom in orbital state l (§4 (*e*))
$\Delta\nu$	$\nu_1 - \nu_0$, (4.1 *a*)
ξ	a constant of order unity (§1 (*c*)); and the quantity defined by (D 6)
Π	probability of absorption for ^{3}He atom striking ion, (4.27)
ρ_4	^{4}He density (§1 (*a*))
σ	effective cross-section for absorption of ^{3}He by ion, (4.35)
$\boldsymbol{\sigma}$	spin of ^{3}He, (4.2)
σ_g	geometric cross-section of ion, (4.27)
$\psi_{l,m}$	wave-function of ^{3}He bound to ion (§1 (*c*))
ω	'cyclotron' frequency of vortex ring (§1 (*a*))
$\boldsymbol{\omega}, \boldsymbol{\omega}'$	roton wave-vector, (4.36)

Appendix B. Tabular vortex nucleation data

A small selection of measured nucleation rates ν is presented in tables 3–5. The data were all obtained for a pressure of 23 bar and, apart from being rounded to three significant figures, they are printed exactly as measured: that is, no correction has been applied to allow for the (small) non-idealities of the collector circuit (see §3 (*a*)) of III). The experimental uncertainties were as discussed in §3 (*a*) and in Appendix B of III.

Table 3. Nucleation rates at $T = 0.329$ K

(The measured nucleation rate is given for various electric fields E and ^{3}He concentrations x_3.)

$10^8 x_3 \ldots$ / $10^{-4} E/(\mathrm{V\ m^{-1}})$	0 (pure)	2.14	4.29	6.44	8.58	10.7	12.9	15.0	17.2
1.05	—	426	784	1540	2730	3610	3920	6180	8140
1.69	—	525	1210	2210	3380	4500	5720	7530	9280
2.32	—	793	1680	2730	4060	5330	6790	8830	10500
3.69	—	1210	2560	3800	5280	6730	8210	10300	12100
5.28	—	1420	2920	4250	5550	7140	8230	10100	11800
7.37	—	1310	2540	3820	5980	6120	7150	8620	9810
10.5	185	1040	1910	2860	3750	4760	5300	6300	7170
16.9	276	904	1450	1950	2440	2990	3580	4080	4690
23.2	540	962	1300	1630	1960	2340	2780	3050	3560
36.9	1430	1640	1730	1850	2040	2250	2410	2550	2890
52.8	3230	3250	3240	3140	3190	3280	3390	3550	3800
63.1	4650	4570	4490	4330	4390	4400	4480	4570	4770

Table 4. Nucleation rates at $T = 0.414$ K

(The measured nucleation rate is given for various electric fields E and ^{3}He concentrations x_3.)

$10^8 x_3 \ldots$ / $10^{-4} E/(\mathrm{V\ m^{-1}})$	0 (pure)	2.14	4.29	6.44	8.58	10.7	12.9	15.0	17.2
1.05	—	426	784	1540	2730	3610	3920	6180	8140
1.69	—	525	1210	2210	3380	4500	5720	7530	9280
2.32	—	151	1680	2730	4060	5330	6790	8830	10500
3.69	—	1210	2560	3800	5280	6730	8210	10300	12100
5.28	—	1420	2920	4250	5550	7140	8230	10100	11800
7.37	126	1310	2540	3820	4980	6120	7150	8620	9810
10.5	147	1040	1910	2860	3750	4760	5300	6300	7170
16.9	302	900	1450	1950	2440	2990	3580	4080	4690
23.2	460	960	1300	1630	1960	2340	2780	3050	3560
36.9	1220	1640	1730	1850	2040	2250	2410	2550	2890
52.8	2820	3250	3240	3140	3190	3280	3390	3550	3800
63.1	4000	4570	4490	4330	4390	4400	4480	4570	4770

Table 5. Nucleation rates at $T = 0.549$ K

(The measured nucleation rate is given for various electric fields E and ^{3}He concentrations x_3.)

$10^8 x_3 \ldots$ / $10^{-4} E/(\mathrm{V\ m^{-1}})$	0 (pure)	2.14	4.29	6.44	8.58	10.7	12.9	15.0	17.2
2.32	—	—	—	—	—	118	101	175	234
3.69	—	—	—	213	267	293	432	632	671
5.28	—	123	305	375	637	764	969	1160	1260
7.37	100	254	553	698	1070	1330	1510	1910	2140
10.5	158	454	803	1220	1670	2060	2460	2790	3270
16.9	417	766	1200	1620	2070	2430	2940	3380	3960
23.2	684	988	1360	1710	2080	2420	2830	3140	3680
36.9	1520	1700	1950	2120	2320	2520	2690	2870	3210
52.8	3270	3300	3360	3500	3530	3650	3700	3770	3940
63.1	4600	4620	4650	4750	4720	4820	4760	4840	5040

Appendix C. ^{3}He Concentration adjustment

In this appendix, we derive the expression (2.1) for the ^{3}He concentration resulting from one pressure cycle of the experimental cell and associated pipework. We assume that the initial pressure and ^{3}He concentration of the He II in the cell are P_i and x_3^i, that the lowest pressure in the cycle is P_l and that the final pressure is P_f. It is most convenient to work in terms of the number density, N_3, of ^{3}He atoms. Initially this is

$$N_3^\mathrm{i} = x_3^\mathrm{i} N_\mathrm{A}/V_\mathrm{m}(\mathrm{P_i}) \tag{C 1}$$

where N_A is Avogadro's constant and V_m is the molar volume of ^{4}He at pressure P_i. In reducing the chamber pressure to P_l, the total helium number density is reduced to

$$N_{\mathrm{T}l} = N_\mathrm{A}/V_\mathrm{m}(P_l), \tag{C 2}$$

although the ^{3}He number density retains the original value of N_3^i. Repressurizing the cell results in helium atoms being pushed into the cell, a fraction x_3^n of which are the ^{3}He atoms. At the final pressure, P_f, the total number density is

$$N_{\mathrm{Tf}} = N_\mathrm{A}/V_\mathrm{m}(P_\mathrm{f}), \tag{C 3}$$

and the increase in the ^{3}He number density is

$$\Delta N_3 = x_3^{\mathrm{n}} N_{\mathrm{A}} \left\{ \frac{1}{V_{\mathrm{m}}(P_{\mathrm{f}})} - \frac{1}{V_{\mathrm{m}}(P_l)} \right\}.$$

The final ^{3}He number density is therefore

$$N_3^{\mathrm{f}} = N_3^{\mathrm{i}} + \Delta N_3 = x_3^{\mathrm{i}} \frac{N_{\mathrm{A}}}{V_{\mathrm{m}}(P_{\mathrm{i}})} + x_3^{\mathrm{n}} N_{\mathrm{A}} \left\{ \frac{1}{V_{\mathrm{m}}(P_{\mathrm{f}})} - \frac{1}{V_{\mathrm{m}}(P_l)} \right\}. \tag{C 4}$$

To determine the final ^{3}He concentration, we note that

$$x_3^{\mathrm{f}} = \{V_{\mathrm{m}}(P_{\mathrm{f}})/N_{\mathrm{A}}\}\, N_3^{\mathrm{f}}, \tag{C 5}$$

which, on substitution of N_3^{f} from (C 4) yields (2.1) directly.

Appendix D. The vortex-borne current

In this appendix we derive an expression for the apparent nucleation rate in low electric fields, where the influence of the vortex current cannot necessarily be assumed to be negligible. To evaluate the integral in (2.7), we require an expression for $v_{\mathrm{r}}(t-t')$. It can be shown (Fetter 1976) that the velocity v_{r} or a vortex ring as a function of its radius r is given by

$$v_{\mathrm{r}} = \frac{\kappa}{4\pi r} \left\{ \ln\left(\frac{8r}{a_0}\right) - \tfrac{1}{2} \right\}, \tag{D 1}$$

where κ is the quantum of circulation and a_0 is the radius of the vortex core. (Here we have assumed the core to be hollow.) When an ion is attached to the vortex ring, there will be changes to this equation; but these will be small provided that the radius of the ring is much larger than that of the ion.

How does the velocity of the charged vortex ring vary with time? This can be calculated by equating the electric force on the ion to the rate of change of impulse of the ring.

$$eE = \frac{\mathrm{d}I}{\mathrm{d}t} = 2\pi\rho\kappa r \frac{\mathrm{d}r}{\mathrm{d}t}. \tag{D 2}$$

Here we have taken the impulse of the ring to be $\pi\rho\kappa r^2$ and have ignored any modifications to (D 1) owing to the presence of the ion trapped on its core. Suppose a ring is created at time t' with an initial radius of r_0. At time t the ring will have expanded to a radius $r(t)$ given by

$$r(t) = r_0\{1 + eE(t-t')/\pi\rho\kappa r_0^2\}^{\frac{1}{2}}, \tag{D 3}$$

as can readily be shown by integration of equation (D 2). We can now substitute this into (D 1) to obtain the velocity of the ring at a time $t-t'$ after its creation. It is useful to define a parameter

$$\alpha = eE/\pi\rho\kappa r_0^2\, \nu. \tag{D 4}$$

The velocity is then

$$v_{\mathrm{r}}(t-t') = \frac{\kappa}{4\pi r_0} \{1 + \alpha\nu(t-t')\}^{-\frac{1}{2}} \left[\ln\left(\frac{8r_0}{a_0}\right) - \tfrac{1}{2} + \tfrac{1}{2} \ln\{1 + \alpha\nu(t-t')\} \right]. \tag{D 5}$$

By putting

$$\xi = \{1 + \alpha\nu(t-t')\}^{\frac{1}{2}} \tag{D 6}$$

and substituting in (2.7), one finds that the total current is given by

$$I(t) = \frac{Q_0 \bar{v}}{L} e^{-\nu t}\left[1 + \frac{\kappa}{2\pi r_0 \alpha \bar{v}} \int_1^{(1+\alpha\nu t)^{\frac{1}{2}}} d\xi \exp\{(\xi^2-1)/\alpha\}\left\{\ln\left(\frac{8r_0}{a_0}\right) - \tfrac{1}{2} + \ln\xi\right\}\right]. \quad \text{(D 7)}$$

The first term in the square brackets is the current due to bare ions, whereas the second term is the current due to ions bound to vortex rings. We now examine the size of the second term relative to the first term and how its presence affects the analysis of the experimental results.

The integral over ξ is dominated by the $\exp(\xi^2)$ term and, in comparison, the $\ln\xi$ term is a slowly varying function. If the maximum value of ξ is much larger than one, then one can replace $\ln\xi$ by the maximum value of $\ln\xi$ with little error. If the maximum of ξ is close to one, then $\ln\xi$ is always small and if we replace $\ln\xi$ by its maximum value then there is hardly any error at all, since $\ln\xi$ is so much smaller than $\{\ln(8r_0/a_0) - \frac{1}{2}\}$. Consequently, replacing $\ln\xi$ by $\frac{1}{2}\ln(1+\alpha\nu t)$ is always a good approximation. The integral in (D 7) now simplifies to

$$\text{Int} = \left\{\ln\left(\frac{8r_0}{a_0}\right) - \tfrac{1}{2} + \tfrac{1}{2}\ln(1+\alpha\nu t)\right\} \int_1^{(1+\alpha\nu t)^{\frac{1}{2}}} d\xi \exp\{(\xi^2-1)/\alpha\}. \quad \text{(D 8)}$$

Let us put $z = \xi\alpha^{-\frac{1}{2}}$ so that this integral becomes

$$\text{Int} = \left\{\ln\left(\frac{8r_0}{a_0}\right) - \tfrac{1}{2} + \tfrac{1}{2}\ln(1+\alpha\nu t)\right\} \alpha^{\frac{1}{2}} e^{-1/\alpha}\left\{\int_0^{(1+\alpha\nu t/\alpha)^{\frac{1}{2}}} dz \exp(z^2) - \int_0^{\alpha^{-\frac{1}{2}}} dz \exp(z^2)\right\}. \quad \text{(D 9)}$$

This can now be written in terms of Dawson's Integral (Gautschi 1965), which is defined as

$$F(x) = \exp(-x^2) \int_0^x dz \exp(z^2). \quad \text{(D 10)}$$

Thus

$$\text{Int} = \left\{\ln\left(\frac{8r_0}{a_0}\right) - \tfrac{1}{2} + \tfrac{1}{2}\ln(1+\alpha\nu t)\right\} \alpha^{\frac{1}{2}} e^{-1/\alpha}\left[\exp\left(\frac{1+\alpha\nu t}{\alpha}\right) F\left\{\left(\frac{1+\alpha\nu t}{\alpha}\right)^{\frac{1}{2}}\right\} - \exp\left(\frac{1}{\alpha}\right) F\left(\frac{1}{\alpha^{\frac{1}{2}}}\right)\right] \quad \text{(D 11)}$$

and substitution into (D 7) gives

$$I(t) = \frac{Q_0 \bar{v}}{L} e^{-\nu t}\left[\left[1 + \frac{A}{\alpha^{\frac{1}{2}}}\left[e^{\nu t} F\left\{\left(\frac{1+\alpha\nu t}{\alpha}\right)^{\frac{1}{2}}\right\} - F\left(\frac{1}{\alpha^{\frac{1}{2}}}\right)\right]\right]\right], \quad \text{(D 12)}$$

where

$$A = \frac{\kappa}{2\pi r_0 \bar{v}}\left\{\ln\left(\frac{8r_0}{a_0}\right) - \tfrac{1}{2} + \tfrac{1}{2}\ln(1+\alpha\nu t)\right\}. \quad \text{(D 13)}$$

Equation (D 12) gives the predicted form of the current as a function of time. In principle it can now be used to obtain values of ν for low electric fields. This is not, however, how we have proceeded in practice. Rather, we have analysed the induction signals on the assumption that the vortex-borne current was zero. Our interest, consequently, is in estimating the size of the error caused by making this approximation.

Let us write

$$I(t) = (Q_0 \bar{v}/L)\, e^{-\nu t}(1+c), \quad \text{(D 14)}$$

where

$$c = \frac{A}{\alpha^{\frac{1}{2}}}\left[e^{\nu t} F\left\{\left(\frac{1+\alpha\nu t}{\alpha}\right)^{\frac{1}{2}}\right\} - F\left(\frac{1}{\alpha^{\frac{1}{2}}}\right)\right] \quad \text{(D 15)}$$

is the correction needed for the vortex current. We will show that for large fields $c \ll 1$ so that

$$\ln I(t) = \ln (Q_0 \bar{v}/L) - \nu t + \ln (1+c) \tag{D 16}$$

and

$$\frac{\mathrm{d}\{\ln I(t)\}}{\mathrm{d}t} \approx -\nu + \frac{\mathrm{d}c}{\mathrm{d}t}. \tag{D 17}$$

Our data have been analysed on the Nicolet 1080 computer by putting the best straight line through the linear part of $\ln I(t)$. Consequently, when we extract values of the nucleation rate by this procedure, the apparent nucleation rate ν_a is given by

$$\nu_a = \nu \left\{ 1 - \frac{1}{\nu} \left(\frac{\mathrm{d}c}{\mathrm{d}t} \right)_{av} \right\} \tag{D 18}$$

where $(\mathrm{d}c/\mathrm{d}t)_{av}$ represents an average over time. Because $\mathrm{d}c/\mathrm{d}t$ is positive, the apparent nucleation rate is always an underestimate of the true nucleation rate.

Now let us try to make a numerical estimate of the size of this error. First we need to know the initial radius of the vortex ring. We take it to be 15 Å, just larger than the radius of the ion. This assumption is not crucial, for the correction c depends only on $\ln (8r_0/a_0)$, so that by changing r_0 by, say, 50 % there is only a 5 % change in c. (The factor $A/\alpha^{\frac{1}{2}}$ is almost independent of r_0.)

For the parameter A we have, with E in volts/m,

$$A = 0.192\{4.0 + 0.5 \ln (1 + 1330 Et)\}. \tag{D 19}$$

The parameter α is

$$\alpha = 1330 E/\nu, \tag{D 20}$$

where we have taken $\bar{v}$ to have a typical value of 55 m s^{-1}. For all the values of ν we have recorded, ν expressed in s^{-1} never exceeds E expressed in V/m. Consequently $\alpha^{-\frac{1}{2}}$ is less than 0.03 and can, where appropriate, be replaced by zero with little error. Then

$$c = 0.0053(\nu/E)^{\frac{1}{2}}\{4.0 + 0.5 \ln (1 + 1330 Et)\}\, \mathrm{e}^{\nu t} F\{(\nu t)^{\frac{1}{2}}\}. \tag{D 21}$$

The main time dependence of c comes from the term $\mathrm{e}^{\nu t} F\{(\nu t)^{\frac{1}{2}}\}$. In figure 29 we plot $\mathrm{e}^x F(x^{\frac{1}{2}})$ as a function of x. It can be seen that this is not a linear function of x (that is, of νt) so that it is not possible to fit a straight line exactly to the data.

Typical values of ν are of order 10^4 s^{-1}, whereas the time that the ion takes to traverse the drift space is *ca.* 10^{-4} s^{-1} for our 5 mm cell. Thus, νt varies from zero to one and so we need to fit a straight line through the curve shown in figure 29 for x in the range zero to one. The best fitting line has a slope of *ca.* 1.3. This gives the average correction to the nucleation rate of

$$\frac{\nu - \nu_a}{\nu} = \frac{1}{\nu} \left(\frac{\mathrm{d}c}{\mathrm{d}t} \right)_{av} = 0.0067 \left(\frac{\nu}{E} \right)^{\frac{1}{2}} \{4.0 + 0.5 \ln (1 + 1330 Et)\}, \tag{D 22}$$

which is the same as (2.8). For a field of 10^4 V/m, with $\nu = 10^4$ s^{-1} (that is, worse than the worst case in practice), this leads to an underestimate of ν of some 5 %. If we were to consider more dilute solutions, so that ν was smaller, then the range of νt would be reduced. Consequently the slope of the best fitting line would increase, roughly as $\nu^{-\frac{1}{2}}$. This means that the dimensionless quantity $\nu^{-1}\mathrm{d}c/\mathrm{d}t$ does not vary significantly with ν, provided $\nu t \lesssim 1$. If $\nu t \gg 1$, then the situation becomes considerably more complicated. The signal for $\nu t > 3$ is attenuated

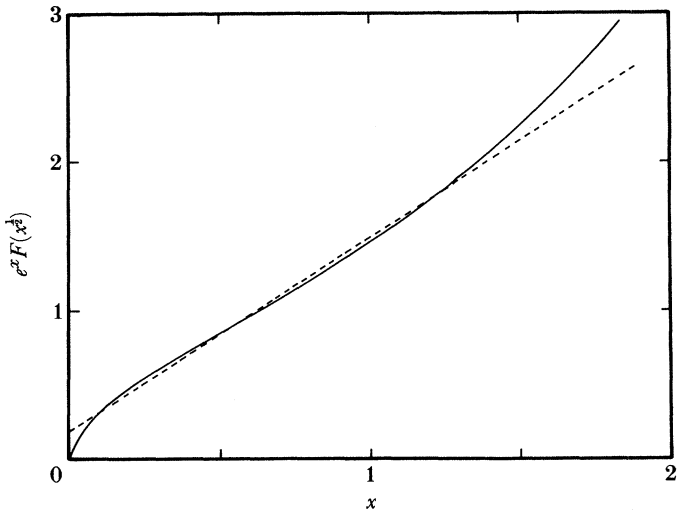

FIGURE 29. Graph to demonstrate the effect of ignoring the vortex current. The full curve shows the true shape of the function $e^x F(x^{\frac{1}{2}})$ discussed in the text; and the dashed line shows best fitting straight line within the range $0 < x = \nu t < 1$.

exceedingly rapidly, however, so that this part of the parameter range is not important in practice. The slope of the best fitting line will in fact increase above 1.3, although not by very much. The quantity $\nu^{-1}\,\mathrm{d}c/\mathrm{d}t$ therefore increases roughly as $\nu^{\frac{1}{2}}$.

APPENDIX E. EQUATIONS FOR THE NONLINEAR TERMS

In this appendix we obtain expressions for ν' and ν'' in terms of the z_m defined by (6.18). In doing so, only terms up to n_3^2 will be needed so that it is sufficient to calculate N_2 to lowest order in n_3, and N_1 to second order in n_3. Rearrangement of (6.17) gives, for $m = 1$,

$$N_1 = \frac{z_1}{1+z_1}\left\{N_0 + 2N_2\left(\frac{1}{n_{\mathrm{eq}}} + \frac{R_2}{N_3 K}\right)\right\} \tag{E 1}$$

and, for $m = 2$,

$$N_2 = \frac{\frac{1}{2}z_2}{1+\frac{1}{2}z_2}\left\{N_1 + 3N_3\left(\frac{1}{n_{\mathrm{ea}}} + \frac{R_3}{n_3 K}\right)\right\}$$

$$= N_1(1+2/z_2)^{-1} \tag{E 2}$$

where we assume N_3 is negligible.

With the aid of (6.9) we can determine N_1, and hence N_2, in terms of variables other than the N_m. Rearranging (E 1) and using (E 2) for N_2 gives

$$N_0 = N_1\left\{\frac{1+z_1}{z_1} - \frac{2}{(1+2/z_2)}\left(\frac{1}{n_{\mathrm{eq}}} + \frac{R_2}{n_3 K}\right)\right\}. \tag{E 3}$$

From (6.18) we have:

$$\frac{1}{n_{\mathrm{eq}}} + \frac{R_2}{n_3 K} = \frac{1}{z_2} - \frac{\nu_2}{2n_3 K}, \tag{E 4}$$

whence

$$N_0 = N_1\left\{\frac{1+z_1}{z_1} - \frac{2}{2+z_2}\left(1 - \frac{z_2\nu_2}{2n_3 K}\right)\right\}. \tag{E 5}$$

We are assuming that N_3, N_4, etc. are negligible and consequently (6.9) becomes

$$N_1 \approx 1 - N_0 - N_2. \tag{E 6}$$

Use of (E 5) for N_0 and (E 2) for N_2 then yields

$$N_1 \approx 1 - N_1\left\{\frac{1+z_1}{z_1} - \frac{2}{2+z_2}\left(1 - \frac{z_2\nu_2}{2n_3K}\right) - \frac{1}{(1+2/z_2)}\right\},$$

which, since $z_2 \ll 1$, gives

$$\begin{aligned} N_1 &\approx \left\{1 + \left(\frac{1+z_1}{z_1} - 1 + \frac{z_2\nu_2}{2n_3K}\right)\right\}^{-1} \\ &= z_1\{1 + z_1(1 + z_2\nu_2/2n_3K)\}^{-1} \\ &\approx z_1 - z_1^2(1 + z_2\nu_2/2n_3K) \end{aligned} \tag{E 7}$$

where $z_1(1 + z_2\nu_2/2n_3K) \ll 1$.

Knowing N_1, and N_2 in terms of N_1, we can now determine ν. From (6.8) we have

$$\begin{aligned} \nu &\approx N_0\nu_0 + N_1\nu_1 + N_2\nu_2 \\ &= (1 - N_1 - N_2)\nu_0 + N\nu_1 + N_2\nu_2 \\ &= \nu_0 + N_1(\nu_1 - \nu_0) + N_2(\nu_2 - \nu_0) \\ &\approx \nu_0 + z_1(\nu_1 - \nu_0) - z_1^2\left(1 + \frac{z_2\nu_2}{2n_3K}\right)(\nu_1 - \nu_0) + \frac{z_1z_2}{2}(\nu_2 - \nu_0) + O(n_3^3), \end{aligned}$$

where we are uninterested in terms of order higher than n_3^2. From a comparison with (5.1) we then obtain

$$\nu' x_3 = (\nu_1 - \nu_0)\, z_1 \tag{E 8}$$

and

$$\nu'' x_3^2 = \frac{z_1z_2}{2}(\nu_2 - \nu_0) - z_1^2\left(1 + \frac{z_2\nu_2}{2n_3K}\right)(\nu_1 - \nu_0). \tag{E 9}$$

Note that z_1 is the same as n_b as given by (4.45) (actually our expression for z_1 has ν_1 instead of $\nu_1 - \nu_0$ but, since $\nu_1 \gg \nu_0$, this is not significant). We have, therefore, already deduced z_1 for both models A and B.

We can simplify (E 7) by making two assumptions. First, we suspect that R_2 will not differ significantly from R_1, which seems reasonable when we remember that we can have at least two bound ^{3}He atoms occupying the same energy level. We shall therefore put $R_1 = R_2 = R$. Secondly, we shall assume that $\nu_2 \gg \nu_1$, which again seems justified since we already know $\nu_1 \gg \nu_0$. Equation (6.18) now gives

$$\frac{1}{z_1} = \frac{1}{n_{eq}} + \frac{R}{n_3K} + \frac{\nu_1}{n_3K},$$

whence

$$\frac{1}{n_{eq}} + \frac{R}{n_3K} = \frac{1}{z_1} - \frac{\nu_1}{n_3K}. \tag{E 10}$$

Also,

$$\frac{1}{z_2} = \frac{1}{n_{eq}} + \frac{R}{n_3K} + \frac{\nu_2}{2n_3K},$$

which, with (E 10), yields

$$z_2 = z_1(1+\nu_2 z_1/2n_3 K)^{-1}. \tag{E 11}$$

Taking each term of equation (E 9) in turn, we find

$$\left.\begin{aligned}\frac{z_1 z_2}{2}(\nu_2-\nu_0) &\approx \frac{z_1^2\nu_2}{2(1+\nu_2 z_1/2n_3 K)}\\ &= \frac{n_3 K z_1}{1+2n_3 K/z_1\nu_2}\end{aligned}\right\} \tag{E 12}$$

and

$$z_2^2\left(1+\frac{z_2\nu_2}{2n_3 K}\right) = z_1^2\left(1+\frac{1}{2n_3 K/\nu_2 z_2+1}\right) \approx 2z_1^2. \tag{E 13}$$

Equation (E9) then becomes

$$\nu'' x_3^2 \approx \frac{n_3 K z_1}{1+2n_3 K/z_1\nu_2} - 2z_1^2(\nu_1-\nu_0), \tag{E 14}$$

which is the same as (6.20).

References

Allum, D. R., McClintock, P. V. E., Phillips, A. & Bowley, R. M. 1977 *Phil. Trans. R. Soc. Lond.* A **284**, 179–224 (referred to in text as I).

Andreev, A. F. 1966 *Zh. éksp. teor. Fiz.* **50**, 1415–1419 (transl. as *Soviet Phys. JETP* **23**, 939–941, 1966).

Bevington, P. R. 1969 *Data reduction and error analysis for the physical sciences*, pp. 237–240. New York: McGraw-Hill.

Bowley, R. M. 1984 *J. Phys. C: solid St. Phys.* **17**, 595–613.

Bowley, R. M. & Lekner, J. 1970 *J. Phys. C: solid St. Phys.* **3**, L127–130.

Bowley, R. M., McClintock, P. V. E., Moss, F. E., Nancolas, G. G. & Stamp, P. C. E. 1982 *Phil. Trans. R. Soc. Lond.* A **307**, 201–260 (referred to in text as III).

Bowley, R. M., Nancolas, G. G. & McClintock, P. V. E. 1984 *Phys. Rev. Lett.* **52**, 659–662.

Bowley, R. M. & Sheard, F. W. 1977 *Phys. Rev.* B **16**, 244–254.

Brooks, J. S. & Donnelly, R. J. 1977 *J. phys. Chem. ref. Data* **6**, 51–104.

Chang, C. C. & Cohen, M. 1973 *Phys. Rev.* A **8**, 3131–3134.

Dahm, A. J. 1969 *Phys. Rev.* **180**, 259–262.

Donnelly, R. J. & Roberts, P. H. 1971 *Phil. Trans. R. Soc. Lond.* A **271**, 41–100.

Edwards, D. O. & Saam, W. F. 1978 In *Progress in low temperature physics* (ed. D. F. Brewer), vol. VIIA, pp. 283–369. Amsterdam: North Holland.

Ellis, T., McClintock, P. V. E. & Bowley, R. M. 1983 *J. Phys. C: solid St. Phys.* **16**, L485–489.

Ellis, T., McClintock, P. V. E., Bowley, R. M. & Allum, D. R. 1980 *Phil. Trans. R. Soc. Lond.* A **296**, 581–595 (referred to in text as II).

Fetter, A. L. 1976 In *The physics of liquid and solid helium* (ed. K. H. Bennemann and J. B. Ketterson), pp. 207–305. New York: Wiley.

Gautschi, W. 1965 In *Handbook of mathematical functions* (ed. M. Abramowitz and I. A. Stegun), pp. 295–329. New York: Dover.

Hetzler, M. C. & Walton, D. 1968 *Rev. scient. Instrum.* **39**, 1656–1657.

Jones, C. A. & Roberts, P. H. 1982 *J. Phys. A: Math. Gen. Phys.* **15**, 2599–2619.

Ketterson, J. B., Kuchnir, M. & Roach, P. R. 1971 *Proc. 12th Int. Conf. Low Temp. Phys.* (ed. E. Kanda), pp. 105–106. Kyoto: Academic Press of Japan.

Kuchnir, M., Ketterson, J. B. & Roach, P. R. 1972 *Phys, Rev.* A **6**, 341–355.

Lekner, J. 1970 *Phil. Mag.* **22**, 669–673.

Muirhead, C. M., Vinen, W. F. & Donnelly, R. J. 1984 *Phil. Trans. R. Soc. Lond.* A **311**, 433–467.

Nancolas, G. G. & McClintock, P. V. E. 1982 *Phys. Rev. Lett.* **48**, 1190–1192.

Neeper, D. A. & Meyer, L. 1969 *Phys. Rev.* **182**, 223–234.

Ngan, T. H., Small, J. C. H. & McClintock, P. V. E. 1981 *Physica* **107B**, 597–598.

Rayfield, G. W. 1968 *Phys. Rev. Lett.* **20**, 1467–1468.

Rayfield, G. W. & Reif, F. 1964 *Phys. Rev.* A **136**, 1194–1208.

Saam, W. F. 1971 *Phys. Rev.* A**4**, 1278–1281.

Schwarz, K. W. & Jang, P. S. 1973 *Phys. Rev.* A**8**, 3199–3210.
Shikin, V. B. 1973 *Zh. éksp. teor. Fiz.* **64**, 1414–1424 (transl. as *Soviet Phys. JETP* **37**, 718–722, 1973).
Vinen, W. F. 1963 In *Liquid Helium: Proc. Int. School Phys. Enrico Fermi: course XXI* (ed. G. Careri), pp. 336–355. New York: Academic Press.
Zoll, R. 1976 *Phys. Rev.* B **14**, 2913–2926.
Zoll, R. & Schwarz, K. W. 1973 *Phys. Rev. Lett.* **31**, 1440–1443.

PHILOSOPHICAL TRANSACTIONS OF THE ROYAL SOCIETY A MATHEMATICAL, PHYSICAL & ENGINEERING SCIENCES